Energy-saving method for changing periodic air temperature field in greenhouse crop cultivation

THIRI SHOON WAI

A thesis submitted for the degree of

Doctor of Engineering

Division of System Engineering

Graduate School of Engineering

Mie University, Japan

March 2025

Abstract

In control agricultural section, the greenhouse and plant factories are increasingly popular. The greenhouse cultivation is an enclosed environment that creates suitable conditions for the high-quality crops production. In contrast to traditional open-field cultivation, greenhouses allow for higher production levels, better crop quality, and out-of-season production. Regarding energy consumption, greenhouse cultivation is a major energy consumer where the entire facility environment is controlled. High energy consumption of creating an appropriate climate for crop growth becomes the main limiting issue in greenhouse cultivation. In particular, some crops like strawberry require periodic temperature field in day and nighttimes. To address this issue, this study proposed periodic local climate control using a simple serpentine copper tube heat exchanger near the crop areas in greenhouse cultivation. Since the environment far away from the crops is not very essential, the environment only near the crops is controlled to provide a suitable climate for crops. In this way, the energy consumption of climate control can be reduced due to a smaller volume compared to climate control for the whole volume of greenhouse cultivation.

The first objective of this thesis was to investigate the local air temperature profiles as well as the performance of the serpentine heat exchanger such as the heat flux and pressure drop in them. Copper tubes were arranged in the shape of serpentine and used as a heat exchanger. In contrast to fin-and-tube heat exchangers, the serpentine heat exchanger has a simple design, provides minimal shade for plants, and is easy to maintain for agriculture. To employ this system for practical use, its scale can be expanded by connecting heat exchangers in series and parallel. The experimental system was constructed under with the assumption that a part of actual plant cultivation was being left out. This study was conducted in a laboratory. Experiments were performed by varying inlet fluid temperature and fluid flow rates. Inlet fluid temperature varies from −5 to 10 ºC for cooling, and 30 to 50 ºC for heating. The fluid flow rate is changed from 0.3 to 3.0 L/min (Reynolds number = 50 – 3,480) for cooling and heating. The local air temperatures, tube surface temperatures, air temperature inside and outside of the experimental area, inlet and outlet fluid temperatures, and pressure drop were measured. The relative humidity was monitored for reference. In terms of cooling, the local air temperature can be reduced by 4–10 °C from the initial air temperature of 22 °C in the area below the heat exchanger at a distance of 150 mm. In terms of heating, the local air temperature can be increased by 6–13 °C from the initial air temperature of 22 °C in the area above the heat exchanger at a distance of 150 mm. For cooling, the average heat flux values in the heat exchanger at inlet fluid temperatures of 5, 0, and −5 °C are enhanced by 55%, 120%, and 170% for all flow rates compared with that at inlet fluid temperature of 10 °C. The average heat flux values in the heat exchanger at inlet fluid temperatures of 40 and 50 °C are increased by 100% and 197% at all flow rates compared with that at inlet fluid temperature of 30 °C. Considering both cooling and heating operations, the pressure drop in the heat exchanger reaches a minimum of 0.3 kPa and a maximum of approximately 5.0 kPa for flow rate of 0.3 to 3.0 L/min. Based on the results, inlet fluid temperature markedly affects the heat flux in the heat exchanger, subsequently influencing the local air

temperature. Particularly, the local air temperature control and heat flux in the heat exchanger are more strongly affected by inlet fluid temperature than by the flow rate.

The second objective of this thesis was to evaluate the change in the periodic air temperature field characteristics of the serpentine copper tube heat exchanger. For this, the air temperature difference between the area below and the area above of the heat exchanger as well as the transition time were examined. The periodic air temperature change was evaluated at the inlet fluid temperatures of −5 and 50 ºC for all flow rates. The results showed that the air temperature difference between the areas below and above the heat exchanger of the cooling and heating processes is approximately 15 ºC. Increasing flow rate does not notably change the air temperature at the areas below of cooling and above of heating the heat exchanger. Larger flow rate of 0.9 L/min, the local air temperatures and air temperatures in the experimental system were not substantially changed. When the flow rate increases from 0.3 to 1.3 L/min, the quick change state and moderate change state from cooling to heating (heating transition) took approximately twenty minutes and two hours, respectively. On one hand, for heating to cooling process (cooling transition), the quick change state took around forty-nine minutes and the moderate change state took about one hour and forty minutes. When the flow rates were 1.5 to 3.0 L/min, the quick change state and moderate change state of heating transition took about eighteen minutes and one hour, respectively. On the other hand, quick change state and moderate change state of the cooling transition took approximately forty minutes and one hour, correspondingly. Regarding the transition time, the cooling transition seems to be more gradual compared to the heating transition, indicating that while the system heats up quickly, it cools down more slowly. The transition time reduces with flow rate increases. When the flow rate increases, the tube surface temperature becomes close to the value of inlet fluid temperature enhancing the heat exchange between the tube wall and surroundings.

The last objective was to estimate the energy requirements theoretically between the whole area and the local area control of practical greenhouse crop cultivation. Here the volume of the cultivation area per unit length was approximated from a practical greenhouse. The maximum system capacity requirement of the whole area control is around 62 W/m whereas that of the local area control is approximately 10 W/m which is more than 80% reduction compared to the whole area control. The total energy requirement of the whole area control was about 152 kJ/m. On the other hand, the total energy requirement of the local area control was approximately 37 kJ/m. The total energy requirement of the local area control was more than 70% reduced compared to that of the whole area control of practical greenhouse crop cultivation. This theoretical calculation is a simple and taking into some assumptions to show the advantage of the local climate control heat exchanger system.

This energy-saving method for periodic air temperature change with local climate control could be applied for crop cultivation in greenhouses.

Acknowledgements

First of all, I would like to express my deepest gratitude to Professor Dr. Naoki Maruyama for his guidance, suggestions, and support throughout this Ph.D. course. This work would not be possible without his consistent encouragement. It has been an honor to work with someone with such professionalism and personal skills. It has been an amazing experience during 3 years of study and I have learned a lot from him.

I am deeply indebted to Professor Dr. Masafumi Hirota, Department of Mechanical Engineering, Faculty of Engineering, Aichi Institute of Technology for his valuable suggestions while conducting experiments. His unassuming approach to research and engineering is a source of inspiration.

I am very grateful to Professor Dr. Takao Maeda of the Division of Mechanical Engineering, Graduate School of Engineering, Mie University for his kind support and valuable suggestions throughout my study which has significantly contributed to my academic.

I am also grateful to Professor Dr. Koichi Tsujimoto, and Professor Dr. Takane Terashima of the Division of Architecture, Graduate School of Engineering, Mie University for their constructive comments and suggestions, which have significantly improved the quality of this work. I would like to express my gratitude to Assistant Professor Dr. Chatchawan Chaichana, Faculty of Engineering Chiang Mai University, Thailand for being patient as well as for giving valuable suggestions while doing research.

Furthermore, I would like to acknowledge the financial support provided by JST SPRING, grant number JPMJSP2137.

I also would like to mention and thank the students from Thermal Energy Laboratory, Mie University who encouraged and helped me in one way or the other throughout the study, especially Jyoji Keeni, who assisted me with the Japanese language and helped me during the stay in Mie University.

I would like to express my deepest gratitude to my friend, Supasuta Leangpanich, for her unwavering support, encouragement, and invaluable insights throughout this journey. Thank you for encouraging me and staying beside me when I felt down. Your friendship has been a source of strength and inspiration.

Finally, I would like to express my warmest thanks to my family for being very supportive both morally and spiritually throughout this tough journey. My parents and my brother allowed me to study without any worries. I am forever indebted to you for your boundless love and the opportunities you created for me. This accomplishment is as much yours as it is mine. Your love, resilience, and faith in me have shaped who I am.

I would also like to offer my regards to all of those who supported me in any aspect of this journey. This accomplishment would not have been possible without all of them.

THIRI SHOON WAI

March, 2025

Table of contents

Abstract i
Acknowledgments iii
List of figures vii
List of tables xiii
Nomenclature xiv

1. Introduction

1.1 Research background and motivation 1
1.2 Literature reviews 2
1.2.1 Literature review on heat exchanger technologies applications 2
1.2.2 Literature review on the environmental control system for greenhouse cultivation 6
1.2.2.1 Cooling technologies in greenhouse cultivation 6
1.2.2.2 Heating technologies in greenhouse cultivation 17
1.2.3 Literature review of energy use in greenhouses in the European Union 19
1.3 Research objectives 24
1.4 Research scopes 24
1.5 Significance of research 25
1.6 Outline of the thesis 25
References in chapter 1 25

2. Principle and theories

2.1 Heat exchanger 32
2.1.1 Classification of heat exchangers 32
2.1.2 Heat transfer methods and basic heat transfer theory 34
2.1.3 Evaluation of heat exchanger 35
2.2 Fundamental of convection 36

2.3 Internal forced convection 36

2.3.1 Laminar and turbulent flow in tubes 36

2.3.2 Thermal analysis 37

2.3.3 Pressure drop 38

2.4 Natural convection 39

2.4.1 Physical mechanism of natural convection 40

2.4.2 Natural convection over surface 43

Summary 46

References in chapter 2 46

3. Research methodology

3.1 Overall experimental procedure 47

3.2 Overview concept of the experiment for temperature control in practical applications 48

3.3 Experiments in laboratory 49

3.3.1 Configuration of the heat exchanger 49

3.3.2 Experimental system set-up 49

3.3.3 Data acquisitions 50

3.3.4 Specifications of sensors and equipment 56

3.3.4.1 Temperature measurement 57

3.3.4.2 Pressure drop measurement 58

3.3.4.3 Volume flow rate monitoring 59

3.3.4.4 Relative humidity monitoring 61

3.4 Experimental conditions and procedure 63

References in chapter 3 66

4. Results and discussion

4.1 Local air temperature 67

4.1.1 Local air temperature profile (cooling) 68

4.1.2 Local air temperature profile (heating) 76

4.2 Heat flux in the heat exchanger 86

4.2.1 Fluid temperature difference and heat flux in the heat exchanger (cooling) 86

4.2.2 Fluid temperature difference and heat flux in the heat exchanger (heating) 87

4.3 Pressure drop in the heat exchanger 89

4.4 Periodic air temperature 89

4.5 Theoretical estimation of energy consumption 98

Summary 103

References in chapter 4 104

5. Conclusions 105

Appendix

List of publications

List of figures

Figures **Page**

Figure 1.1. Plain and different oval rib surface parabolic trough collector geometries 2
Figure 1.2. Obstacles mounted on absorber plate 3
Figure 1.3. Schematic diagram of double-dimpled corrugated pipe 4
Figure 1.4. Schematic diagram of different corrugated channels 4
Figure 1.5. Schematic diagrams of helically corrugated pipe 5
Figure 1.6. Isometric view of the helical pipe with different shapes of jackets 6
Figure 1.7. Different shapes of greenhouses 7
Figure 1.8. Sunrays fall on a East-West oriented greenhouse in a day: in the morning (left side), at noon (in center), in the evening (at right) 8
Figure 1.9. Photographs of the experimental greenhouses: (a) External view of fully removable and half removable back wall greenhouse 8
Figure 1.9. Photographs of the experimental greenhouses: (b) Greenhouse with a fully removable back wall 9
Figure 1.9. Photographs of the experimental greenhouses: (c) Greenhouse with a half removable back wall 9
Figure 1.10. A model polyethylene film for greenhouse covering 10
Figure 1.11. Schematic diagram for the greenhouse shaded at different locations: (a) Outside roof (black plastic net) 11
Figure 1.11. Schematic diagram for the greenhouse shaded at different locations: (b) Outside roof and side walls (black plastic net) 11
Figure 1.11. Schematic diagram for the greenhouse shaded at different locations: (c) Inside roof (white net and thermal screen) 11
Figure 1.11. Schematic diagram for the greenhouse shaded at different locations: (d) Inside roof (white net), side walls (black plastic net) 11
Figure 1.12. Layout of the experimental solar greenhouse system 12
Figure 1.13. Naturally ventilated greenhouse 13
Figure 1.14. Fan and pad evaporative cooling in greenhouse 13
Figure 1.15. Proposed liquid filter ceiling in greenhouse 14
Figure 1.16. Schematic diagram of the solar desiccant assisted distributed fan-pad ventilated greenhouse system 14
Figure 1.17. Heat exchange between tube air and soil 15
Figure 1.18. Earth air heat exchanger system and greenhouse 16
Figure 1.19. Air circulation in a closed-greenhouse 16

Figure 1.20. Active Solar Heating System and greenhouse: (a) Description of experimental greenhouse 17
Figure 1.20. Active Solar Heating System and greenhouse: (b) Functioning scheme of the Active Solar Heating System (ASHS) system 17
Figure 1.21. Root zone heating system: (a) Heating pot with a heating source 18
Figure 1.21. Root zone heating system: (b) Experimental heating system 18
Figure 1.22. Arch shed heat exchange tube in a greenhouse 18
Figure 1.23. Energy consumption in high energy intensity tomato greenhouse production in Spain (GJ/ha) 19
Figure 1.24. Energy consumption in high energy intensity greenhouse production in Greece (GJ/ha) 20
Figure 1.25. Energy consumption in low energy intensity greenhouse production in Greece (GJ/ha) 21
Figure 1.26. Energy consumption in low energy intensity greenhouse production in Italy (GJ/ha) 21
Figure 1.27. Energy consumption in German greenhouse sector (GJ/ha) 22
Figure 1.28. Energy inputs in high energy intensity tomato production systems (GJ/ha) 23
Figure 1.29. Energy inputs in low energy intensity tomato production systems (GJ/ha) 23
Figure 2.1. Related temperature profiles and different flow pattern in a double-pipe heat Exchanger (a) Parallel flow 33
Figure 2.1. Related temperature profiles and different flow pattern in a double-pipe heat Exchanger (b) Counter flow 33
Figure 2.2. Shell and tube heat exchanger (one-shell pass and one-tube pass) 33
Figure 2.3. A plate-and-frame liquid-to-liquid heat exchanger 34
Figure 2.4. Internal forced convection caused by a fan or pump 36
Figure 2.5. Heat transfer to a fluid flowing in a tube 37
Figure 2.6. Schematic diagram of pressure drop in a pipe 38
Figure 2.7. Cooling process of hot ball in cooler environment by natural convection 40
Figure 2.8. Buoyancy force keeps the ship floating in water ($W = F_{buoyancy}$ for floating objects) 41
Figure 2.9. The Grashof number is a measure of the relative magnitudes of the buoyancy force and the opposing viscous force acting on the fluid 42
Figure 2.10. Isotherms in natural convection over a hot plate in air 43
Figure 2.11. Typical temperature and velocity profiles for natural convection flow over a hot vertical plate 44
Figure 3.1. Methodological flow chart 47
Figure 3.2. Overview concept of periodic temperature control for cultivation: (a) Cooling 48
Figure 3.2. Overview concept of periodic temperature control for cultivation: (b) Heating 48
Figure 3.3. Serpentine copper tube heat exchanger (All units are in mm.) 49

Figure 3.4. Overall dimension of the experimental system 50
Figure 3.5. Schematic diagram of air temperature measurement are below and above the heat exchanger 51
Figure 3.6. Physical thermocouples setup and positioning at the area below and above the heat exchanger (a) Area below 51
Figure 3.6. Physical thermocouples setup and positioning at the area below and above the heat exchanger (b) Area above 51
Figure 3.7. Upper area and lower area air temperature measurement in the experimental system 52
Figure 3.8. Layout of the experimental system 53
Figure 3.9. Overall view of the experimental system including data loggers and chiller 53
Figure 3.10. Hioki 8422-50 data logger 54
Figure 3.11. GL840-WV midi logger 55
Figure 3.12. T-type thermocouple 57
Figure 3.13. Photos of resistance thermal detector: (a) Resistance thermal detector 57
Figure 3.13. Photos of resistance thermal detector: (b) Physical photo of inlet fluid temperature measurement 58
Figure 3.13. Photos of resistance thermal detector: (c) Physical photo of outlet fluid temperature measurement 58
Figure 3.14. GC 50 multifunctional digital differential pressure gauge 59
Figure 3.15. Flow meter sensor 60
Figure 3.16. Globe valve for controlling flow rate 60
Figure 3.17. Humidity sensors photo: (a) Humidity sensors in the area below 61
Figure 3.17. Humidity sensors photo: (b) Humidity sensors in the area above 61
Figure 3.18. NCC-3000 D chiller 62
Figure 4.1. Configuration for air temperature measurements in each layer around the heat exchanger 68
Figure 4.2. Air temperature contour of the area below and above the heat exchanger for all flow rates under steady state condition (cooling): (a) $\dot{V}$ = 0.3 L/min 69
Figure 4.2. Air temperature contour of the area below and above the heat exchanger for all flow rates under steady state condition (cooling): (b) $\dot{V}$ = 0.5 L/min 69
Figure 4.2. Air temperature contour of the area below and above the heat exchanger for all flow rates under steady state condition (cooling): (c) $\dot{V}$ = 0.7 L/min 70
Figure 4.2. Air temperature contour of the area below and above the heat exchanger for all flow rates under steady state condition (cooling): (d) $\dot{V}$ = 0.9 L/min 70
Figure 4.2. Air temperature contour of the area below and above the heat exchanger for all flow rates under steady state condition (cooling): (e) $\dot{V}$ = 1.1 L/min 71

Figure 4.2. Air temperature contour of the area below and above the heat exchanger for all flow rates under steady state condition (cooling): (f) $\dot{V}$ = 1.3 L/min 71
Figure 4.2. Air temperature contour of the area below and above the heat exchanger for all flow rates under steady state condition (cooling): (g) $\dot{V}$ = 1.5 L/min 72
Figure 4.2. Air temperature contour of the area below and above the heat exchanger for all flow rates under steady state condition (cooling): (h) $\dot{V}$ = 2.0 L/min 72
Figure 4.2. Air temperature contour of the area below and above the heat exchanger for all flow rates under steady state condition (cooling): (i) $\dot{V}$ = 2.5 L/min 73
Figure 4.2. Air temperature contour of the area below and above the heat exchanger for all flow rates under steady state condition (cooling): (j) $\dot{V}$ = 3.0 L/min 73
Figure 4.3. Average local air temperatures at all flow rates (cooling): (a) $\dot{V}$ = 0.3 L/min 74
Figure 4.3. Average local air temperatures at all flow rates (cooling): (b) $\dot{V}$ = 0.5 L/min 74
Figure 4.3. Average local air temperatures at all flow rates (cooling): (c) $\dot{V}$ = 0.7 L/min 75
Figure 4.3. Average local air temperatures at all flow rates (cooling): (d) $\dot{V}$ = 0.9 L/min 75
Figure 4.3. Average local air temperatures at all flow rates (cooling): (e) $\dot{V}$ = 1.1 L/min 75
Figure 4.3. Average local air temperatures at all flow rates (cooling): (f) $\dot{V}$ = 1.3 L/min 75
Figure 4.3. Average local air temperatures at all flow rates (cooling): (g) $\dot{V}$ = 1.5 L/min 75
Figure 4.3. Average local air temperatures at all flow rates (cooling): (h) $\dot{V}$ = 2.0 L/min 75
Figure 4.3. Average local air temperatures at all flow rates (cooling): (i) $\dot{V}$ = 2.5 L/min 75
Figure 4.3. Average local air temperatures at all flow rates (cooling): (j) $\dot{V}$ = 3.0 L/min 75
Figure 4.4. Air temperature contour of the area below and above the heat exchanger for all flow rates under steady state condition (heating): (a) $\dot{V}$ = 0.3 L/min 77
Figure 4.4. Air temperature contour of the area below and above the heat exchanger for all flow rates under steady state condition (heating): (b) $\dot{V}$ = 0.5 L/min 77
Figure 4.4. Air temperature contour of the area below and above the heat exchanger for all flow rates under steady state condition (heating): (c) $\dot{V}$ = 0.7 L/min 78
Figure 4.4. Air temperature contour of the area below and above the heat exchanger for all flow rates under steady state condition (heating): (d) $\dot{V}$ = 0.9 L/min 78
Figure 4.4. Air temperature contour of the area below and above the heat exchanger for all flow rates under steady state condition (heating): (e) $\dot{V}$ = 1.1 L/min 79
Figure 4.4. Air temperature contour of the area below and above the heat exchanger for all flow rates under steady state condition (heating): (f) $\dot{V}$ = 1.3 L/min 79
Figure 4.4. Air temperature contour of the area below and above the heat exchanger for all flow rates under steady state condition (heating): (g) $\dot{V}$ = 1.5 L/min 80

Figure 4.4. Air temperature contour of the area below and above the heat exchanger for all flow rates under steady state condition (heating): (h) $\dot{V}$ = 2.0 L/min 80
Figure 4.4. Air temperature contour of the area below and above the heat exchanger for all flow rates under steady state condition (heating): (i) $\dot{V}$ = 2.5 L/min 81
Figure 4.4. Air temperature contour of the area below and above the heat exchanger for all flow rates under steady state condition (heating): (j) $\dot{V}$ = 3.0 L/min 81
Figure 4.5. Average local air temperatures at all flow rates (heating): (a) $\dot{V}$ = 0.3 L/min 82
Figure 4.5. Average local air temperatures at all flow rates (heating): (b) $\dot{V}$ = 0.5 L/min 82
Figure 4.5. Average local air temperatures at all flow rates (heating): (c) $\dot{V}$ = 0.7 L/min 82
Figure 4.5. Average local air temperatures at all flow rates (heating): (d) $\dot{V}$ = 0.9 L/min 82
Figure 4.5. Average local air temperatures at all flow rates (heating): (e) $\dot{V}$ = 1.1 L/min 83
Figure 4.5. Average local air temperatures at all flow rates (heating): (f) $\dot{V}$ = 1.3 L/min 83
Figure 4.5. Average local air temperatures at all flow rates (heating): (g) $\dot{V}$ = 1.5 L/min 83
Figure 4.5. Average local air temperatures at all flow rates (heating): (h) $\dot{V}$ = 2.0 L/min 83
Figure 4.5. Average local air temperatures at all flow rates (heating): (i) $\dot{V}$ = 2.5 L/min 83
Figure 4.5. Average local air temperatures at all flow rates (heating): (j) $\dot{V}$ = 3.0 L/min 83
Figure 4.6. External convective heat transfer coefficient with different flow rates for all inlet fluid temperatures 84
Figure 4.7. Internal convective heat transfer coefficient with different flow rates for all inlet fluid temperatures 85
Figure 4.8. Fluid temperature difference and heat flux for all conditions (cooling) 87
Figure 4.9. Fluid temperature difference and heat flux for all conditions (heating) 88
Figure 4.10. Pressure drop in the heat exchanger under cooling and heating conditions 89
Figure 4.11. Experimental system enclosed with polyvinyl chloride transparent film 90
Figure 4.12. Schematic diagram of showing duration of time for transition 90
Figure 4.13. Periodic air temperature changes for conditions of T_{inlet}= −5 and 50 ºC with all flow rates: (a) $\dot{V}$ = 0.3 L/min 92
Figure 4.13. Periodic air temperature changes for conditions of T_{inlet}= −5 and 50 ºC with all flow rates: (b) $\dot{V}$ = 0.5 L/min 93
Figure 4.13. Periodic air temperature changes for conditions of T_{inlet}= −5 and 50 ºC with all flow rates: (c) $\dot{V}$ = 0.7 L/min 93
Figure 4.13. Periodic air temperature changes for conditions of T_{inlet}= −5 and 50 ºC with all flow rates: (d) $\dot{V}$ = 0.9 L/min 94
Figure 4.13. Periodic air temperature changes for conditions of T_{inlet}= −5 and 50 ºC with all flow rates: (e) $\dot{V}$ = 1.1 L/min 94

Figure 4.13. Periodic air temperature changes for conditions of T_{inlet}= −5 and 50 ºC with all flow rates: (f) $\dot{V}$ = 1.3 L/min 95
Figure 4.13. Periodic air temperature changes for conditions of T_{inlet}= −5 and 50 ºC with all flow rates: (g) $\dot{V}$ = 1.5 L/min 95
Figure 4.13. Periodic air temperature changes for conditions of T_{inlet}= −5 and 50 ºC with all flow rates: (h) $\dot{V}$ = 2.0 L/min 96
Figure 4.13. Periodic air temperature changes for conditions of T_{inlet}= −5 and 50 ºC with all flow rates: (i) $\dot{V}$ = 2.5 L/min 96
Figure 4.13. Periodic air temperature changes for conditions of T_{inlet}= −5 and 50 ºC with all flow rates: (j) $\dot{V}$ = 3.0 L/min 97
Figure 4.14. The schematic structure of the greenhouse with whole area control 98
Figure 4.15. Photo of the strawberry crop rows in greenhouse 99
Figure 4.16. The schematic structure of the greenhouse with local area control 99

List of tables

Tables **Page**

Table 2.1. Empirical correlations for the average Nusselt number for natural convection over surfaces 45
Table 3.1. Specifications of Hioki 8422-50 data logger 54
Table 3.2. Specifications of the GL 840 data logger 55
Table 3.3. Specifications of the measuring devices 56
Table 3.4. General specifications of resistance thermal detector 58
Table 3.5. Specifications of GC 50 multifunctional digital differential pressure gauge 59
Table 3.6. Specifications of flow meter sensor 60
Table 3.7. Specifications of the humidity sensors 62
Table 3.8. Specifications of NCC-3000 D chiller 63
Table 3.9. Experimental conditions: (a) Cooling conditions 64
Table 3.9. Experimental conditions: (b) Heating conditions 64
Table 4.1. The characteristic of periodic air temperature change 97
Table 4.2. Calculation of heating and cooling amount and energy requirements of the different states for the whole area and local area control in greenhouse cultivation ($\dot{V}$ = 0.9 L/min) 101
Table 4.3. Maximum system capacity and total energy requirements for the whole and local area control for greenhouse cultivation 103

Nomenclature

A	area of the below and above the heat exchanger for cooling and heating, respectively, m^2
A_s	outer surface area of the copper tube except U-bends, m^2
A_t	heat transfer surface area, m^2
c_p	specific heat of the fluid, kJ/(kg·K)
c_{pa}	specific heat capacity of air at certain temperature, kJ/(kg·K)
c_{pf}	specific heat of the fluid, J/(kg·K)
c_{pl}	specific heat of liquid at the average film temperature, kJ/(kg·K)
d_{inner}	inner diameter, m
D	diameter, m
E	energy requirements, kJ/m
f	friction factor
$F_{buoyancy}$	buoyancy force, N
g	gravitational acceleration, m/s^2
Gr	Grashof number
h	convection heat transfer coefficient, $W/(m^2 \cdot K)$
h_a	external convective heat transfer coefficient, $W/(m^2 \cdot K)$
h_f	internal convective heat transfer coefficient, $W/(m^2 \cdot K)$
h_L	head loss, m
k	thermal conductivity of air at film temperature, W/(m·K)
k_{air}	thermal conductivity of air at a certain air temperature, W/(m·K)
k_f	thermal conductivity of working fluid, W/(m·K)
k_l	thermal conductivity of liquid, W/(m·K)
K	coefficient of performance, (dimensionless)
L_c	characteristic length, m
$\dot{m}$	mass flow, kg/s
Nu	Nusselt number of natural convection , dimensionless
Nu_i	Nusselt number of internal force convection, dimensionless
p	perimeter, m
P	heat amount to be removed/added with unit length including transition time, kW/m
P_1	pressure at the inlet tube, kPa
P_2	pressure at the outlet tube, kPa
ΔP	pressure drop, kPa
Pr	Prandtl number, dimensionless
$\dot{q}_a$	heat flux in the heat exchanger, W/m^2

$\dot{q}_s$	constant surface heat flux, W
Q	heat amount to be removed/added with unit length, kJ/m
Q_{loss}	heat diffusion from the local area to the nearby surroundings, W
$\dot{Q}_{conv}$	convective heat transfer, W
$\dot{Q}_{total}$	rate of the total heat loss, W
R	radius, m
Ra_L	Rayleigh number, dimensionless
Re	Reynolds number, dimensionless
S	system capacity, kW/m
T_e	average temperature at the exit, °C
T_i	average temperature at the inlet, °C
T_{inlet}	inlet fluid temperature, °C
T_l	local air temperature, °C
T_{l,avg_ab}	average local air temperature of the area above the heat exchanger, °C
T_{l,avg_be}	average local air temperature of the area below the heat exchanger, °C
T_{outlet}	outlet water temperature, °C
T_{room}	room air temperature, °C
T_s	surface temperature, °C
T_∞	temperature of the fluid sufficiently far from the surface, °C
ΔT	air temperature difference between two vertical layers of the heat exchanger, °C
ΔT_a	air temperature difference, °C
ΔT_f	absolute fluid temperature difference in the heat exchanger = $\lvert T_{outlet} - T_{inlet} \rvert$, °C
V	volume of the whole greenhouse or local area greenhouse, m^3/m
$\dot{V}$	volume flow rate, m^3/s
V_{avg}	average velocity for incompressible flow in a circular pipe, m/s
V_{body}	volume of the portion of the body immersed in the fluid, m^3
v	kinematic viscosity of the fluid, m^2/s
$\dot{W}_{pump,L}$	pumping power to overcome the pressure loss, W
Δz	vertical distance, m

Greek letters

β	coefficient of volume expansion, 1/K
μ	dynamic viscosity, Pa·s
μ_l	dynamic viscosity of liquid, Pa·s
ρ_a	density of air, kg/m^3
ρ_{body}	density of the body, kg/m^3

ρ_{fluid}	density of the fluid, kg/m^3
ρ_l	density of liquid, kg/m^3
τ	time, hour
τ_1	quick change state (heating transition), minute, hour
τ_2	moderate change state (heating transition), minute, hour
τ_3	steady state (heating transition), minute, hour
τ_4	quick change state (cooling transition), minute, hour
τ_5	moderate change state (cooling transition), minute, hour
τ_6	steady state (cooling transition), minute, hour
τ_w	shear stress, N/m^2
v	flow velocity, m/s

Abbreviations

ASHS	active solar heating system
COP	coefficient of performance, dimensionless
RH	relative humidity, %

Subscript

a	air
ab	above
avg	average
be	below
c	cold fluid
h	hot fluid
i	inside
f	fluid
l	local

Chapter 1

Introduction

1.1 Research background and motivation

With the economic growth of developing countries, there is a need for improvements in the quantity and quality of food products in the control agricultural section. Control cultivations like greenhouse and plant factory are becoming increasingly common all over the world because the desirable environment (air temperature and relative humidity) is controllable using a greenhouse cultivation system [1,2]. Cooling/heating systems are employed in greenhouse cultivation to provide uniform environmental control throughout greenhouse areas of crop cultivation [3–6]. Thus, the control agriculture is one of the promising methods to secure food products and avoid adverse weather conditions. Moreover, the benefits include off-seasons growing, high yield, and quality of crops. The main drawback of control greenhouse agriculture is the high use of energy from the environmental controlling system compared to traditional cultivation in the outdoor environment [7,8].

Several types of heat exchangers are available, each with its own advantages and disadvantages. Commonly used heat exchangers include shell-and-tube and fin-and-tube exchangers [9–12]. Fin-and-tube heat exchangers are known for their excellent thermal performance [13–17]. However, fins can accumulate dirt in humid areas in addition to debris, leading to difficulties in maintenance. Additionally, the fin-and-tube heat exchanger creates shade, which may inhibit plant growth. Therefore, different types of heat exchangers are required for different applications. Among them, serpentine coils are the smallest and most adaptable heat exchangers available for cooling/heating and refrigerant evaporator/condenser applications for an agricultural field. Serpentine heat exchangers are inexpensive and are widely used because of their compactness [18].

This study targeted strawberries crop, because they require daytime and nighttime temperature differences almost every day. Frequent cooling and heating are necessary to obtain high-quality strawberries [19–22].

Generally, greenhouses and plant factories require a suitable constant temperature setting for a certain time. Periodic air temperature control is essential for greenhouse cultivation. As mentioned previously, the periodic temperature control of the entire facility results in substantial energy consumption. Plants are generally not affected by environments that are far from them. Thus, the novelty of this study is to provide local climate control only near the plant area with periodic air temperature control. The surrounding air temperature far from the plants remains steady. Moreover, this local climate control can reduce energy consumption because the climate is controlled only near the crop area.

To provide climate control near the crop area, copper tubes are arranged in a simple serpentine shape, serving as a heat exchanger. Furthermore, the shape of a serpentine copper tube is selected because it does not considerably prevent sunlight and will be suitable in humid areas. In addition, the serpentine heat exchanger is compact and easy to handle. Studies addressing the use of serpentine copper tube heat exchangers for

greenhouse cultivation are currently limited. Researchers have explored investigating diverse greenhouse designs, and heating and cooling systems as parameters to obtain high thermal efficiency to control the entire greenhouse area. However, in greenhouse cultivation, a crucial research gap exists in exploring climate control only near the plants. Therefore, a novel approach, which is local climate control, needs to be thoroughly studied.

This thesis aims to address the change of periodic air temperature field near the strawberry crops using energy-saving method. To save energy requirements, a simple serpentine copper tube shape is introduced to use as a heat exchanger near the crops area. Periodic air temperature indicates that air temperature control is alternating (cooling and heating) to create a desirable climate near the crops. Moreover, this local climate control will be applicable in both temperate and tropical regions. This study was conducted in a laboratory. The experimental system was constructed under with the assumption that a part of actual plant cultivation was being left out.

1.2 Literature reviews

The literature review of previous studies concerning with heat exchanger technologies applications, and the environmental control systems in greenhouse cultivations such as cooling and heating systems are described detailed in below.

1.2.1 Literature review on heat exchanger technologies applications

Heat exchangers are designed to exchange heat between media. They are widely used in several industrial applications ranging from power plants to heating, ventilation, and air-conditioning refrigeration [23–26]. They are typically installed as air-conditioning components in various cooling and heating systems.

Numerous studies and research have been conducted to develop and enhance heat exchanger technologies, aiming to improve performance, energy efficiency, and reliability [27]. A. Kumar et al. [28] focus on improving the efficiency of parabolic trough solar collectors equipped with oval ribbed receiver tube using TiO_2/water nanofluid. Oval ribs are symmetrically positioned on the inner surface of the receiver tube as shown in Fig. 1.1. They found that parameters such as relative major diameter ratio, relative minimum diameter ratio, and relative spanwise and streamwise hydraulic diameter ratios will lead to enhanced heat transfer performance.

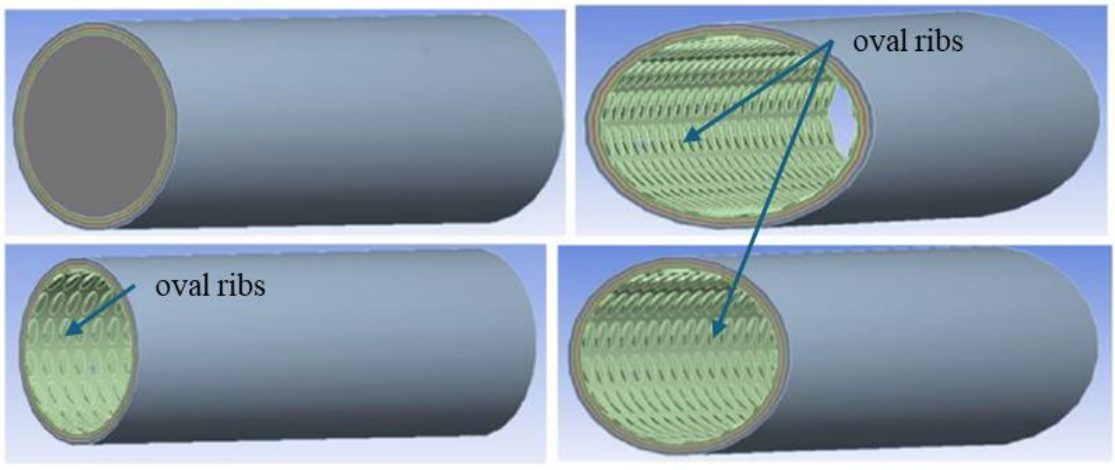

Figure 1.1. Plain and different oval rib surface parabolic trough collector geometries [28].

R. Kant et al. [29] explored enhancing heat transfer in solar air heaters using triangular winglet obstacles with sharp corners as depicted in Fig. 1.2. They used four types of triangular winglet configurations as obstacles such as single, dual, triple, and quadruple triangular winglets. Different obstacle configurations impact heat transfer and friction factors in the system. Their outcomes showed that Nusselt number increases up to 3.85 with the triple triangular winglet obstacle configuration, resulting in improving heat transfer efficiency.

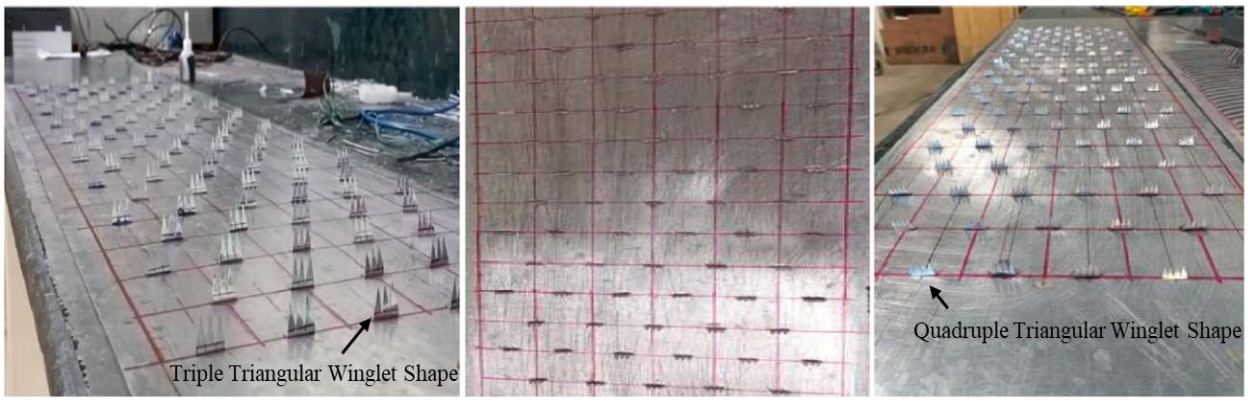

Figure 1.2. Obstacles mounted on absorber plate [29].

Nanofluids enhance heat transfer in various aspects of applications through improved properties [30]. S. Salehin et al. [31] emphasized the use of nanofluid in solar energy systems, such as solar thermal collectors and solar water heaters, to improve solar to thermal energy conversion efficiency.

F. Ahmad et al. [32] examined the influence of nanofluids in spherical double-dimpled surfaces on heat transfer and pressure drop characteristics. To assess the heat transfer performance, both single and hybrid nanofluids in terms of varying Reynolds numbers and nanoparticle volume concentrations in a double-dimpled pipe were analyzed using computational methods. Assuming a constant and uniform heat flux of 10,000 W/m^2 as shown in Fig. 1.3, the numerical simulations are conducted at Reynolds numbers ranging from 10,000 to 30,000. Their result showed that double-dimpled surface tubes had 20–25% higher heat transfer coefficient compared to smooth tubes.

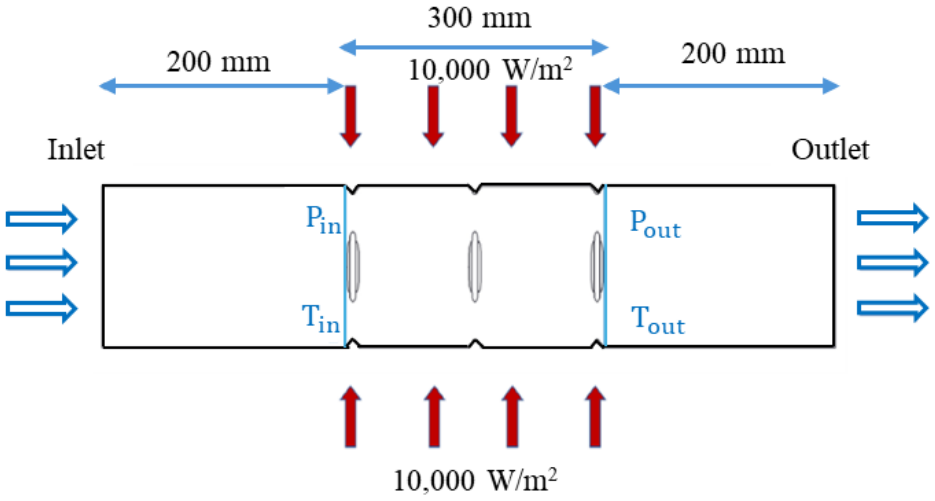

Figure 1.3. Schematic diagram of double-dimpled corrugated pipe [32].

R. Ahamed et al. [33] conducted a numerical investigation of a curved trapezoidal-corrugated channel with E-shaped baffles for thermal-hydraulic performance and flow behavior involving the use of single and hybrid nanofluids. Their results demonstrate that the effects of baffles and corrugations can result in the creation of vortex flow and greater turbulence, which promote the heat transfer enhancement.

F. Ahmad et al. [34] investigated the impact of different corrugation patterns on heat transfer and nanofluids performance in mini channels, focusing on single-phase turbulent flow. Corrugated mini channels have the following structural properties: The dimensions specified are a 500 mm long channel, a 25 mm wavelength of the corrugation, and a 2 mm thick wall as shown in Fig. 1.4. Their results stated that various nanoparticle compositions exhibited a 25–30% increased heat transfer coefficient.

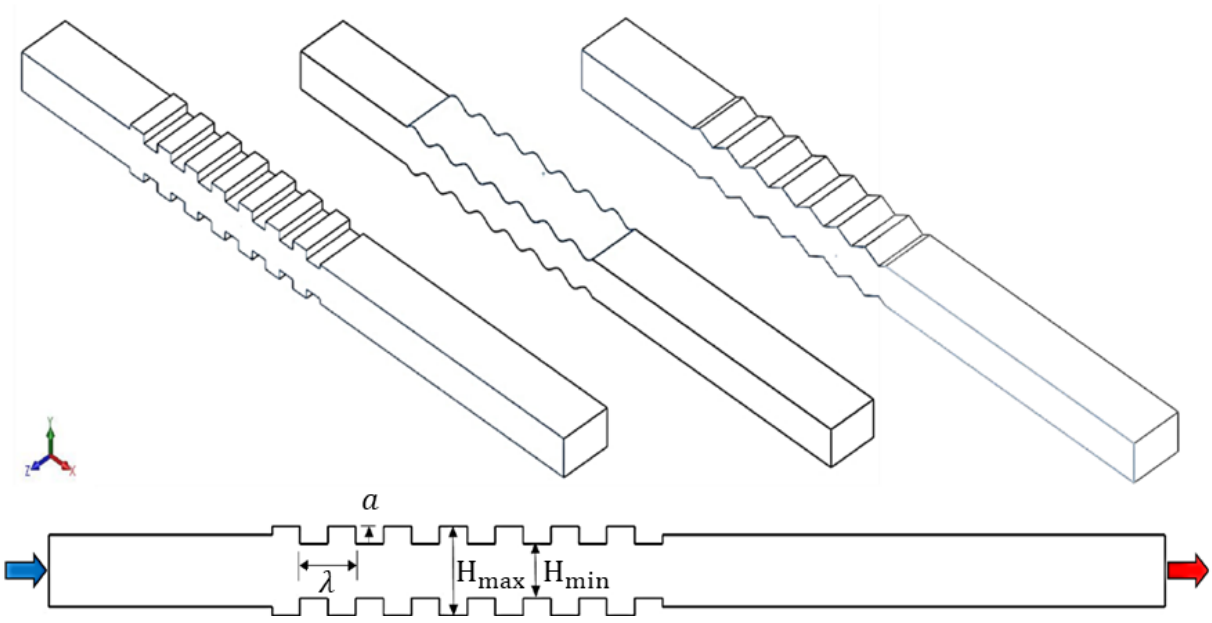

Figure 1.4. Schematic diagram of different corrugated channels [34].

A. Mustakim et al. [35] evaluated the thermo-hydrodynamic performance of single and hybrid nanofluids in a helically featured straight pipe, considering different Reynolds numbers and nanoparticle concentrations. With dimensional modifications, such as helical corrugation pitch (P) and height (e) at the inlet, different case studies were performed for comparison in heat exchanger performance. The schematic diagram of helically corrugated pipe is shown in Fig. 1.5. The simulations were conducted using the ANalysis SYStem (ANSYS) commercial program, employing the Realizable k-epsilon turbulence model. The results showcased that the smallest corrugation pitch notably increased performance.

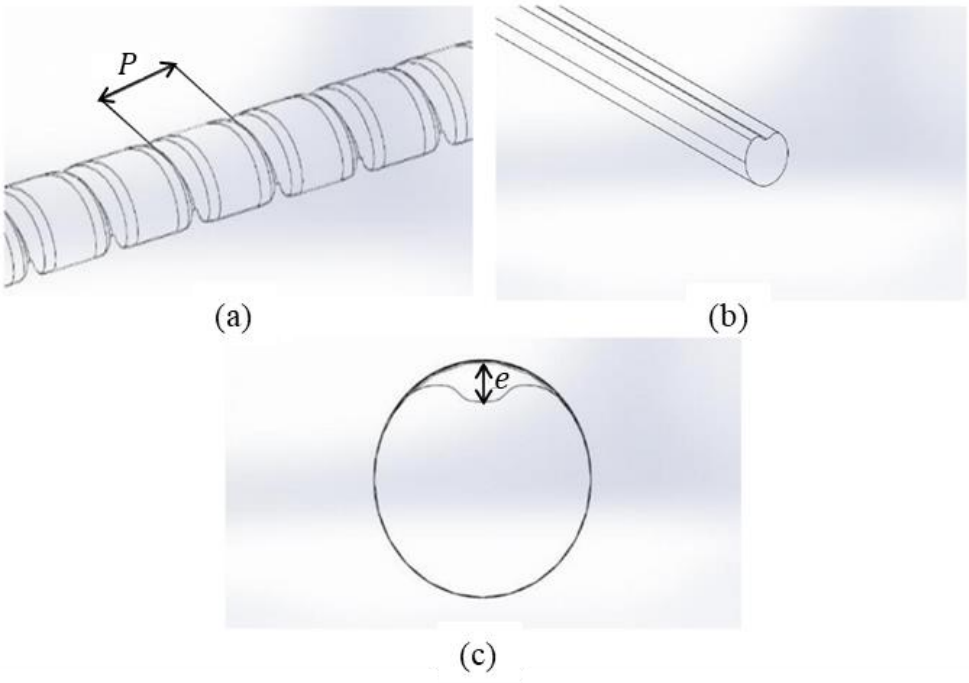

Figure 1.5. Schematic diagrams of helically corrugated pipe [35].

S.M.N.U. Islam et al. [36] simulated characterizing the thermos-hydraulic performance of nanofluids and hybrid nanofluids in helical pipes with various jacket shapes. Three jacket shapes (circular, square, and triangle) were used in this study are as shown in Fig. 1.6. A computational framework was employed to analyze turbulent flow in three dimensional helical pipes with Reynolds numbers ranging from 5,000 to 30,000 and a constant heat flux of 1,000 W/m^2. The results showed that using different nanofluids significantly improves the Nusselt number value and heat transfer coefficients, from 36 % to 60 % compared to water in a smooth coiled pipe.

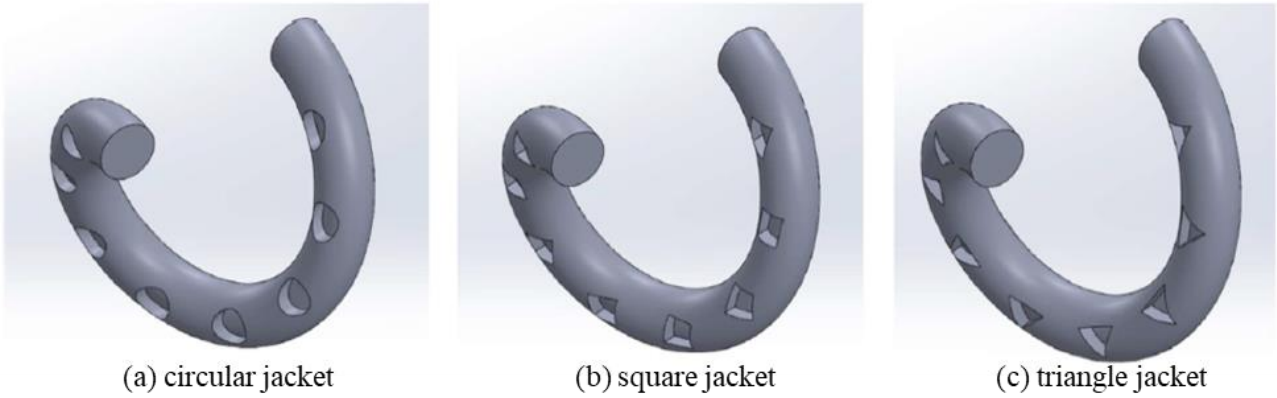

Figure 1.6. Isometric view of the helical pipe with different shapes of jackets [36].

Furthermore, M. Awais et al. [37] evaluated thermo-hydraulic performance of a serpentine tube heat exchanger using computational fluid dynamics to optimize heat transfer and pressure drop. The results showed that low-to-high serpentine tube provided higher heat transfer performance than the other cases.

All the above studies highlighted heat transfer enhancement of the heat exchangers using nanofluids and improving the shape of the heat transfer surface area. This indicates that innovative heat exchanger technologies are increasingly popular in many industrial applications.

1.2.2 Literature review on the environmental control system for greenhouse cultivation

Maintaining optimal environmental conditions within greenhouses is crucial for successful crop cultivation. Cooling/heating systems play a key role in greenhouse cultivation to create a favorable environment for crop cultivation.

One of the primary challenges in greenhouse cultivation is regulating the air temperature. In cool regions, heating the greenhouse air is a well-established and straightforward process. However, in hot and sunny regions, cooling the greenhouse air is a more complex task, as the available cooling technologies are still limited compared to heating systems. Additionally, cooling systems are generally more expensive to install and operate than heating systems. However, both the cooling and heating systems' high energy consumption is still an issue in greenhouse cultivation compared to open-field agriculture.

1.2.2.1 Cooling technologies in greenhouse cultivation

The cooling technologies inside the greenhouse plantation are usually necessary for tropical and subtropical regions as the weather is usually warm throughout the year. The cooling in greenhouse cultivaiton can be classified into two main categories: passive and active systems. Passive systems include greenhouse orientation and shape, shading systems, and natural ventilation to reduce the temperature inside the greenhouse without consuming additional water or power. Furthermore, the active systems such as evaporative cooling and earth-air heat exchanger systems where electricity is required to operate pumps, fans or heat pumps.

Several design features strongly contribute to the decrease in the cooling requirements, namely, the orientation and shape, covering materials and shading sytems in the greenhouse [38]. The structural layout of

greenhouses consists of typical frames with different kinds of shapes [39]. The most common shapes of the greenhouses are gabic even/uneven span, modiefied quonsent, quonset, and modified arch shapes as shown in Fig. 1.7. According to Choab et al. [40] and Sethi [41], independently of the considered location, the quonset form corresponds to the minimal values of the temperature and solar collection, as opposed to the uneven-span shape, which allows for maximum solar capture, as well as high heat records. As for the orientation, it is concluded in many comparative studies that the East–West (E–W) orientation is more convenient at all latitudes, except near the equator, where summer is weakly insolated compared to winter.

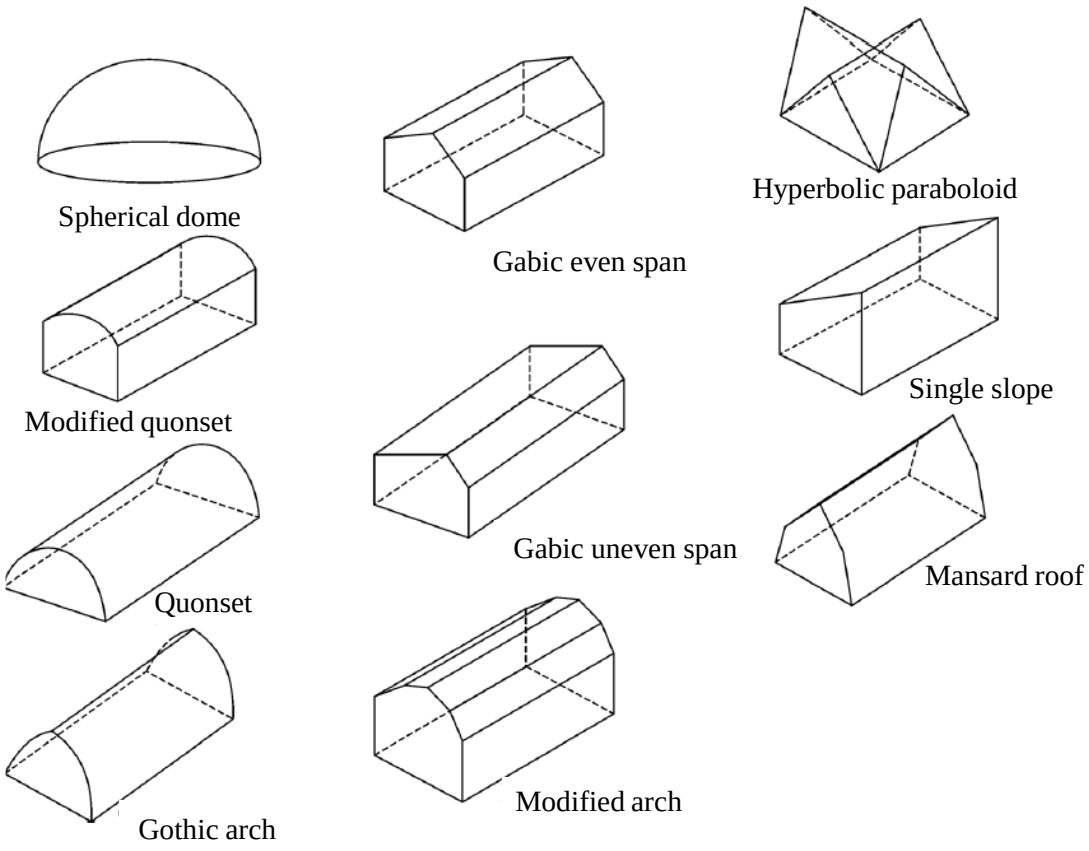

Figure 1.7. Different shapes of greenhouses [38].

Stanciu et.al [42] studied the effect of the greenhouse orientation, with respect to the E–W axis, on its required heating and cooling loads for an even-span greenhouse of 180 m2 at 44.25 ºN latitude as shown in Fig.1.8. They found that, for the E–W orientation, the cooling and heating requirements were reduced by 125 kWh/day in June, and by 87 kWh/day in January, respectively. These energy savings for the E–W orientation, with respect to North- South axis, in both the summer and winter periods, has been confirmed by previous studies [43,44].

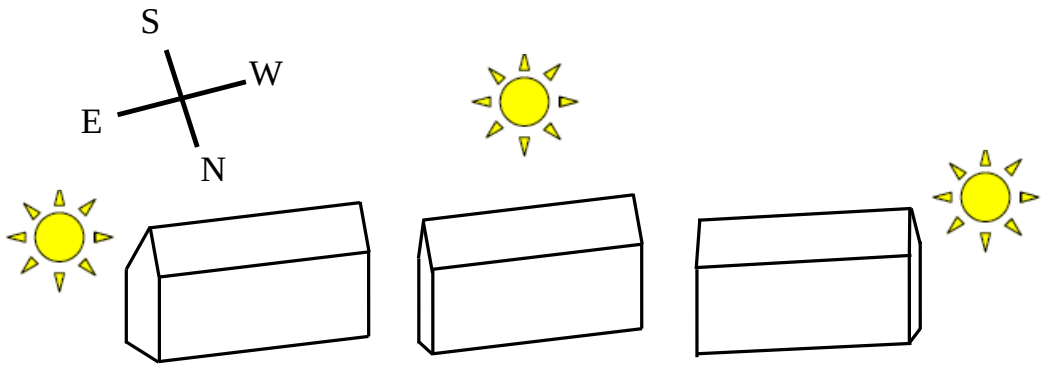

Figure 1.8. Sunrays fall on a East-West oriented greenhouse in a day: in the morning (left side), at noon (in center), in the evening (at right) [42].

On the other hand, specific covering materials can also provide the appropriate shading/reflection effect, namely, colored plastic films and near infrared radiation (NIR) filtering plastic films [45]. The selection of the appropriate covering material is realized on the basis of the amount of intercepted radiation, as well as crop types. The minimum transmissivity of the covering material was around 0.7 [46].

B. Wei et.al [47] investigated two types of greenhouses with removable back walls that are suitable for the climate in southern Jiangsu province, China to improve the thermal performance of conventional single-span greenhouses as shown in Fig. 1.9 (a). One type of the greenhouse with a fully removable back wall and one with a half-removable back wall as shown in Figs. 1.9 (b) and (c). Their results suggested that the air temperature inside the greenhouse is lowered by 5 ºC, and the energy requirements for cooling are reduced by 8%.

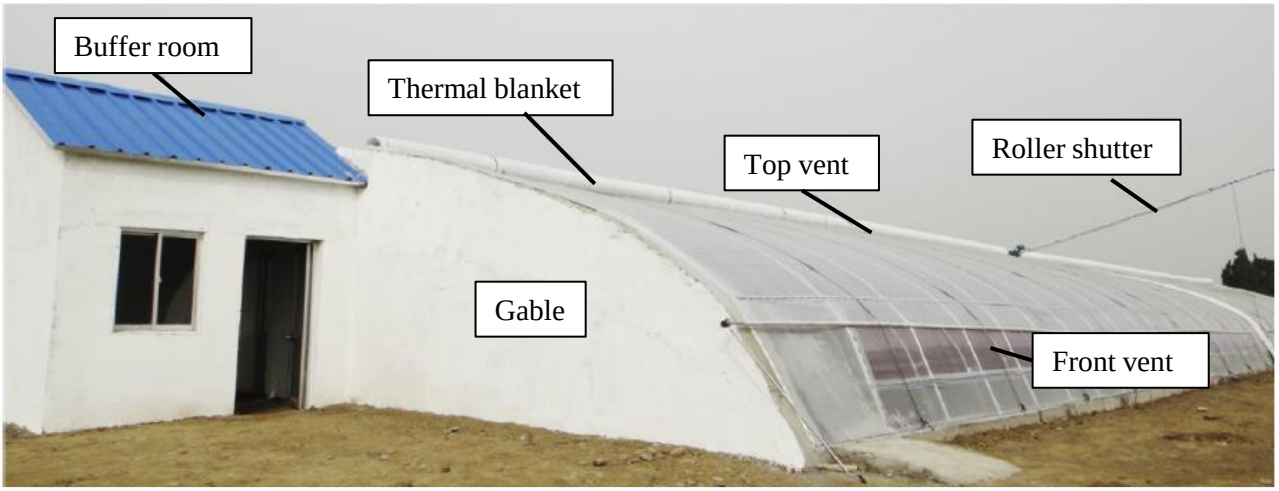

(a) External view of fully removable and half removable back wall greenhouse

(b) Greenhouse with a fully removable back wall

(c) Greenhouse with a half removable back wall

Figure 1.9 Photographs of the experimental greenhouses [47].

Near infrared radiation (NIR) filtering films are recommended for harsh climates since they reflect the near infrared radiation without affecting the crop photosynthesis or the plant growth. A. M. Abdel-Ghany et al.[48] reviewed the advantages of greenhouse covers that incorporate NIR reflectors. The most important characteristics of greenhouse covering films are ability to provide cooling, high mechanical strength, and durability against photodegradation. A model of such a film covering is shown in Fig. 1.10. Their survey focused on how the cover type affects the transmittance of photosynthetically active radiation, the reflectance or absorptance of NIR, and the greenhouse air temperature. NIR-reflecting plastic films seem to be the most suitable, low cost and simple cover for greenhouses under arid conditions. They concluded that NIR-reflecting covers are able to reduce greenhouse air temperature by no more than 5◦C. This reduction is not enough in regions where the ambient temperature may exceed 45 ºC in summer. C. Stanghellini et al. [49] investigated the effect of NIR-reflective screen material on ventilation requirement, crop transpiration and water use efficiency of a greenhouse rose crop in an experiment whereby identical climate was ensured in greenhouse

compartments installed with either NIR-reflective or conventional material as internal movable screens. They pointed out that the NIR-filter reduced the energy load of the greenhouse by 8%.

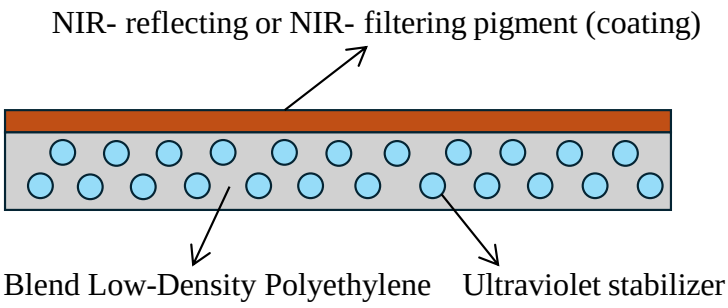

Figure 1.10. A model polyethylene film for greenhouse covering [48].

Shading and reflection are the basic concepts in the reduction and avoidance of intense solar radiation, and they therefore reduce the cooling requirements. Several shading methods have been used and investigated, such as roof shading, external shading, and different material shading nets.

A. Baille [50] studied the influence of whitening a greenhouse roof on microclimate and canopy behaviour during summer in a greenhouse located in the coastal area of eastern Greece. They measured the microclimate variables such as intercepted net radiation, canopy temperature and canopy transpiration rate of a well-watered soilless rose canopy over several days before and after roof whitening. They stated that whitening reduced the average glasshouse transmission coefficient for solar radiation from 0.62 to 0.31. As a consequence, air temperature, vapour pressure deficit and canopy-to-air temperature difference experienced drastic changes while transpiration rate was not strongly affected, being slightly higher (about 18%) after whitening.

A M. Abdel-Ghany et al.[51] evaluated the effect of different shading configurations on the solar and thermal radiation in a greenhouse. Nets at four different locations were employed to shade the roof and side-walls of a polycarbonate, mechanically ventilated greenhouse as shown in Fig. 1.11. The net solar and thermal radiations and air temperature were measured outside and inside two identical shaded and unshaded greenhouses. One greenhouse

was kept without shading and the other was shaded using five different configurations: (1) horizontally above the roof using a black plastic net of 250 μm thickness and 30% porosity; (2) horizontally above the roof using the black plastic net and vertically inside the side-walls using the black plastic net; (3) horizontally below the roof using a white plastic net of 185 μm thickness and 50% porosity; (4) horizontally below the roof using a thermal screen of 183 μm thickness and 15% porosity; (4) horizontally below the roof using the white plastic net and vertically, inside the side-walls, using the black plastic net as shown in Figs. 1.11 (a) – (d). They carried out the experiments on clear sunny days in the period from 18 to 26 December 2014. Their results showed that external roof-shading is desirable, as it reduced the generated thermal radiation in the greenhouse by 21% and 15% during the day and night time, respectively and reduced the greenhouse air temperature during the day.

The internal shading (roof and side walls) is undesirable, since it drastically increased the generated thermal radiation in the greenhouse by 147% and strongly increased the greenhouse air temperature during the day. Shading the side-walls is not recommended because it significantly reduces the transmitted solar radiation in the morning and afternoon (when the outside irradiance is low) and is useless at around noon when the outside irradiance is extremely high. It was proven that external shading is more effective in radiation control than under-roof and side-wall placements.

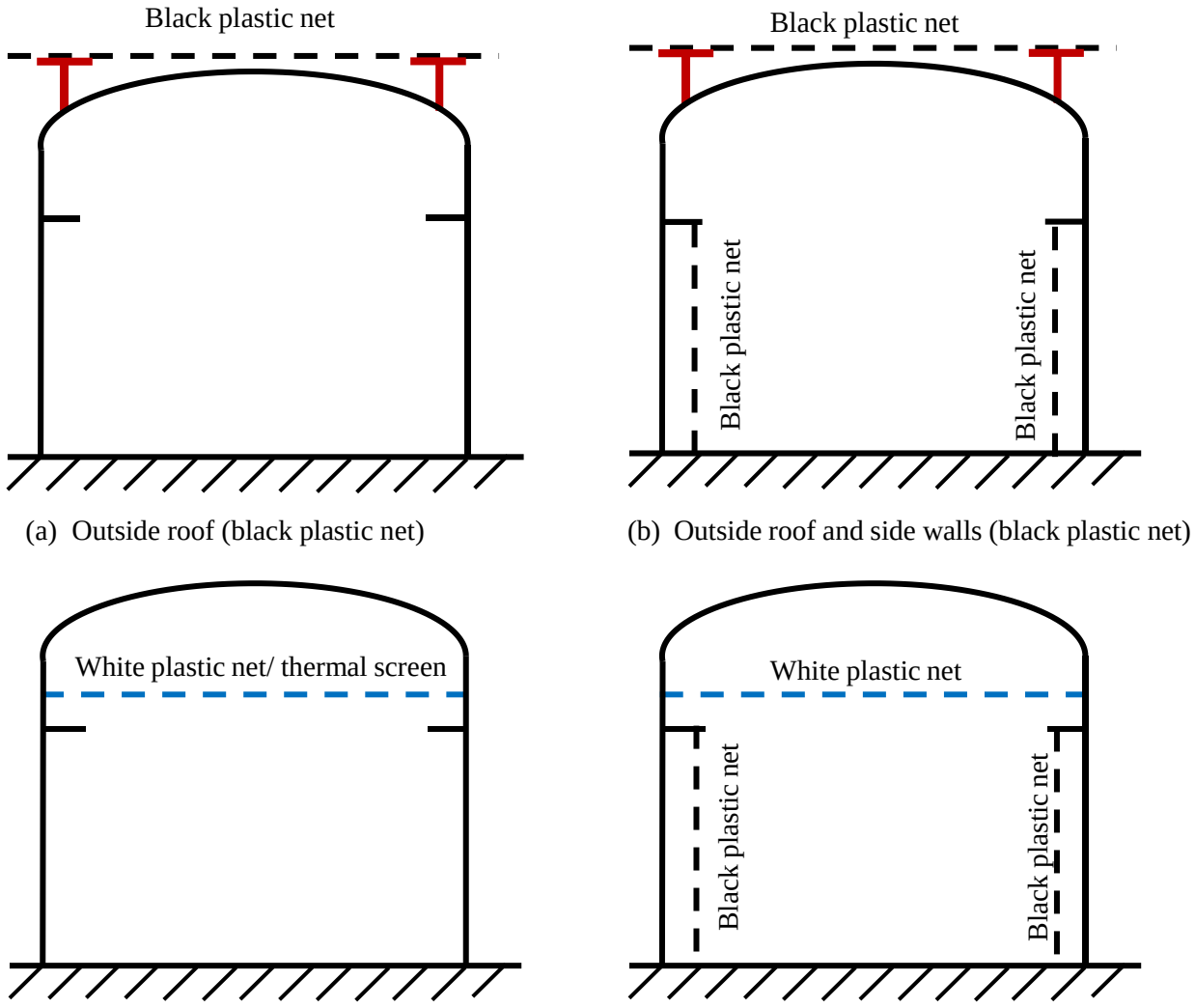

(a) Outside roof (black plastic net)

(b) Outside roof and side walls (black plastic net)

(c) Inside roof (white net and thermal screen)

(d) Inside roof (white net), side walls (black plastic net)

Figure 1.11. Schematic diagram for the greenhouse shaded at different locations [51].

Y. Tang et al. [52] assessed the impact of differences in both temperature and light factors caused by opaque photovoltaic modules and solar heating on strawberry growth and quality in a constructed greenhouse. A solar greenhouse with opaque photovoltaic modules and a solar combined air source heat pump system was built for strawberry production. The experimental device shown in Fig. 1.12 was built in Kunming, China (longitude 102.68°E and latitude 25.07°N). The greenhouse was installed on the roof of a solar energy research

institute building, with an east-west orientation. Opaque photovoltaic modules were installed on the roof of the greenhouse. Their results showed that the yield of the shaded strawberry was 1.2 times higher than that of the unshaded samples. In summary, strawberry plants shaded by opaque photovoltaic modules were superior to unshaded strawberry plants in terms of growth, quality, and yield.

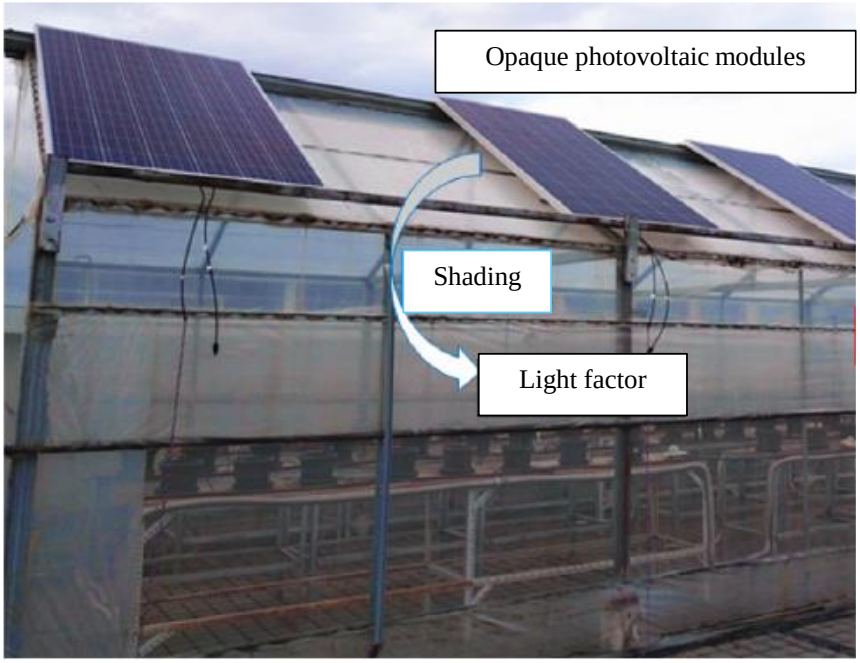

Figure 1.12. Layout of the experimental solar greenhouse system [52].

In recent decades, natural ventilation methods for greenhouse cooling have been studied in depth and many passive design techniques have been successful to various degrees. This method is straightforward and does not necessarily require much external energy. The air is driven by the disparity in the pressure between the outside and inside greenhouse environment [53]. A. Reyes-Rosas et.al [54] predicted temperatures of airflow, crops, cover, and soil in a naturally ventilated greenhouse using a dynamic semi-empirical model as shown in Fig. 1.13. Synopta software (Hortisystems UK Ltd, West Sussex, UK) was used to control the vent opening. Their study revealed that decreasing air movement produced an important heterogeneity in the distribution of temperature, with the difference of 7−8 ºC between the zones near the plants, and close to the greenhouse covering in the middle of spans, where the hot air accumulated because of buoyancy driven flows. Although natural ventilation is a useful way to cool air with little energy consumption, using it alone is sometimes not sufficient to lower air temperature for some crops cultivation.

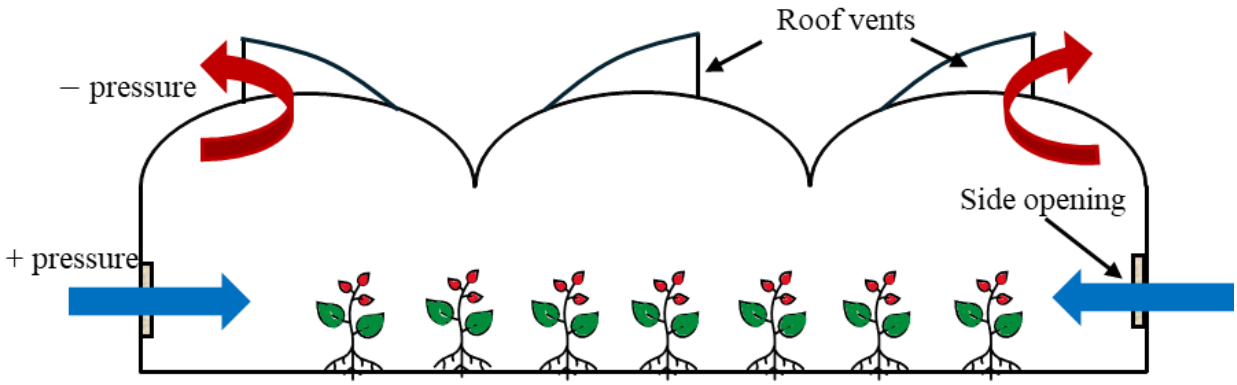

Figure 1.13. Naturally ventilated greenhouse [54].

Generally, evaporative cooling is the technology that uses water that evaporates and absorbs heat from the air, thereby reducing its temperature [55]. E. Romantchik et al. [56] determined the energy required by a fan-pad system in the span-type greenhouse with a double layer of polyethylene plastic cover. Then, the size of the photovoltaic system to generate the energy required by the fan-pad system was also predicted. Figure 1.14 shows fan and pad evaporative cooling in greenhouse. A model calibrated with experiments was developed to predict the greenhouse temperatures, ventilation rates, and energy consumption which allowed the reliable sizing of the photovoltaic systems. The work highlighted that the grid-connected photovoltaic system was able to generate all the energy consumed by the fans.

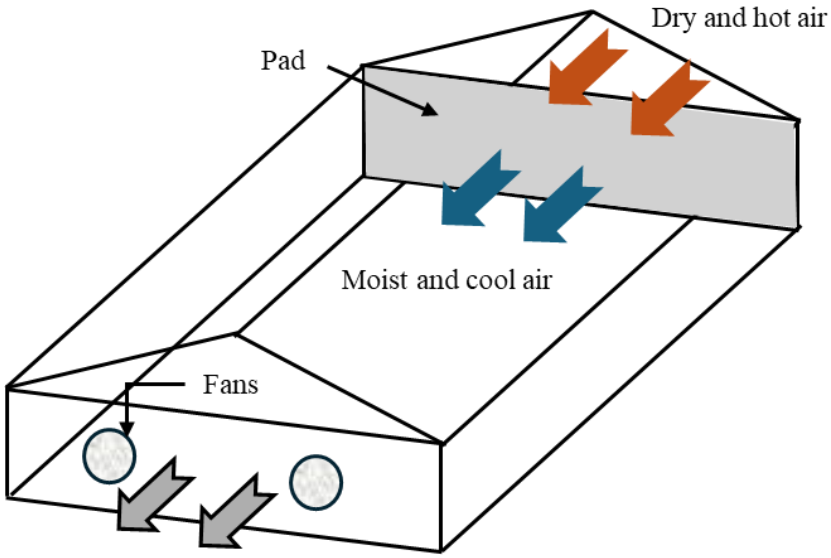

Figure 1.14. Fan and pad evaporative cooling in greenhouse [56].

J. H. AlSadah [57] proposed a new design that features a layer of liquid or water solution between two layers of commercial-grade glass as shown in Fig 1.15. This design effectively absorbs thermal radiation and can be integrated with an active heat dissipation system to enhance cooling efficiency. Their results indicated that the liquid filter can significantly reduce thermal load, with reductions ranging from 31-62%. Additionally, the filter allows for a reduction in the photosynthetically active portion of the solar spectrum between 32-79%.

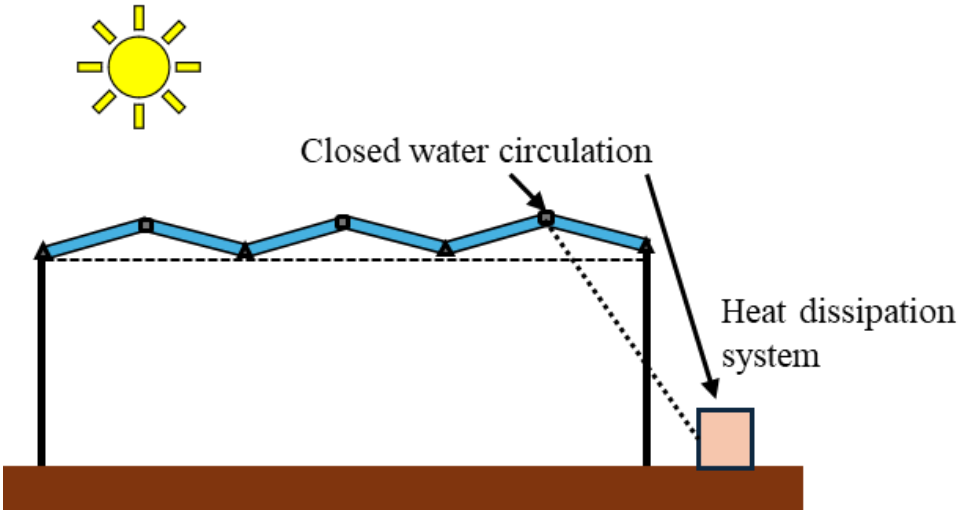

Figure 1.15. Proposed liquid filter ceiling in greenhouse [57].

P. Banik et al. [58] developed a thermal model of a distributed fan-pad evaporative cooler coupled with solar desiccation as shown in Fig. 1.16, used in a floricultural greenhouse in Indian sub-continent. The study considered the influence of crop transpiration and other parameters such as area index and characteristic length of crop leaf. Their study concluded that coupling desiccants with evaporative cooling provides improved cooling effect. The maximum temperature in the greenhouse was predicted as 26.6 ºC in June, while the temperature of the conventional fan pad system reached up to 28 ºC.

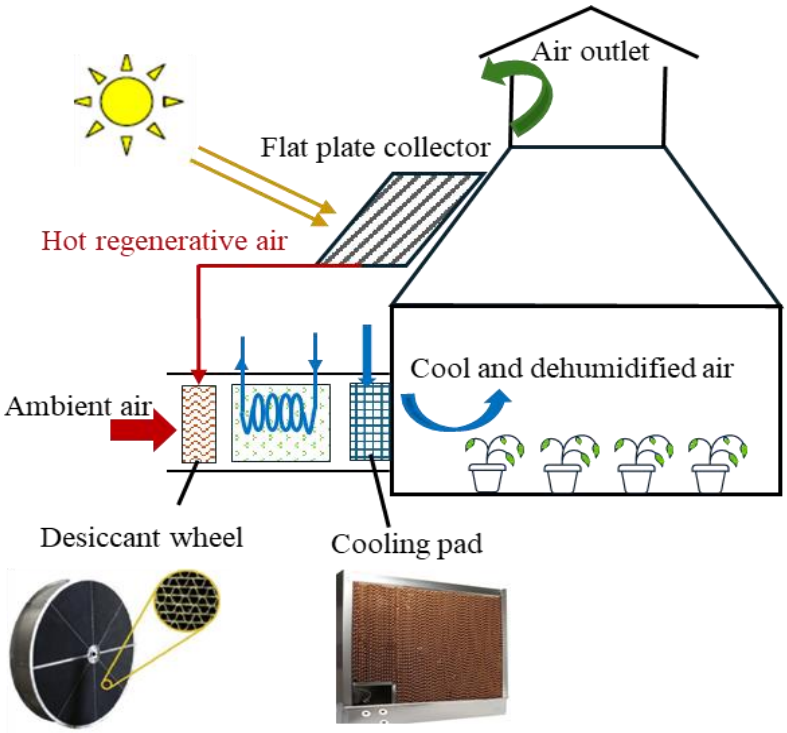

Figure 1.16. Schematic diagram of the solar desiccant assisted distributed fan-pad ventilated greenhouse system [58].

Earth-air heat exchangers have emerged as a promising technology that can efficiently utilize the underground thermal potential to preheat the greenhouse air temperature in summer and vice versa in winter [59]. The earth-air heat exchangers use underground pipes under certain depth of the soil and carry indoor or outdoor air into the pipes. The temperature difference between the soil and air can be applied to substitute the heated or cooled air in the greenhouse [60].

The mechanism of heat transfer of earth-air heat exchanger is as shown in Fig.1.17 .The pulled air is pushed by an air blower to flow through the tubes of the exchanger as a mediator heat carrier to the medium required to be conditioned by a process of heat exchange between it and the soil through the walls of the tubes, where the heat is transferred from the air flowing through the tube to its walls by convection and then transmitted through it by conduction to the surrounding soil [61]. In this way, the earth-air heat exchanger system provides air temperature control in the greenhouse.

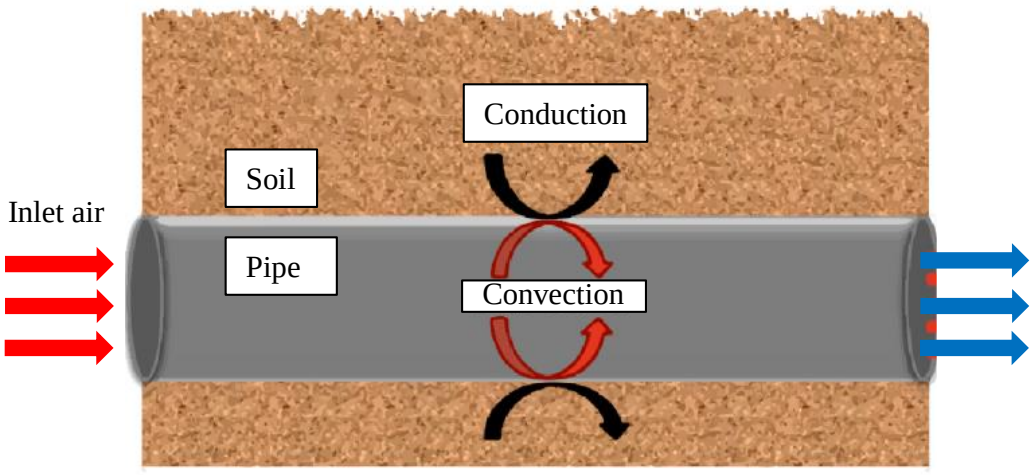

Figure 1.17. Heat exchange between tube air and soil [61].

J. Xiao et al. [62] investigated the thermal performance of an earth-air heat exchanger applied in a greenhouse. Figure 1.18 shows the earth-air heat exchanger and greenhouse in their study. A mathematical heat balance model and the three-dimensional unsteady Computational Fluid Dynamics (CFD) model predicted the greenhouse and system outlet temperature and analyzed the main parameters. Their result showed that earth-air heat exchanger can increase the night temperature by 1.41 ºC and decrease the day temperature by 1.87 ºC in winter and summer, respectively, and effectively reduce the fluctuation of indoor temperature.

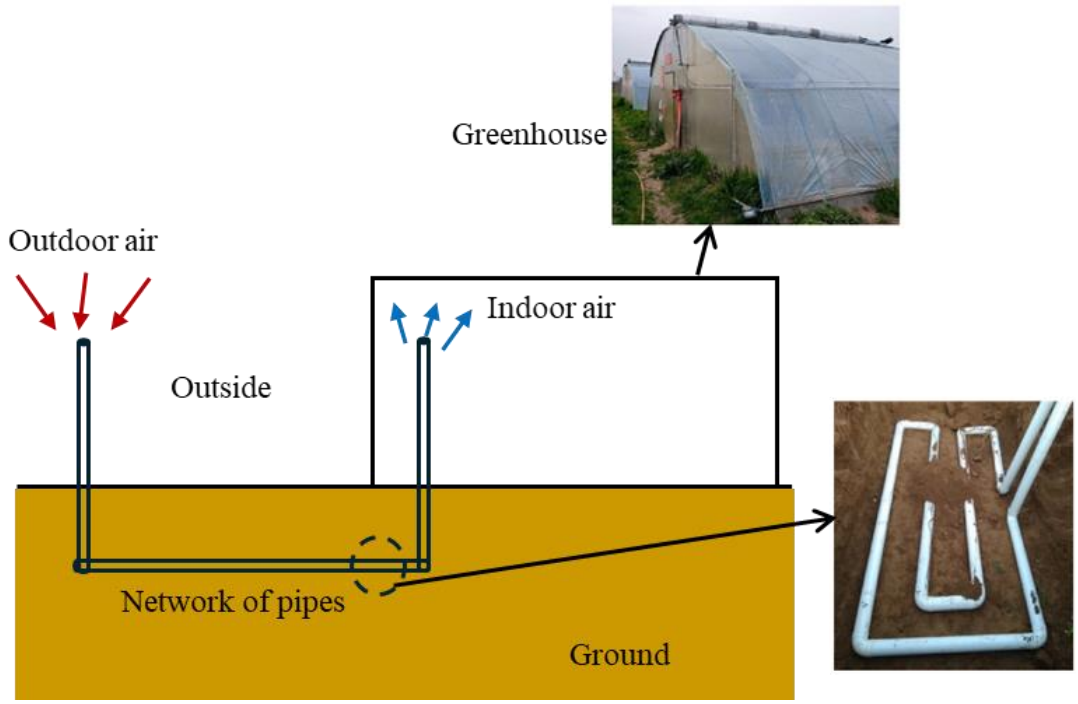

Figure 1.18. Earth air heat exchanger system and greenhouse [62].

In recent decades, the innovative idea of using closed greenhouse was formed to conserve water and energy [63]. In the closed greenhouse, concept aquifers are used to store excess heat in summer to heat the greenhouse in winter. Air is circulated in a greenhouse as shown in Fig.1.19. This technique is already applied in hundreds of office buildings, hospitals, and apartment blocks, but is rather new to greenhouses. In winter, water from the warm side is pumped up to heat the greenhouse using heat pumps, and the cooled water is stored at the cold side of the aquifer. Much more heat is stored than can be used in the closed greenhouse.

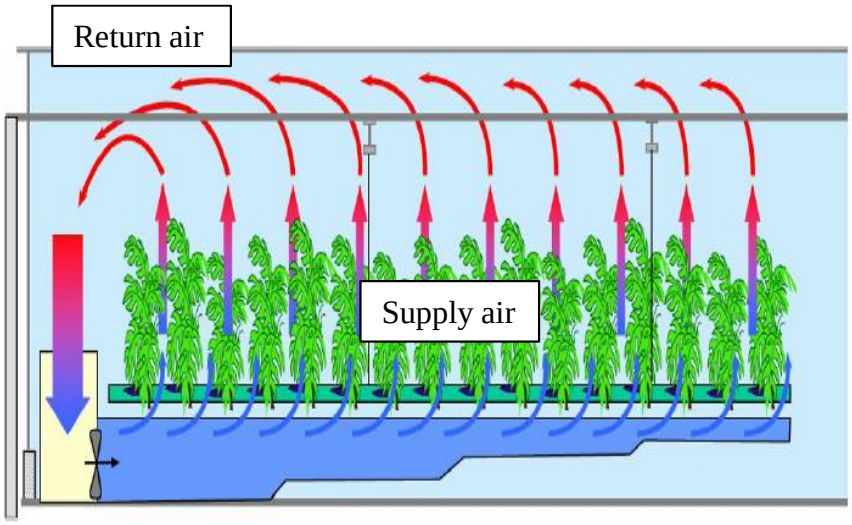

Figure 1.19. Air circulation in a closed-greenhouse [63].

1.2.2.2 Heating technologies in greenhouse cultivation

Heating greenhouses is essential to provide favorable climatic conditions for growing plants under cold periods. A. Bazgaou et al. [64] studied the performance of an Active Solar Heating System (ASHS) consisting of two solar water heaters equipped with flat solar collectors, two storage tanks, and exchanger pipes. Figure 1.20 (a) shows their experimental greenhouse system and Figure 1.20 (b) depicts the functioning diagram of the ASHS system for greenhouse. During the day, the water is heated in the thermosyphon solar collectors and stored in tanks before being placed into circulation in the exchanger pipes to distribute the heat to the greenhouse area of tomato cultivation. Their experimental results showed that the ASHS system improved the nocturnal climatic conditions under greenhouse. The suitable heated environment created by the ASHS system increased the absorption of nutrients, which improved the external quality (color, size, weight, and firmness) and the internal quality (sugar content, acidity, and taste) of tomato fruits. This improvement was also reflected by increasing total tomato yield by 55% in the winter period.

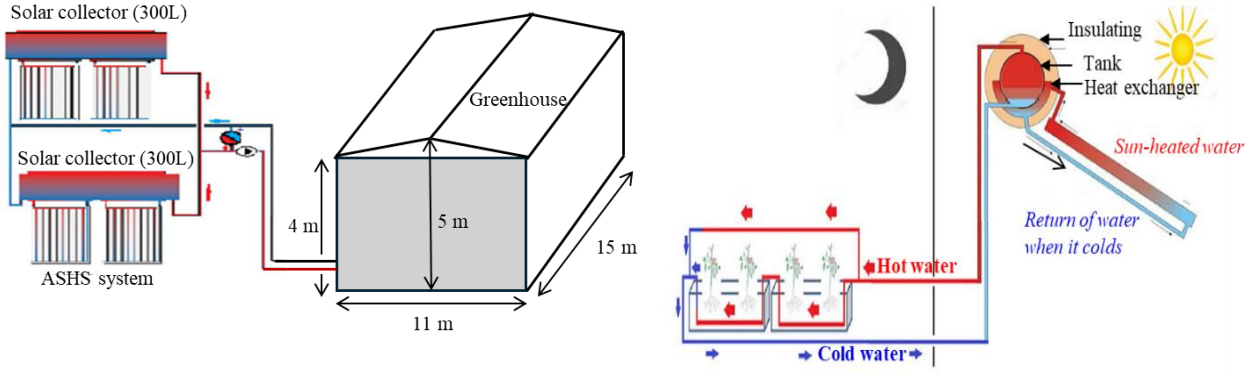

(a) Description of experimental greenhouse (b) Functioning scheme of the Active Solar Heating System (ASHS) system

Figure 1.20. Active Solar Heating System and greenhouse [64].

M. Ameen et al. [65] evaluated a heating system that can provide heat directly to the root zone instead of heating the entire greenhouse for winter-grown green peppers as shown in Fig 1.21. Figure 1.21 (a) shows the pot equipped with a heating source and Figure 1.21 (b) the experimental setup with the heating system. They stated that this heating system is a viable option to reduce energy consumption. Root zone heating could be an effective alternative for the sustainable development of plants during the winter.

(a) Heating pot with a heating source (b) Experimental heating system

Figure 1.21. Root zone heating system [65].

M. Zhao et al. [66] developed vertical heat exchange tube arrays specifically designed for greenhouses. The tube arrays are one-third buried in the soil and the rest is in the air to regulate the indoor air temperature of the greenhouse as shown in Fig. 1.22. The hollow aluminum heat exchange tube has a cross-sectional square size of 80 mm × 40 mm and a wall thickness of 2 mm. As a group, 16 hollow vertical heat exchange tubes were arranged in the arch shed in the greenhouse. The greenhouse dimension is 3 m in width, 2 m in depth, and 2.2 m in height. Their focus is on enhancing the passive heat absorption and heat storage efficiency of the device and its influence on the thermal environment of the greenhouse. In order to improve the heat absorption and storage efficiency of the heat exchanger device and its impact on the greenhouse thermal environment, experimental comparative analysis was conducted using air, water, and phase-change materials as working fluids inside the pipes. Notably, their results concluded that when the working fluid is a phase-change material, it has the most significant impact on the thermal environment of the greenhouse.

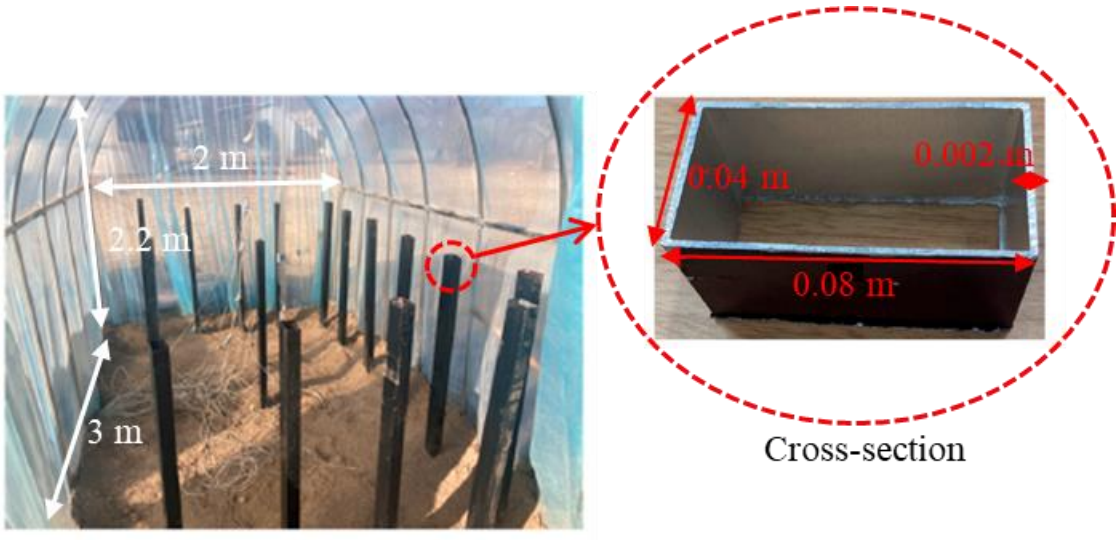

Figure 1.22. Arch shed heat exchange tube in a greenhouse [66].

1.2.3 Literature review of energy use in greenhouses in the European Union

Energy use in the European Union greenhouse agriculture sector was reviewed. It is important to noted that data on the energy use in greenhouse cultivation in the European Union are fragmented and that available data are extremely limited. Thus, the literature provided data on greenhouse energy use both on a country level, for which there is some data available (for The Netherlands, Italy, Spain, Germany), and specifically for tomato production, a crop which has by far the most available data.

High energy systems, which are more dominant in northern Europe, are generally heavily climate controlled and energy use is dominated by heating and cooling processes, while low energy systems, which are dominant in southern Europe, show a mixture of energy uses including heating, cooling, irrigation, lighting, fertilisers, and pesticides.

Spain has the largest greenhouse sector by area in the European Union with an estimated 43,964 hectares under greenhouse production and is the largest supplier of greenhouse vegetables in Europe. F.J. Baptista et al. [67] studied the greenhouses which are heavily climatically controlled and exhibit large energy inputs. As shown in Fig. 1.23, the heating and cooling comprises for tomato production depending upon the locations of the greenhouses in Spain. It was found out that the energy consumption are the highest in the cities of Madrid and Navarra.

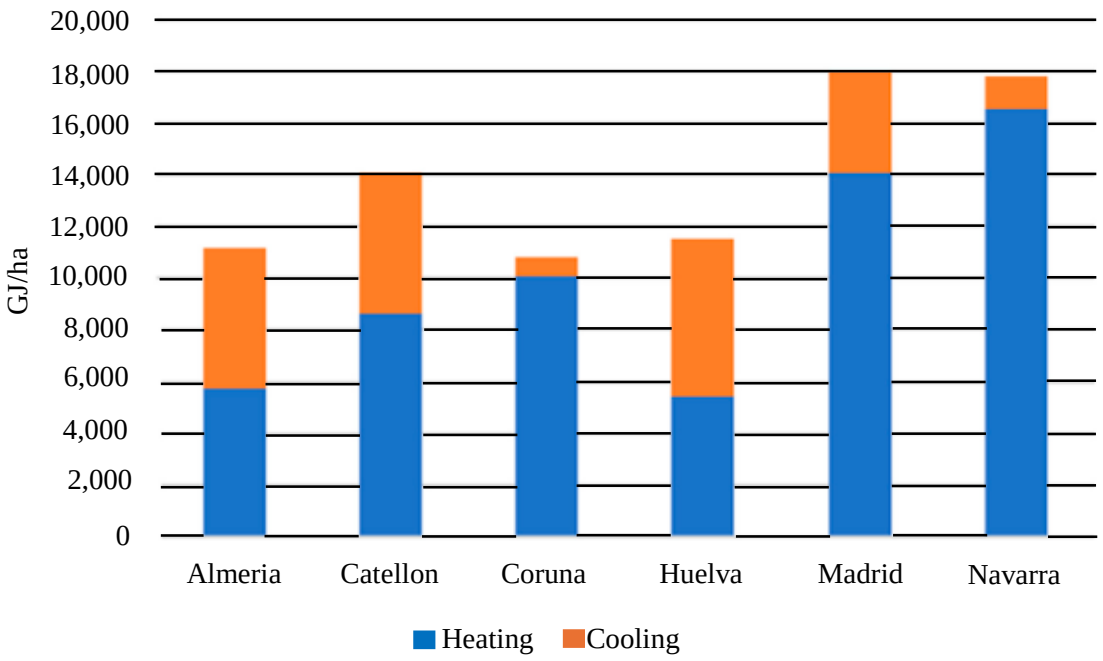

Figure 1.23. Energy consumption in high energy intensity tomato greenhouse production in Spain (GJ/ha) [67].

In Greece, the area under greenhouse cultivation is approximately 5600 ha, which represents around 0.12% of the country's total cultivated land area. The most common vegetable crops grown in Greek greenhouses are tomato, cucumber, and pepper. Figure 1.24 shows energy consumption in high energy intensity greenhouse production in Greece for specific crop including tomato [68], lettuce [69], and flowers [70]. Since the greenhouse use high energy intensity, heating is the main energy consumption in all three crops.

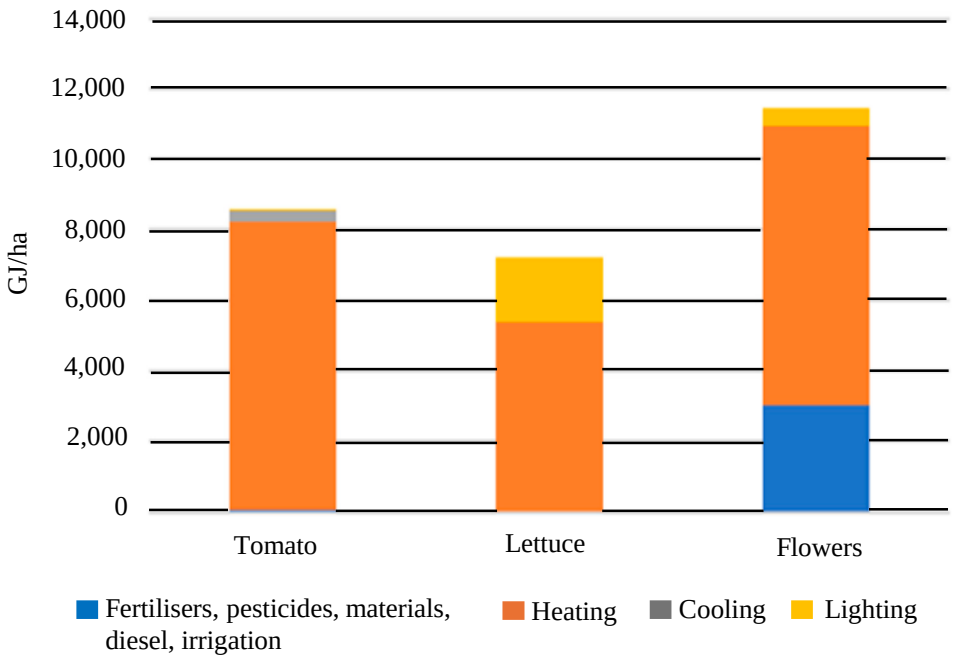

Figure 1.24. Energy consumption in high energy intensity greenhouse production in Greece (GJ/ha) [68,69,70].

D. Visser et al. [71] conducted tomato and cucumber for low energy intensity greenhouse production. Figure 1.25 illustrates that low energy intensive greenhouses, demand for energy inputs is spread across fertilizers, materials, irrigation, pesticide, lighting, heating, and cooling. consumption. For both crops covered in the low energy intensity greenhouses, the energy inputs are around 250 GJ/ha, whereas in high energy intensity greenhouses they are many times higher, ranging from around 7,000 GJ/ha to 11,500 GJ/ha. By contrast, in high energy intensity greenhouses, energy used for heating dominates the consumption.

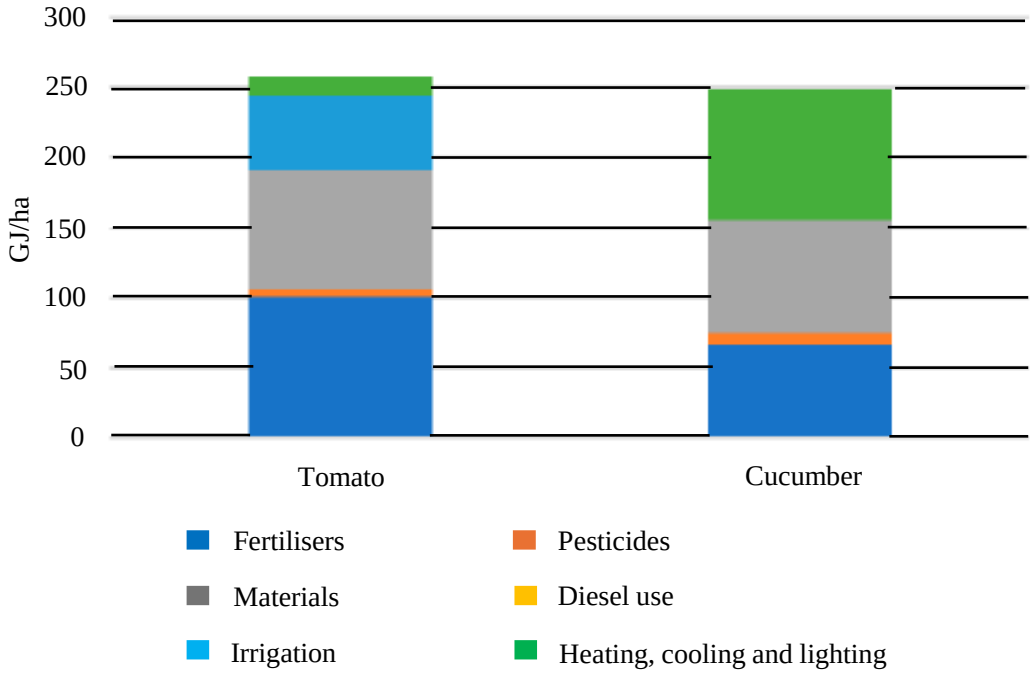

Figure 1.25. Energy consumption in low energy intensity greenhouse production in Greece (GJ/ha) [71].

The greenhouses in Italy are distributed all over the Italian peninsula with the majority, about 60%, located in southern regions. Italian greenhouse sector is of considerable economic importance for the national agricultural systems and a significant energy consumer. Data for Italy were only located for crop cultivated in low energy intensity greenhouses in central Italy as shown in Fig.1.26. Within these data, energy use ranges between 60 GJ/ha to 140 GJ/ha and suggest that electricity accounts for around half of all the energy inputs, followed by diesel at around a quarter of all energy inputs [72].

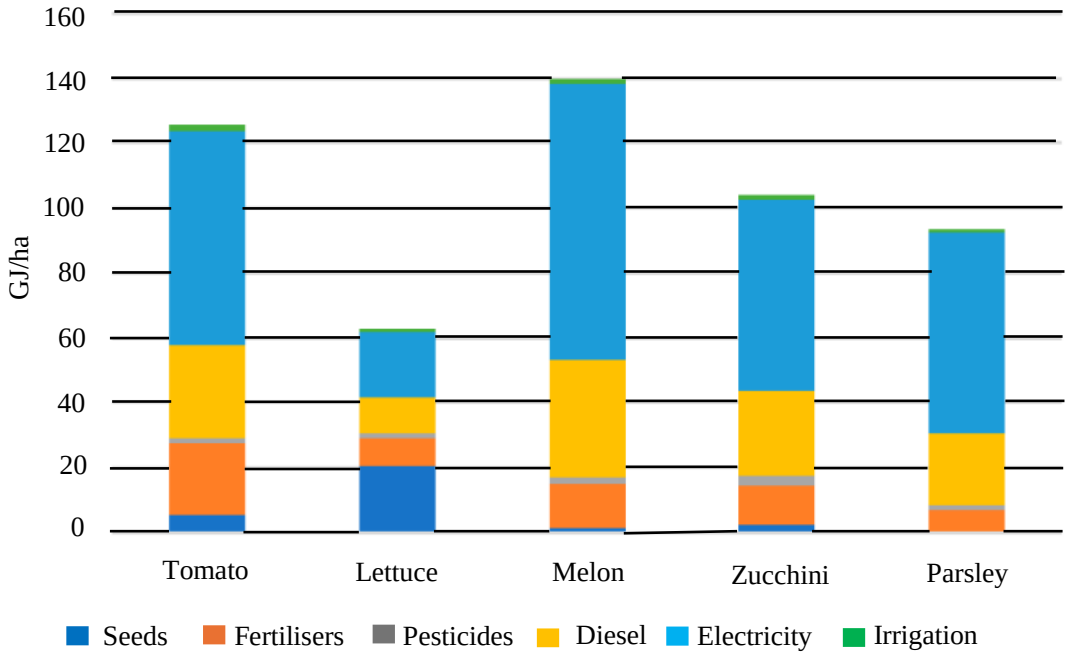

Figure 1.26. Energy consumption in low energy intensity greenhouse production in Italy (GJ/ha) [72].

Data on greenhouse production in Germany is relatively scarce. J. Voss [73] suggested that only 3,689 hectares are covered by greenhouses, of which an estimated 80% are glass greenhouses, 15% foil, and 5% stiff plastics, while 2,500 hectares are heated. The main crops cultivated in the German greenhouses are tomato, cucumber, certain plants and other crops. It is important to note that most of the facilities are relatively old; 43.1% of the total number of greenhouses, which corresponds to almost 1,600 ha, were built before 1,982. Even though some of these facilities were upgraded to comply with the modern-day standards, most of them are still outdated and only 10.6% of the total facilities were built after 2,000. Furthermore, most the production area under glass which is specialized for vegetable crops is owned by "small" farmers.

For Germany, D. Visser et al. [71] investigated the energy consumption in greenhouses for tomato and cucumber production as shown in Fig.1.27. The biggest share of the energy inputs is attributed to heating purposes, whereas a small portion of the energy inputs account for fertilizers. The available data suggested that close to 13,000 GJ/ha are consumed in the greenhouse cultivation of both crops, of which 99.6% accounts for heating purposes.

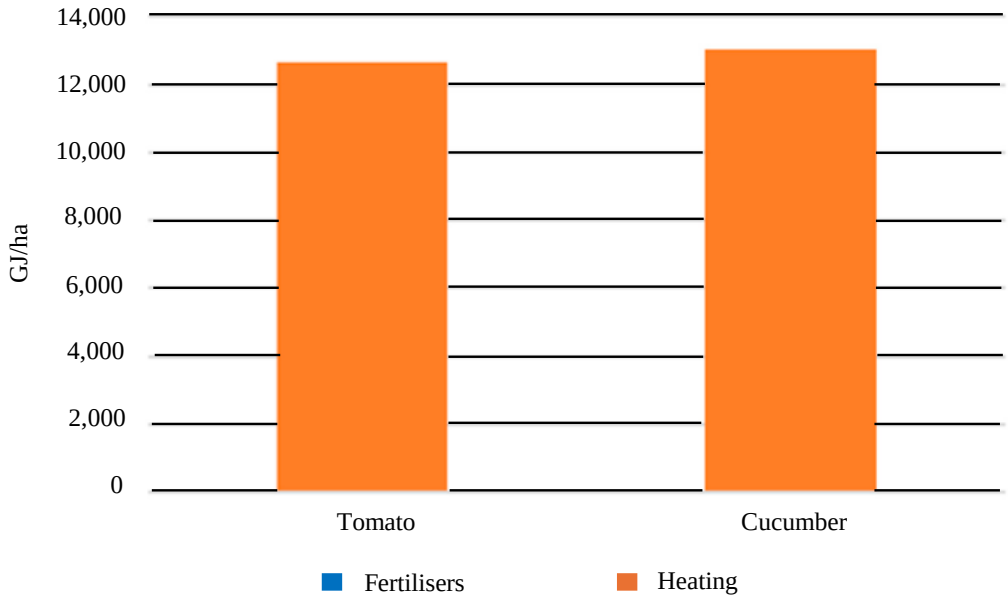

Figure 1.27. Energy consumption in German greenhouse sector (GJ/ha) [71].

Figures 1.28 and 1.29 provide an overview of the energy data of high and low energy intensity greenhouse tomato production. They are presented according to country and in cases where multiple data points are available for one country simple averages were calculated. These data show some variations within categories, with energy inputs for high energy systems ranging from around 8,000 GJ/ha in Greece to around 15,000 GJ/ha in the Netherlands. In the high energy intensity systems, the vast majority of energy inputs are associated with heating and cooling activities, while in the low energy intensity systems fertilizers are the largest energy inputs. Importantly, this illustrates that energy inputs in high energy intensive tomato production systems are around 50 times greater per hectare than in low energy intensive systems. This energy intensity translates into large differences in final yield, for instance, in the Netherlands the average tomato yield is around 50 kg/m^2 while in southern Italy it is 7.6 kg/m^2.

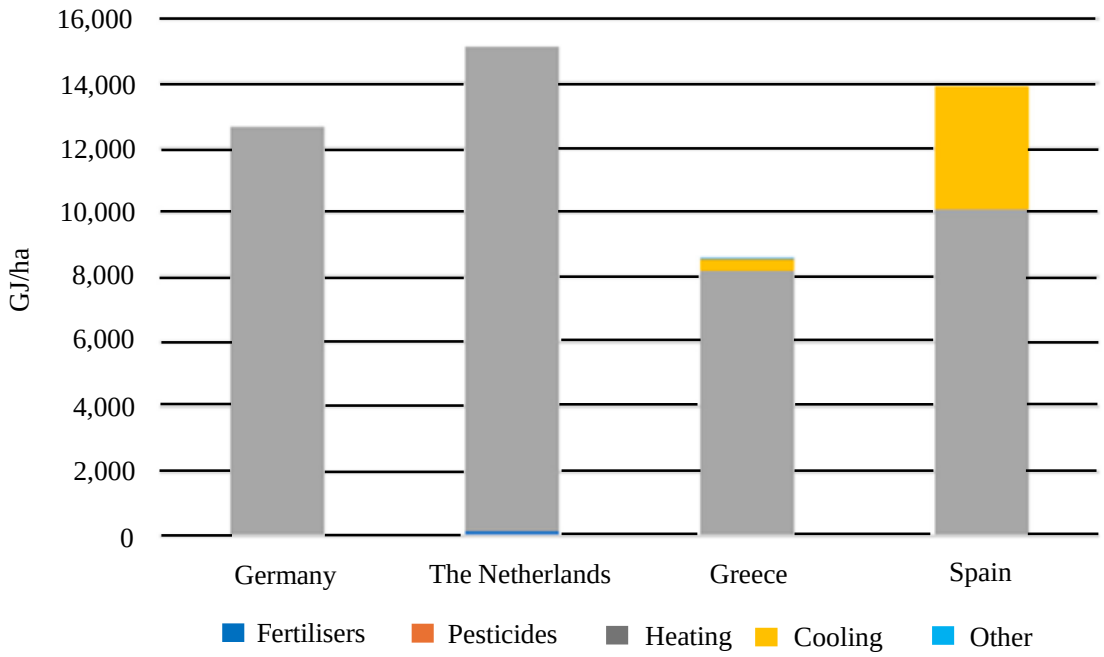

Figure 1.28. Energy inputs in high energy intensity tomato production systems (GJ/ha) [67, 71, 73].

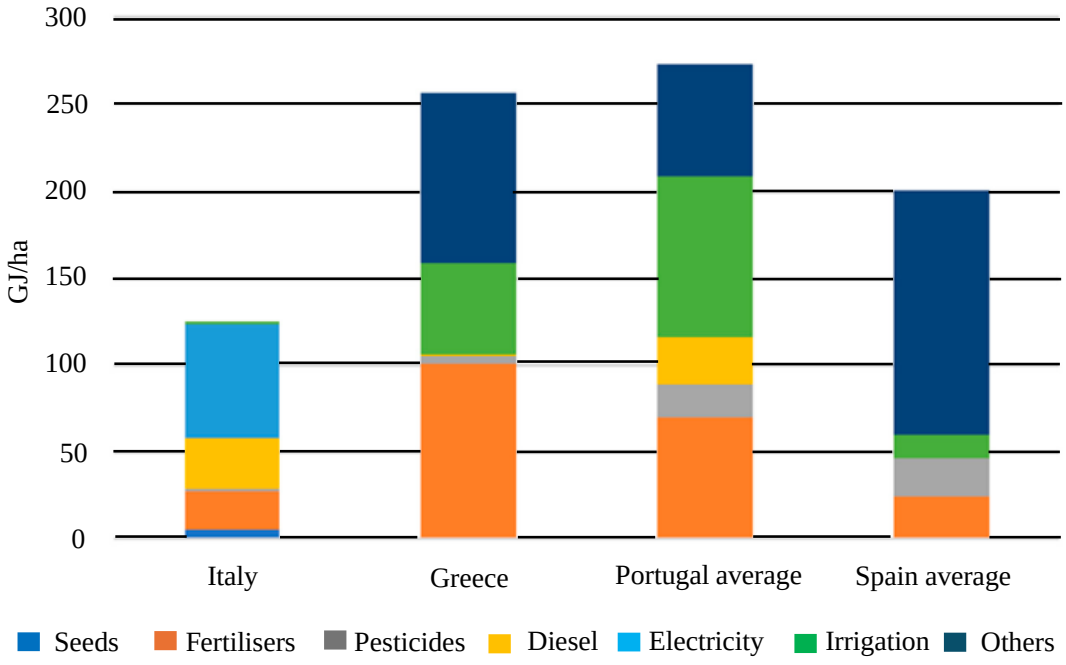

Figure 1.29. Energy inputs in low energy intensity tomato production systems (GJ/ha) [71, 72, 75].

The above energy inputs literature review showcased the energy use in greenhouses in European Union. The literature review data depending upon the type of greenhouse, geographical area and crop grown. Overall, it can be indicated that the energy requirements for heating and cooling in energy intensive systems are very considerable that other energy inputs, such as fertilisers, are extremely minor. Indeed, it has been estimated that the heating and cooling of greenhouses represents 1.5% of Europe's total energy consumption. In most

cases, heating and cooling systems are powered by energy from fossil fuels but in recent years sustainable sources of heat, mainly geothermal, have been grown rapidly.

The cooling and heating processes, which aim to maintain the greenhouse environment under optimal conditions, and which are suitable for crop growth, have the highest share of energy consumption, at about 65 to 85% [76]. The cooling energy consumption in the Mediterranean region is about 100,000 kWh/ha per year, while no numerical estimate for the hot regions is available in the existing literature; however, the amount of energy consumed definitely reaches much higher values in the hot countries. For instance, the cooling energy consumption for protected crops in the United Arab Emirates ranged from 10.43 to 14.67 kWh/m^2 during the production cycle.

This energy consumption is mainly based on electric power, which is essentially produced from fossil energy, which is increasingly being depleted, which threatens the energy supply. Consequently, selecting and developing appropriate climate control techniques and more efficient cooling systems that aim to decrease the high amounts of energy and water consumption is considered to be the major challenge in the upcoming years, particularly in hot and arid countries.

Challenges remain, such as the increased energy consumption associated with mentioned cooling and heating systems. To overcome this challenge, researchers have explored on minimizing energy consumption and obtaining suitable environmental conditions for cultivating crops [77]. Therefore, most of the researchers have intensively researched the methods for greenhouse cultivation to achieve the required environmental control as well as the minimum energy consumption.

Moreover, many researchers focus on the entire facility environment in control agriculture. Limited studies existed focus for local climate control in greenhouse cultivation. Unlike the above-mentioned literature review, this thesis will focus on periodic air temperature control for the local area cooling and heating which is near the strawberry crop in greenhouse cultivation.

1.3 Research objectives

In particular, this thesis will address the periodic local climate control near the crops using a simple serpentine heat exchanger. The research objectives of this thesis are as follows:

1.3.1 To investigate the local air temperature near the crops, the heat flux and pressure drop in the heat exchanger

1.3.2 To examine the characteristics of periodic air temperature field change for local climate area cultivation

1.3.3 To estimate and compare the theoretical energy requirement based on the experimental results between the whole area and the local area control of the practical greenhouse cultivation

1.4 Research scopes

1.4.1 An experimental system was set up for serpentine copper tube heat exchangers with the assumption that the actual crops were being left out.

1.4.2 Experiments were carried out in the laboratory.

1.4.3 Inlet fluid temperature and fluid flow rate were experimental parameters.

1.5 Significance of research

1.5.1 A simple-shaped serpentine heat exchanger for local climate control appropriate for greenhouse agriculture is introduced.

1.5.2 Local climate control for periodic air temperature field in the practical greenhouse application using a heat exchanger is proposed.

1.5.3 Energy-saving method for changing periodic air temperature field for crop cultivation is presented.

1.5.4 This heat exchanger system can be applied to tropical and temperate regions since the local climate control can provide for both cooling and heating.

1.6 Outline of the thesis

The thesis comprises 5 chapters. This chapter addresses the research background and motivation to address the novelty of this research, the literature review to highlight similar research work, the research objectives, the research scopes, and the significance of the research.

Chapter 2 consists of the principles and theories related to basic heat transfer theory, evaluation of heat exchanger, internal forced convection, and natural convection.

Chapter 3 describes the overview of the experimental concept, configuration of heat exchanger, experimental setup, and experimental conditions of this study. The sensors and equipment used for data collection are also described in detail. The calculating heat transfer in a serpentine copper tube heat exchanger is stated. The estimation of theoretical energy requirement method is stated as well.

Chapter 4 discusses the experimental results such as local air temperature, heat flux, and pressure drop in the heat exchanger. Furthermore, periodic air temperature control such as the temperature difference between cooling and heating processes and transition time between them is evaluated. Moreover, the theoretical consideration of energy requirement for whole area and local area of the greenhouse crop cultivation was also estimated.

Chapter 5 presents the concluding remarks and significant findings in this thesis.

References in chapter 1

[1] L. Ouazzani Chahidi, M. Fossa, A. Priarone, A. Mechaqrane, Greenhouse cultivation in Mediterranean climate: Dynamic energy analysis and experimental validation, Thermal Science Engineering Progress, vol. 26, pp. 1–9, 2021.

[2] O. Abedrabboh, M. Koç, Y. Biçer, Computational modeling and assessment of novel irradiation-controlled geothermally cooled greenhouse in hot arid climates, Solar Energy, vol. 277, pp. 1–19, 2024.

[3] B. Paris et al., Energy Use in Greenhouses in the EU: A Review Recommending Energy Efficiency Measures and Renewable Energy Sources Adoption, Applied Science, vol. 12, No. 10, pp. 1–19, 2022.

[4] A. Ahmadbeyki, M. Ghahderijani, A. Borghaee, H. Bakhoda, Energy use and environmental impacts analysis of greenhouse crops production using life cycle assessment approach: A case study of cucumber and tomato from Tehran province, Iran, Energy Reports, vol. 9, pp. 988–999, 2023.

[5] A. Banakar, M. Montazeri, B. Ghobadian, H. Pasdarshahri, F. Kamrani, Energy analysis and assessing heating and cooling demands of closed greenhouse in Iran, Thermal Science. Engineering Progress, vol. 25, pp. 1–7, 2021.

[6] T. S. Wai, C. Chaichana, N. Maruyama, Energy cost analysis of growing strawberries in a controlled environment chamber, Energy Reports, vol. 9, pp. 677–687, 2023.

[7] L. Ouazzani Chahidi, M. Fossa, A. Priarone, A. Mechaqrane, Energy saving strategies in sustainable greenhouse cultivation in the mediterranean climate – A case study, Applied Energy, vol. 282, pp. 1–12, 2021.

[8] A. D. Thomas, Yara, Liping Wang, Energy Savings Analysis of a Greenhouse Heated by Waste Heat, Proceeding 15th IBPSA Conference, pp. 2821–2826, 2017.

[9] P. Bichkar, O. Dandgaval, P. Dalvi, R. Godase, T. Dey, Study of Shell and Tube Heat Exchanger with the Effect of Types of Baffles, Procedia Manufacturing, vol. 20, pp. 195–200, 2018.

[10] M. R. Saffarian, F. Fazelpour, M. Sham, Numerical study of shell and tube heat exchanger with different cross-section tubes and combined tubes, International Journal of Energy and Environmental Engineering, vol. 10, No. 1, pp. 33–46, 2019.

[11] Y. Maghsoudali, A. Rastegarkoutenaei, M. Sahami, M. G. Bandpy, Investigation of the effect of using the finned tubes on the performance of shell and tube heat exchanger by 3D modeling, Journal of Energy Storage, vol. 56, pp. 1–16, 2022.

[12] M. Chaanaoui, K. Ettahi, S. Abderafi, S. Vaudreuil, T. Bounahmidi, Comparative analysis between optimum configurations of finned tube heat exchanger: Application for solar drying, Case Study in Thermal Engineering, vol. 22, pp. 1–15, 2020.

[13] P. Tong, G. Fan, Z. Sun, M. Ding, Experimental study of steam-air condensation over a vertically longitudinal finned tube, International Journal of Heat and Mass Transfer, vol. 89, pp. 1230–1238, 2015.

[14] S. Unger, M. Beyer, M. Arlit, P. Stasch, U. Hampel, An experimental investigation on the air-side heat transfer and flow resistance of finned short oval tubes at different tube tilt angles, International Journal of Thermal Science, vol. 140, pp. 225–237, 2019.

[15] H. Zhou, D. Liu, Q. Sheng, M. Hu, Y. Cheng, K. Cen, Research on gas side performance of staggered fin-tube bundles with different serrated fin geometries, International Journal of Heat and Mass Transfer, vol. 152, pp 1–9, 2020.

[16] C. Wang, Z. Cui, H. Yu, K. Chen, and J. Wang, Intelligent optimization design of shell and helically coiled tube heat exchanger based on genetic algorithm, International Journal of Heat and Mass Transfer, vol. 159, pp 1–11, 2020.

[17] Y. Maghsoudali, A. Rastegarkoutenaei, M. Sahami, M. G. Bandpy, Experimental investigating the thermal and hydraulic performance of heat exchangers with helix wire finned tube, Applied Thermal Engineering, vol. 231, pp. 1–13, 2023.

[18] Q. Jiang et al., Improved heat transfer and friction correlations of aluminum offset-strip fin heat exchangers for helium cryogenic applications, Applied Thermal Engineering, vol. 192, pp. 1–15, 2021.

[19] P. Palencia, F. Martínez, J. J. Medina, J. López-Medina, Strawberry yield efficiency and its correlation with temperature and solar radiation, Horticultural Brasileira, vol. 31, No. 1, pp. 93–99, 2013.

[20] J. F. Hancock, Strawberries, 2nd Ed. Crop Production Science in Horticulture Series CABI, 2021.

[21] R. M. Sharma, Strawberries_Production Psotharvest Management and Protection, vol. 01, 2019.

[22] M. Pritts, D. Handley, C. Walker, Strawberry Production Guide, 1998.

[23] Kurapalli Shivareddy Madhu, Ramareddy Shankararеddy, Shantappa Gurubasappa Sangashetty, Experimental Study on the Effect of TiO_2–Water Nanofluid on Heat Transfer and Pressure Drop in Heat Exchanger with Varying Helical Coil Diameter, Journal of Advanced Research in Fluid Mechanics and Thermal Science, vol. 107, No. 2, pp. 50–67, 2023.

[24] Q. Chen, G. Xu, and P. Xia, The performance of a solar-driven spray flash evaporation desalination system enhanced by microencapsulated phase change material, Case Study in Thermal Engineering, vol. 27, pp. 1–15, 2021.

[25] B. I. Master, K. S. Chunangad, A. J. Boxma, D. Kral, P. Stehlík, Most frequently used heat exchangers from pioneering research to worldwide applications, Heat Transfer Engineering, vol. 27, no. 6, pp. 4–11, 2006.

[26] A. E. Kabeel, E. M. S. El-Said, A hybrid solar desalination system of air humidification, dehumidification and water flashing evaporation: Part II. Experimental investigation, Desalination, vol. 341, No. 1, pp. 50–60, 2014.

[27] S. Ishaque, M. I. H. Siddiqui, M. H. Kim, Effect of heat exchanger design on seasonal performance of heat pump systems, International Journal of Heat and Mass Transfer, vol. 151, pp. 1–12, 2020.

[28] A. Kumar et al., Effect of oval rib parameters on heat transfer enhancement of TiO_2/water nanofluid flow through parabolic trough collector, Case Study in Thermal Engineering, vol. 55, pp. 1–16, 2024.

[29] R. Kant, T. Alam, D. Singh, A. Sabeeh, M. I. H. Siddiqui, Heat transfer and flow behavior in solar thermal collector equipped with obstacles, International Journal of Heat and Fluid Flow, vol. 107, pp. 1–10, 2024.

[30] M. Monjurul Ehsan, S. Noor, S. Salehin, A. K. M. Sadrul Islam, Application of Nanofluid in Heat Exchangers for Energy Savings. Elsevier Inc., 2016.

[31] S. Salehin, M. Monjurul Ehsan, S. Rafat Faysal, A. K. M. Sadrul Islam, Utilization of nanofluid in various clean energy and energy efficiency applications, Green energy and Technology, pp. 1–32, 2018.

[32] F. Ahmad, S. Mahmud, M. M. Ehsan, M. Salehin, Thermo-hydrodynamic performance evaluation of double-dimpled corrugated tube using single and hybrid nanofluids, International Journal of Thermofluids, vol. 17, pp. 1–15, 2023.

[33] R. Ahamed, M. Salehin, M. M. Ehsan, Thermal-hydraulic performance and flow phenomenon evaluation of a curved trapezoidal corrugated channel with E-shaped baffles implementing hybrid nanofluid, Heliyon, vol. 10, No. 7, pp. 1–40, 2024.

[34] F. Ahmad, S. Mahmud, M. M. Ehsan, M. Salehin, Numerical Assessment of Nanofluids in Corrugated Minichannels: Flow Phenomenon and Advanced Thermo-hydrodynamic Analysis, International Journal of Thermofluids, vol. 20, pp. 1–19, 2023.

[35] A. Mustakim, S. M. N. U. Islam, R. Ahamed, M. Salehin, M. M. Ehsan, Numerical Assessment of Advanced Thermo-Hydrodynamic Characteristics of Nanofluid Inside a Helically Featured Straight Pipe, International Journal of Thermofluids, vol. 21, pp. 1–20, 2024.

[36] S. M. N. U. Islam, A. Mustakim, R. Ahamed, M. Salehin, M. M. Ehsan, Advanced Thermo-Hydraulic Assessment of Helical Pipes with Different Shapes of Jackets Using Single-Phase and Hybrid Nanofluids, Int. J. International Journal of Thermofluids, vol. 22, pp. 1–20, 2024.

[37] M. Awais, M. Saad, H. Ayaz, M. M. Ehsan, A. A. Bhuiyan, Computational assessment of Nano-particulate (Al_2O_3/Water) utilization for enhancement of heat transfer with varying straight section lengths in a serpentine tube heat exchanger, Thermal Science and Engineering Progress, vol. 20, pp. 1–15, 2020.

[38] R. K. Sahdev, M. Kumar, A. K. Dhingra, A comprehensive review of greenhouse shapes and its applications, Frontiers in Energy, vol. 13, No. 3, pp. 427–438, 2019.

[39] C. Maraveas, K. D. Tsavdaridis, Strengthening Techniques for Greenhouses, AgriEngineering, vol. 2, pp. 37–54, 2020.

[40] N. Choab, A. Allouhi, A. El Maakoul, T. Kousksou, S. Saadeddine, A. Jamil, Review on greenhouse microclimate and application: Design parameters, thermal modeling and simulation, climate controlling technologies, Solar Energy, vol. 191, pp. 109–137, 2019.

[41] V. P. Sethi, On the selection of shape and orientation of a greenhouse : Thermal modeling and experimental validation, Solar Energy, vol. 83, pp. 21–38, 2009.

[42] C. Stanciu, D. Stanciu, A. Dobrovicescu, Effect of Greenhouse Orientation with Respect to E-W Axis on its Required Heating and Cooling Loads, Energy Procedia, vol. 85, pp. 498–504, 2016.

[43] W. M. El-Maghlany, M. A. Teamah, H. Tanaka, Optimum design and orientation of the greenhouses for maximum capture of solar energy in North Tropical Region, Energy Conversion and Management, vol. 105, pp. 1096–1104, 2015.

[44] S. M. Dragićević, Determining the optimum orientation of a greenhouse on the basis of the total solar radiation availability, Thermal Science, vol. 15, pp. 215–221, 2011.

[45] S. Ghani et al., Design challenges of agricultural greenhouses in hot and arid environments – A review, Engineering in Agricultural Environment and Food, vol. 12, pp. 48–70, 2019.

[46] V. P. Sethi, S. K. Sharma, Survey of cooling technologies for worldwide agricultural greenhouse applications, vol. 81, pp. 1447–1459, 2007.

[47] B. Wei et al., Thermal performance of single span greenhouses with removable back walls, Biosystems Engineering, vol. 141, pp. 48–57, 2016.

[48] A. M. Abdel-Ghany, I. M. Al-Helal, S. M. Alzahrani, A. A. Alsadon, I. M. Ali, R. M. Elleithy, Covering materials incorporating radiation-preventing techniques to meet greenhouse cooling challenges in arid regions: A review, Scientific World Journal, vol. 1, pp. 1.11, 2012.

[49] C. Stanghellini, J. Dai, F. Kempkes, Effect of near-infrared-radiation reflective screen materials on ventilation requirement, crop transpiration and water use efficiency of a greenhouse rose crop, Biosystems Engineering, vol. 110, No. 3, pp. 261–271, 2011.

[50] A. Baille, C. Kittas, N. Katsoulas, Influence of whitening on greenhouse microclimate and crop energy partitioning, Agricultural and Forest Meteorology, vol. 107, No. 4, pp. 293–306, 2001.

[51] A. M. Abdel-Ghany, P. Picuno, I. Al-Helal, A. Alsadon, A. Ibrahim, M. Shady, Radiometric characterization, solar and thermal radiation in a greenhouse as affected by shading configuration in an arid climate, Energies, vol. 8, No. 12, pp. 13928–13937, 2015.

[52] Y. Tang, X. Ma, M. Li, Y. Wang, The effect of temperature and light on strawberry production in a solar greenhouse, Solar Energy, vol. 195, pp. 318–328, 2020.

[53] M. Ghoulem, K. El Moueddeb, E. Nehdi, R. Boukhanouf, J. Kaiser Calautit, Greenhouse design and cooling technologies for sustainable food cultivation in hot climates: Review of current practice and future status, Biosystem Engineering, vol. 183, pp. 121–150, 2019.

[54] A. Reyes-Rosas, F. D. Molina-Aiz, D. L. Valera, A. López, S. Khamkure, Development of a single energy balance model for prediction of temperatures inside a naturally ventilated greenhouse with polypropylene soil mulch, Computer and Electronics in Agriculture, vol. 142, pp. 9–28, 2017.

[55] G. Lychnos, P. A. Davies, Modelling and experimental verification of a solar-powered liquid desiccant cooling system for greenhouse food production in hot climates, Energy, vol. 40, pp. 116–130, 2012.

[56] E. Romantchik, E. Ríos, E. Sánchez, I. López, J. Reyes, Determination of energy to be supplied by photovoltaic systems for fan-pad systems in cooling process of greenhouses, Applied Thermal Engineering, vol. 114, pp. 1161–1168, 2017.

[57] J. H. Alsadah, Efficient Cooling for Agricultural Greenhouses in Hot Climates: A Novel Water Light Filter Design, Journal of Physics: Conference Series, vol. 2751, pp. 1–14, 2024.

[58] P. Banik, A. Ganguly, Performance and economic analysis of a floricultural greenhouse with distributed fan-pad evaporative cooling coupled with solar desiccation, Solar Energy, vol. 147, pp. 439–447, 2017.

[59] M. Benhammou, B. Draoui, M. Hamouda, Improvement of the summer cooling induced by an earth-to-air heat exchanger integrated in a residential building under hot and arid climate, Applied Energy, vol. 208, pp. 428–445, 2017.

[60] S. Hamdane, L. C. C. Pires, P. D. Silva, P. D. Gaspar, Evaluating the Thermal Performance and Environmental Impact of Agricultural Greenhouses Using Earth-to-Air Heat Exchanger: An Experimental Study, Applied Science, vol. 13, No. 2, pp. 1–13, 2023.

[61] W. Morshed, L. Abbas, H. Nazha, Heating performance of the PVC earth-air tubular heat exchanger applied to a greenhouse in the coastal area of west Syria: An experimental study, Thermal Science and Engineering Progress, vol. 27, pp. 1–8, 2022.

[62] J. Xiao, Q. Wang, X. Wang, Y. Hu, Y. Cao, J. Li, An earth-air heat exchanger integrated with a greenhouse in cold-winter and hot-summer regions of northern China: Modeling and experimental analysis, Applied Thermal Engineering, vol. 232, pp. 1–17, 2023.

[63] E. Heuvelink, M. Bakker, L. F. M. Marcelis, M. Raaphorst, Climate and yield in a closed greenhouse, Acta Horticulturae, vol. 801, pp. 1083–1092, 2008.

[64] A. Bazgaou et al., Effect of active solar heating system on microclimate, development, yield and fruit quality in greenhouse tomato production, Renewable Energy, vol. 165, pp. 237–250, 2021.

[65] M. Ameen et al., An investigation of a root zone heating system and its effects on the morphology of winter-grown green peppers, Energies, vol. 12, No. 5, pp. 1–15, 2019.

[66] M. Zhao et al., Comparative Analysis of the Filling Mass of Vertical Heat Exchanger Tubes on the Thermal Environment of Arched Greenhouses, Energies, vol. 16, No. 13, pp. 1–28, 2023.

[67] F. J. Baptista, A. T. Silva, L. M. Navas, A. C. Guimarães, J. F. Meneses, Greenhouse energy consumption for tomato production in the Iberian Peninsula countries, Acta Horticulturae, vol. 952, pp. 409–416, 2012.

[68] C. Kittas, A. Elvanidi, N. Katsoulas, K. P. Ferentinos, T. Bartzanas, Reflectance indices for the detection of water stress in greenhouse tomato (Solanum lycopersicum), Acta Horticulturae, vol. 1112, pp. 63–70, 2016.

[69] G. Trypanagnostopoulos, A. Kavga, Souliotis, Y. Tripanagnostopoulos, Greenhouse performance results for roof installed photovoltaics, Renewable Energy, vol. 111, pp. 724–731, 2017.

[70] J. Vourdoubas, Overview of Heating Greenhouses with Renewable Energy Sources a Case Study in Crete- Greece, Journal of Agriculture and Environmental Sciences, vol. 4, pp. 70–76, 2015.

[71] C. de Visser, J. Gołaszewski, Z. Brodziński, R. Myhan, State of the Art on Energy Efficiency in Agriculture, Country Data on Energy Consumption in Different Agroproduction Sectors in the European Countries; The Netherlands, pp. 1–70, 2012.

[72] E. Campiglia, G. Colla, R. Mancinelli, Y. Rouphael, A. Marucci, Energy balance of intensive vegetable cropping systems in central Italy, Acta Horticulturae, vol. 747, pp. 185–191, 2007.

[73] J. Voss, Market Special: Greenhouse Farming in Germany, EVD International: Hague, The Netherlands, 2011.

[74] C. Kittas, N. Katsoulas, T. Bartzanas, J.C. Bakker, Greenhouse Climate Control and Energy Use; FAO: Rome, Italy, pp. 63–95, 2013.

[75] A. M. Alonso, G. J. Guzmán, Comparison of the efficiency and use of energy in organic and conventional farming in Spanish agricultural systems, Journal of Sustainable Agriculture, vol. 34, No. 3, pp. 312–338, 2010.

[76] S. Gorjian et al., A review on opportunities for implementation of solar energy technologies in agricultural greenhouses, Journal of Cleaner Production, vol. 285, pp. 1–30, 2021.

[77] R. Ben Ali, S. Bouadila, A. Mami, Experimental validation of the dynamic thermal behavior of two types of agricultural greenhouses in the Mediterranean context, Renewable Energy, vol. 147, pp. 118–129, 2020.

Chapter 2

Principle and theories

The environmental climate control system for crop cultivation is essential in controlled environment agriculture, such as greenhouse cultivation. Currently, greenhouse cultivation is a popular trend in agriculture because it has the ability to produce crops all year round, with the possibility of increased crops yield. In greenhouse cultivation, cooling/heating (constant temperature control) is primarily provided throughout greenhouse areas for crop cultivation. Accordingly, the energy consumption in greenhouse cultivation is high.

As the minimal energy consumption of the environmental control system is also important, the local climate control near the crops is of interest. In particular, some crops like strawberry require periodic temperature field in the day and nighttimes. Therefore, this thesis focuses on periodic air temperature control of local climate area near the strawberry crops in greenhouse cultivation.

The fundamental theories relating to heat exchangers, forced convection, and natural convection are stated as below.

2.1 Heat exchanger

Heat exchangers are devices that enable the exchange of heat between two fluids that are at different temperatures while preventing them from mixing with each other. Heat exchangers are extensively employed in various practical applications, from heating and air-conditioning systems in a household, to chemical processing and power production in large plants. Heat exchangers differ from mixing chambers in that they do not allow the two fluids involved to mix.

2.1.1 Classification of heat exchangers

Various heat transfer applications require different types of hardware and different configurations of heat transfer equipment. A double-pipe heat exchanger has two concentric pipes with different diameters as shown in Fig. 2.1. In the double-pipe heat exchanger, the smaller pipe carries one fluid, and the annular space between the two pipes carries another fluid. The double-pipe heat exchanger can have two different flow arrangements: in parallel flow, the hot and cold fluids enter the heat exchanger at the same end and flow in the same direction. The second one is the counter flow, where the hot and cold fluids flow into the heat exchanger at opposite ends and move in the opposite directions [1].

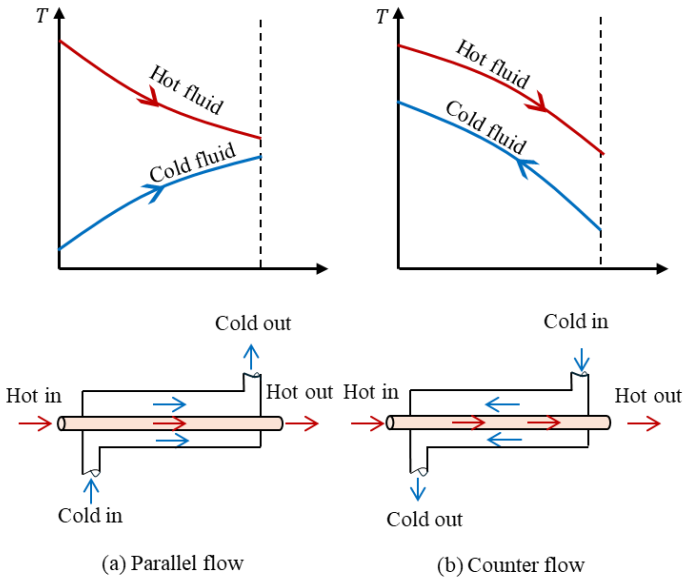

Figure 2.1. Related temperature profiles and different flow pattern in a double-pipe heat exchanger.
(Source: Yunus A. Cengel and Afshin J. Ghajar, Heat and mass transfer. McGraw Hill, 2015)

The most commonly used heat exchanger is the shell and tube type as shown in Fig 2.2. It has many applications in the power generation, petroleum refinery, chemical, and process industries. They are used as oil coolers, condensers, feedwater heaters, etc. This type of heat exchanger consists of a shell (a large pressure vessel) with a bundle of tubes inside it. One fluid runs through the tubes, and another fluid flows over the tubes (through the shell) to transfer heat between the two fluids. The set of tubes is called a tube bundle. Typically, the ends of each tube are terminated through holes in a tubesheet. The tubes are mechanically rolled or welded into the tubesheet face. Baffles are frequently inserted into the shell to improve heat transfer and preserve consistent tube spacing by forcing the fluid on the shell's outside to flow across the shell. Despite their widespread use, shell-and-tube heat exchangers are not suitable for use in automotive and aircraft applications because of their relatively large size and weight [2].

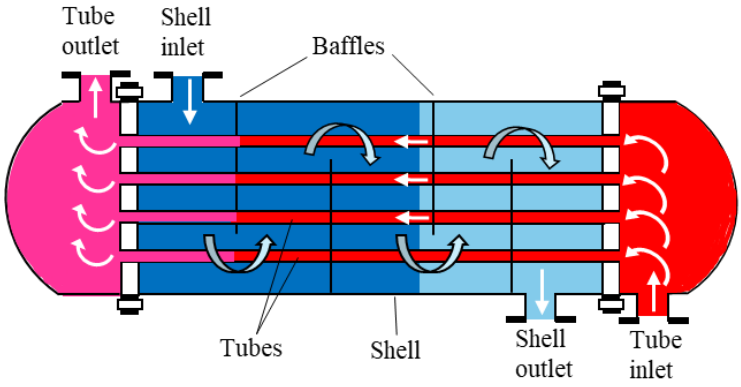

Figure 2.2. Shell and tube heat exchanger (one-shell pass and one-tube pass).
(Source: Kuppan Thulukkanam, Heat Exchangers Classification, Selection, and Thermal Design. Taylor & Francis Group, 2024)

The plate and frame heat exchanger, sometimes known as the plate heat exchanger, is another innovative type of heat exchanger that has become widely used. It consists of several plates with corrugated flat flow passages as shown in Fig. 2.3. The hot and cold fluids pass through alternate passages, and thus each cold fluid stream is surrounded by two hot fluid streams. As a result, very effective heat transfer can be obtained. Additionally, by just adding additional plates, plate heat exchangers can expand to meet the increasing demand for heat transfer. They are well suited for liquid-to-liquid heat exchange applications, provided that the hot and cold fluid streams are at about the same pressure.

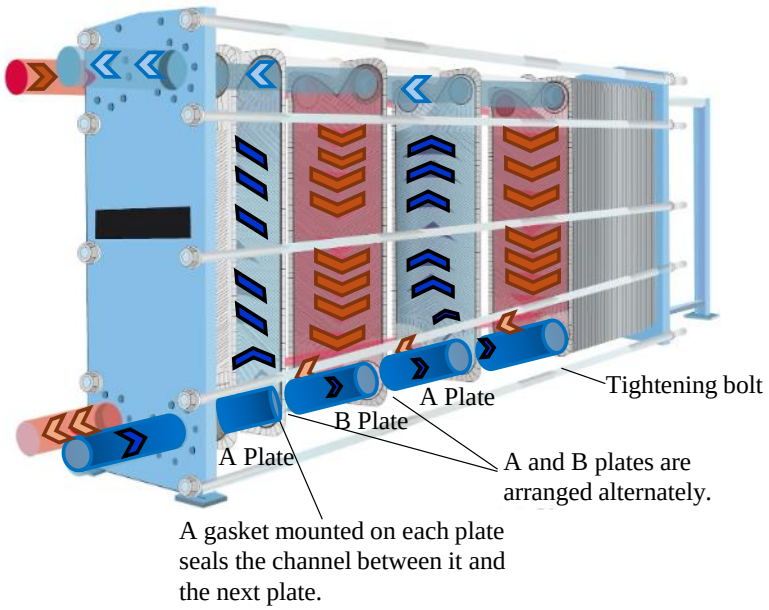

Figure 2.3. A plate-and-frame liquid-to-liquid heat exchanger.
(Source: Yunus A. Cengel and Afshin J. Ghajar. Heat and mass transfer. McGraw-Hill, 2015)

2.1.2 Heat transfer methods and basic heat transfer theory

Heat can be transferred by three methods.

(a) Conduction – Energy is transferred between solids in contact

(b) Convection – Convection is the mechanism of heat transfer through a fluid in the presence of bulk fluid motion.

(c) Radiation – Energy is transferred by electromagnetic radiation. An example is the heating of the Earth by the sun.

The natural principles of physics always allow the driving energy in a system to flow until equilibrium is reached. As long as there is a temperature differential, heat moves from the warmer body or the hottest fluid to the cold medium. A heat exchanger follows this principle in its endeavor to reach equalization. Heat is transferred between the hot and cold media in a heat exchanger by means of the surface. As a result, it is possible to heat or cool fluids or gases which have minimal energy levels. The theory of heat transfer from one fluid to another is determined by several factors such as

i. Heat is always transferred from a hot medium to a cold medium.
ii. There must always be a temperature difference between the media, i.e., thermal gradient.
iii. The heat lost from the hot medium is equal to the amount of heat gained by the cold medium.

2.1.3 Evaluation of heat exchanger

Heat exchangers typically run for a long time without changing their operating conditions. Thus, they can be considered as steady-flow devices. Consequently, the mass flow rate of each fluid remains unchanged, and the fluid properties such as temperature and velocity at any inlet or outlet remain constant. Furthermore, there is little to no change in the velocities and elevations of the fluid streams, which means that the kinetic and potential energy changes are negligible. In general, specific heat of the fluid varies with temperature. However, within a certain temperature range, it can be considered a constant at some average value with little loss in accuracy. Typically, axial heat conduction along the tube is usually insignificant and can be considered negligible. Lastly, the heat exchanger's outside is assumed to be completely insulated, meaning that any heat transfer happens solely between the two fluids and that there is no heat loss to the surrounding medium.

The heat transfer rate, also known as the heat capacity or heat load, is a measure of the heat energy transferred in the heat exchanger per unit time. This is the most fundamental specification for describing heat exchanger performance. The idealizations stated above are closely approximated in practical applications and they significantly facilitate the analysis of a heat exchanger with little sacrifice from accuracy. Thus, they are commonly used. Under these assumptions, the first law of thermodynamics requires that the rate of heat transfer from the hot fluid be equal to the rate of heat transfer to the cold one, which can be described as,

$$\dot{Q}_{total} = \dot{m}_c c_{pc}(T_{c,outlet} - T_{c,inlet}) \tag{2.1}$$

and

$$\dot{Q}_{total} = \dot{m}_h c_{ph}(T_{h,inlet} - T_{h,outlet}) \tag{2.2}$$

where the scripts c and h denote cold and hot fluids, respectively, $\dot{m}$ represents the mass flow rate of the flow rate, c_p represents the specific heat of the fluid, T_{inlet} is the inlet fluid and T_{outlet} is the outlet fluid temperatures.

It should be noted that the heat transfer rate $\dot{Q}_{total}$ which is assumed to be a positive amount, is from the hot fluid to the cold one along with the second law of thermodynamics. The multiplication of mass flow rate and the specific heat of the fluid is the heat capacity rate in heat exchanger analysis. This heat capacity rate is defined for the cold and hot fluids as

$$C_c = \dot{m}_c c_{pc} \tag{2.3}$$

and

$$C_h = \dot{m}_h c_{ph} \tag{2.4}$$

Thus, the equations 2.1 and 2.2 become

$$\dot{Q}_{total} = C_c(T_{c,outlet} - T_{c,inlet}) \tag{2.5}$$

and

$$\dot{Q}_{total} = C_h(T_{h,inlet} - T_{h,outlet}) \tag{2.6}$$

2.2 Fundamental of convection

Convection is classified as forced convection and natural (or free), depending on how the fluid motion is initiated. In forced convection, the fluid is forced to flow over a surface or in a pipe by external means such as a pump or a fan. In natural convection, any fluid motion is caused by natural means such as the buoyancy effect, which manifests itself as the rise of warmer fluid and the fall of the cooler fluid. Convection is also classified as external and internal, depending on whether the fluid is forced to flow over a surface or in a pipe.

2.3 Internal forced convection

Gas or liquid passing through pipes or ducts is usually utilized in heating and cooling applications. In these applications, a fan or pump forces the fluid to pass through a flow section long enough to achieve the required heat transfer.

Circular cross section flow sections are generally referred to as pipes (particularly when the fluid is a liquid), while noncircular cross section flow sections are referred to as ducts (particularly when the fluid is a gas) can be seen in Fig. 2.4. Pipes with a small diameter are commonly called tubes.

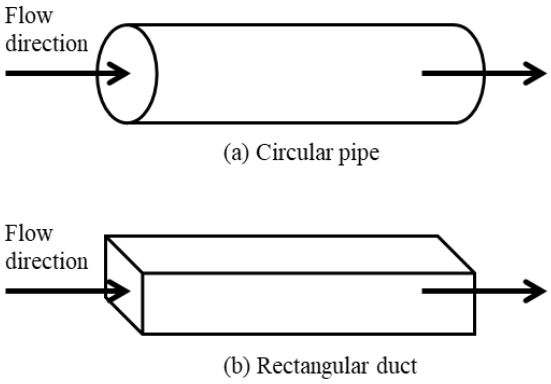

Figure 2.4. Internal forced convection caused by a fan or pump.

2.3.1 Laminar and turbulent flow in tubes

Flow in a tube can be laminar or turbulent based on the flow conditions. At low velocities, fluid flow is streamlined and hence laminar; but, as velocity increases beyond a threshold value, the flow becomes turbulent. The change from laminar to turbulent flow happens gradually over a range of velocities, with the flow

fluctuating between laminar and turbulent before reaching its full turbulent state. In practical applications, most pipe flows are turbulent. Laminar flow occurs when highly viscous fluids such as oils flow in small diameter tubes or narrow passages.

The Reynolds number is expressed as follows for flow in circular tubes.

$$Re = \frac{V_{avg}D}{v} = \frac{\rho V_{avg}D}{\mu} = \frac{\rho D}{\mu}\left(\frac{\dot{m}}{\rho\pi D^2/4}\right) = \frac{4\dot{m}}{\mu\pi D} \tag{2.7}$$

where V_{avg} is the average flow velocity, $v = \mu/\rho$ is the kinematic viscosity of the fluid and D is the diameter of the tube.

Reynolds number, Nusselt number, and the friction factor for flow in the noncircular tubes are based on the hydraulic diameter. It is defined as

$$D_h = \frac{4A_c}{p} \tag{2.8}$$

where A_c is the cross sectional area of the tube and p is its wetted perimeter. Therefore, for circular tubes, this hydraulic diameter equivalent to the ordinary diameter D.

It is desirable to know precise values of Reynolds numbers for laminar, transitional, and turbulent flows although this is not the case in practice. The reason is that the transition from laminar to turbulent flow also depends on the degree of disturbance of the flow by surface roughness, pipe vibrations, and fluctuations in the flow. It is stated that the flow in a tube is laminar for Re < 2300, fully turbulent for Re > 10,000, and transitional in between under most practical conditions.

2.3.2 Thermal analysis

In the absence of any work interactions, the conservation of energy equation for the steady flow of a fluid in a tube can be written as follows (Figure 2.5),

$$\dot{Q} = \dot{m}c_p(T_e - T_i) \tag{2.9}$$

where $\dot{Q}$ is the heat transfer rate to or from the fluid, T_i and T_e are the mean fluid temperatures at the inlet and exit of the tube, respectively.

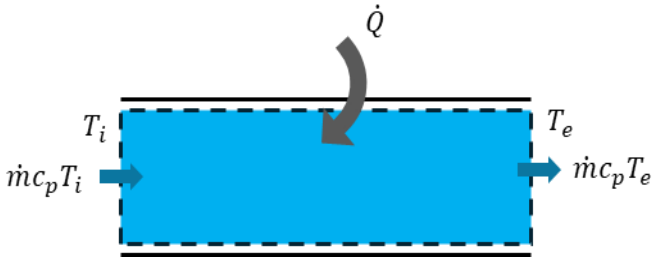

Figure 2.5. Heat transfer to a fluid flowing in a tube.

2.3.3 Pressure drop

Pressure drop (ΔP) is another quantity of interest in the analysis of pipe flow because ΔP is directly related to the power requirements of the fan or pump to maintain flow. Simply, pressure drop is the difference in total pressure between two points in a fluid-carrying network system.

$$\frac{dP}{dx} = \frac{P_1 - P_2}{L} \tag{2.10}$$

where P_1 is the pressure at the inlet tube, P_2 is the pressure at the outlet tube and L is the length of the tube.

With the V_{avg}, the pressure drop in laminar flow is regarded as

$$\Delta P = P_1 - P_2 = \frac{8\mu L V_{avg}}{R^2} = \frac{32\mu L V_{avg}}{D^2} \tag{2.11}$$

The symbol Δ is usually used to indicate the difference between the final and initial values, for example, $\Delta y = y_2 - y_1$. However, in fluid flow, ΔP is used to designate pressure drop, and thus it is $P_1 - P_2$.

From Eq. 2.11, it is noted that the pressure drop is proportional to the viscosity μ of the fluid. ΔP would be zero if there were no friction. Thus, the drop of pressure from P_1 to P_2 in this case is due entirely to viscous effects, and Eq. 2.11 represents the pressure loss ΔP_L when a fluid of viscosity μ flows through a pipe of constant diameter D and length L at average velocity V_{avg}.

Figure 2.6 shows the schematic diagram of pressure drop in a pipe. It is convenient to express the pressure loss for all types of fully developed internal flows (laminar or turbulent flows, circular or noncircular pipes, smooth or rough surfaces, horizontal or inclined pipes) as by the following equation.

$$\Delta P_L = f \frac{L}{D} \frac{\rho {V_{avg}}^2}{2} \tag{2.12}$$

where $\rho {V_{avg}}^2/2$ is the dynamic pressure and f is the Darcy friction factor and it can be expressed as

$$f = \frac{8\tau_w}{\rho {V_{avg}}^2} \tag{2.13}$$

where τ_w is the shear stress.

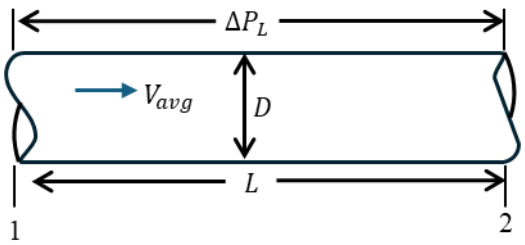

Figure 2.6. Schematic diagram of pressure drop in a pipe.

From Eq. 2.11 and Eq 2.12 equivalent and solving for f becomes friction factor for fully developed laminar flow in a circular tube as shown in Eq. 2.14. This equation shows that in laminar flow, the friction factor is a function of the Reynolds number only and is independent of the roughness of the pipe surface.

$$f = \frac{64\mu}{\rho D {V_{avg}}^2} = \frac{64}{Re} \tag{2.14}$$

Pressure losses in piping system analysis are typically stated in terms of the equivalent fluid column height, named head loss h_L. Since pressure drop $\Delta P = \rho g h$ and ΔP also equal to a fluid height of $h = \Delta P/\rho g$, the pipe head loss can be calculated by dividing ΔP_L by ρg to obtain

$$h_L = \frac{\Delta P_L}{\rho g} = f \frac{L}{D} \frac{{V_{avg}}^2}{2g} \tag{2.15}$$

The heat loss h_L presents the additional height that the fluid needs to be boosted by a pump to overcome the frictional losses in the pipe. Viscosity is the cause of the head loss, which is directly correlated with the wall shear stress. Equation 2.12 is valid for both laminar and turbulent flows in both circular and noncircular tubes. However, Eq.2.14 is valid only for fully developed laminar flow in circular pipes.

When the pressure loss or head loss is known, the required pumping power to overcome the pressure loss can be obtained from

$$\dot{W}_{pump,L} = \dot{V} \Delta P_L = \dot{V} \rho g h_L = \dot{m} g h_L \tag{2.16}$$

where $\dot{V}$ is the volume flow rate and $\dot{m}$ is the mass flow rate.

The average velocity for laminar flow in a horizontal tube of Eq. 2.11 becomes

$$V_{avg} = \frac{(P_1 - P_2)R^2}{8\mu L} = \frac{(P_1 - P_2)D^2}{32\mu L} = \frac{\Delta P\, D^2}{32\mu L} \tag{2.17}$$

Thus, the volume flow rate for laminar flow through a horizontal tube of diameter D and length L is

$$\dot{V} = V_{avg} A_c = \frac{(P_1 - P_2)R^2}{8\mu L} \pi R^2 = \frac{(P_1 - P_2)\pi D^4}{128\mu L} = \frac{\Delta P\, \pi D^4}{128\mu L} \tag{2.18}$$

2.4 Natural convection

Natural convection which is also called free convection is the motion that results from the interaction of gravity with density differences within a fluid. The differences may result from gradients in temperature, concentration, or composition. The fluid motion in forced convection is quite obvious as a fan or a pump can transfer enough momentum to the fluid to move it in a certain direction. However, the fluid motion in natural convection is often not noticeable because of the low velocities involved.

2.4.1 Physical mechanism of natural convection

The hot object can be cooled down naturally in the surrounding air temperature as shown in Fig. 2.7. When the hot object is exposed to cooler air, the temperature of the outside of the object will drop and the temperature of adjacent air to the object will rise. Consequently, the object is surrounded with a thin layer of warmer air and heat will be transferred from this layer to the outer layers of air. In this case, cooling occurs slowly because the object would always be blanketed by warm air and it has no direct contact with the cooler air located farther away.

The temperature of the air adjacent to the hot object is higher, thus its density is lower. As a result, the heated air rises. This movement is called the natural convection current. The heat transfer that is enhanced as a result of this natural convection current is called natural convection heat transfer. It should be noted that in the absence of this movement, heat transfer would be by conduction only and its rate would be much lower.

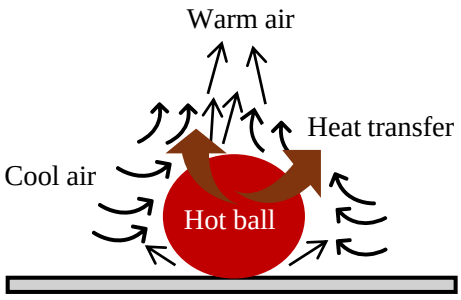

Figure 2.7. Cooling process of hot ball in cooler environment by natural convection.

A net force pushes upward a light fluid placed in a heavier fluid in a gravitational field. The buoyancy force is the upward force exerted by a fluid on a body completely or partially immersed in it. The magnitude of the buoyancy force is equal to the weight of the fluid displaced by the body. It can be expressed as,

$$F_{buoyancy} = \rho_{fluid}\, g\, V_{body} \tag{2.19}$$

where $\rho_{fluid}$is the density of the fluid, V_{body} is the volume of the portion of the body immersed in the fluid, and g is the gravitational acceleration.

When there are no other forces, the net vertical force acting on a body is the difference between the weight of the body and the buoyancy force. That is,

$$F_{net} = W - F_{buoyancy} = \rho_{body}\, g\, V_{body} - \rho_{fluid}\, g\, V_{body} \tag{2.20}$$

And Eq. 2.20 becomes

$$F_{net} = (\rho_{body} - \rho_{fluid})\, g\, V_{body} \tag{2.21}$$

This force is proportional to the difference in the densities of the fluid and the body immersed in it. Hence, a body immersed in a fluid will experience a "weight loss" in an amount equal to the weight of the fluid it displaces. This is known as Archimedes' principle.

In daily life, there are numerous applications of the buoyancy effect. This is because, without buoyancy, heat transfer between a cold (or hot) surface and the fluid around it would occur by condition instead of natural convection. Owing to buoyancy, the natural convection currents exited in the oceans, lakes, and the atmosphere. In addition, due to buoyancy, light boats and even heavy steel battleships float on water as can be seen in Fig. 2.8. The foundation of ship design is the idea that the total weight of a ship, including its cargo, equals the weight of water that the ship's submerged volume can hold.

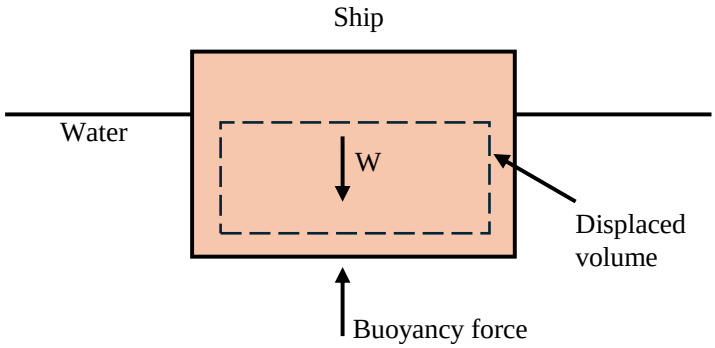

Figure 2.8. Buoyancy force keeps the ship floating in water ($W = F_{buoyancy}$ for floating objects).
(Source: Yunus A. Cengel and Afshin J. Ghajar. Heat and mass transfer. McGraw-Hill, 2015)

Temperature is the main variable in heat transfer studies, and it is desirable to represent the net buoyancy force (Eq. 2.21) in terms of temperature differences. However, this requires expressing the density difference in terms of a temperature difference, which requires a knowledge of a property that represents the variation of the density of a fluid with temperature at constant pressure. The volume expansion coefficient β, is the property that provides this information and can be defined as,

$$\beta = \frac{1}{V}\left(\frac{\partial V}{\partial T}\right)_P = -\frac{1}{\rho}\left(\frac{\partial \rho}{\partial T}\right)_P \tag{2.22}$$

At constant pressure, the volume expansion coefficient can be expressed approximately by replacing differential quantities by differences as

$$\beta \approx -\frac{1}{\rho}\frac{\Delta\rho}{\Delta T} = -\frac{1}{\rho}\frac{\rho_\infty - \rho}{T_\infty - \rho} \tag{2.23}$$

where ρ_∞ is the density and T_∞ is the temperature of the quiescent fluid away from the surface.

The volume expansion coefficient β of an ideal gas ($P = \rho RT$) at a temperature T is equivalent to the inverse of the temperature,

$$\beta_{ideal\ gas} = \frac{1}{T} \tag{2.24}$$

where T is the thermodynamic temperature. It should be noticed that a large value of β for a fluid means a large change in density with temperature and the product $\beta\Delta T$ represents the fraction of volume change of a fluid that corresponds to a temperature change ΔT at constant pressure. Moreover, the buoyancy force at constant pressure is proportional to the difference in density, which is proportional to the variation in temperature. Thus, the larger the temperature difference between the fluid adjacent to a cold(or hot) surface and the fluid away from it, the larger the buoyancy force and the stronger the natural convection currents, leading to a higher heat transfer rate.

The dimensionless Grashof number represents the ratio of buoyant forces to viscous forces. It can be described as

$$Gr = \frac{g\beta(T_s - T_\infty){L_c}^3}{v^2} \tag{2.25}$$

where

g is gravitational acceleration, m/s^2

β is coefficient of volume expansion, 1/K ($\beta = 1/T$ for ideal gas)

T_s is temperature of the surface, °C

T_∞ is temperature of the fluid sufficiently far from the surface, °C

L_c is characteristic length of the geometry, m

v is kinematic viscosity of the fluid, m^2/s

As mentioned before, the dimensionless Reynolds number represents the ratio of inertial forces to viscous forces acting on the fluid. On the other hand, The Grashof number controls the flow regime in natural convection, which presents the ratio of the buoyancy force to the viscous force acting on the fluid as shown in Fig. 2.9.

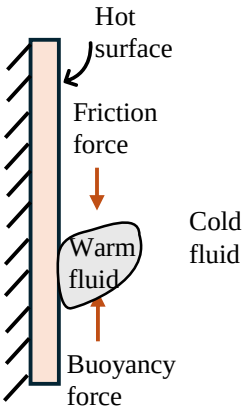

Figure 2.9. The Grashof number is a measure of the relative magnitudes of the buoyancy force and the opposing viscous force acting on the fluid.

Grashof number is important in natural convection while Reynolds number plays a key role in force convection. So, Grashof number can provide information in determining whether the fluid flow is laminar or turbulent. For instance, for vertical plates, the critical Grashof number is observed to be approximately 10^9. Hence, the flow regime on a vertical plate starts to become turbulent at Grashof numbers larger than 10^9.

2.4.2 Natural convection over surface

The orientation and shape of a surface affect the amount of heat transferred by natural convection. It also depends on the fluid's thermophysical characteristics and surface temperature fluctuations. An interferometer produces a map of interference fringes, which can be interpreted as lines of constant temperature as shown in Fig. 2.10. The smooth and parallel lines in Fig. 2.10 (a) show the flow is laminar, whereas the irregularities line in Fig. 2.10 (b) indicate that the flow is turbulent. Note that the lines are closest near the surface, indicating a higher temperature gradient [3].

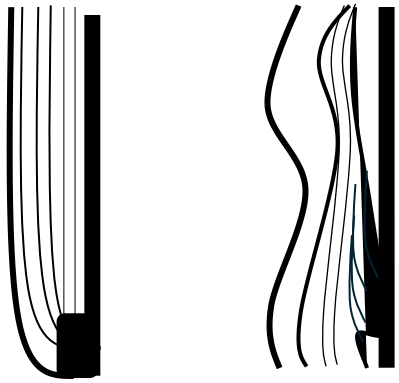

(a) Laminar flow (b) Turbulent flow

Figure 2.10. Isotherms in natural convection over a hot plate in air.
(Source: M. Necati Özisik, Heat transfer: a basic approach, McGraw Hill, 1985)

For another example of natural convection, the velocity and temperature profile for natural convection over a hot vertical plate are shown in Fig. 2.11.

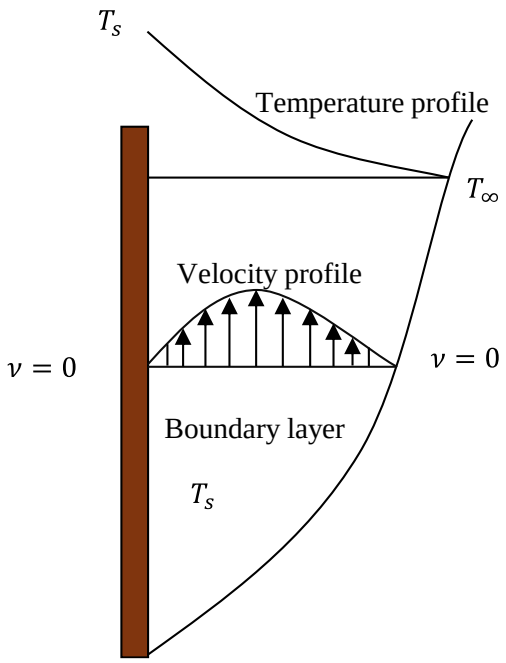

Figure 2.11. Typical temperature and velocity profiles for natural convection flow over a hot vertical plate.

The simple empirical correlations for the average Nusselt number Nu in natural convection can be expressed as

$$Nu = \frac{hL_c}{k} = C(Gr_L Pr)^a = CRa_L^a \tag{2.26}$$

where h is heat transfer coefficient (W/m^2·K), k is thermal conductivity of air at film temperature (W/m·K), Ra_L is the Rayleigh number, which is the product of the Grashof number, which explains the relationship between buoyancy and viscosity within the fluid. The Prandtl number, which describes the relation between momentum diffusivity and thermal diffusivity. C and n values are constant, and both of values depend on the geometry of the surface and the flow regime, which is determined by the range of Rayleigh number. The value of n is usually $\frac{1}{4}$ for laminar and $\frac{1}{3}$ for turbulent flow. Normally, the value of the constant C is less than 1.

The Rayleigh number can be expressed as

$$Ra_L = Gr_L Pr = \frac{g\beta(T_s - T_\infty){L_c}^3}{v^2} Pr \tag{2.27}$$

Table 2.1 presents simple relations for the average Nusselt number for several geometries. The characteristic lengths of the geometries and the ranges of Rayleigh number in which the relation is applicable are also provided. All fluid properties are to be evaluated at the film temperature $T_f = \frac{1}{2}(T_s + T_\infty)$.

Table 2.1. Empirical correlations for the average Nusselt number for natural convection over surfaces.

Geometry	Characteristic length, L_c	Range of Ra_L	Nu
Vertical plate 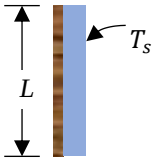	L	10^4-10^9 10^{10}-10^{13} Entire range	$Nu = 0.59Ra_L^{1/4}$ (2.28) $Nu = 0.1Ra_L^{1/3}$ (2.29) $Nu = \left\{0.825 + \frac{0.387Ra_L^{1/6}}{[1+(0.492/Pr)^{9/16}]^{\frac{8}{27}}}\right\}^2$ (2.30) (Complex but more accurate)
Inclined plate 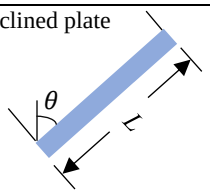	L		Use vertical plate equations for the upper surface of a cold plate and the lower surface of a hot plate. Replace g by $g\cos\theta$ for $0 < \theta < 60°$
Horizontal plate (Surface area A_s and perimeter p) (a) Upper surface of a hot plate (or lower surface of a cold plate) 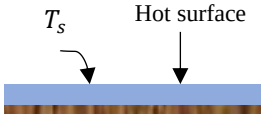 (b) Lower surface of a hot plate (or upper surface of a cold plate) 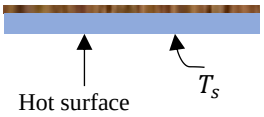	A_s/p	10^4-10^7 10^7-10^{11} 10^5-10^{11}	$Nu = 0.59Ra_L^{\frac{1}{4}}$ (2.31) $Nu = 0.1Ra_L^{1/3}$ (2.32) $Nu = 2.7Ra_L^{1/4}$ (2.33)
Vertical cylinder 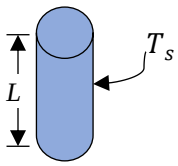	L		A vertical cylinder can be treated as a vertical plate when $D \geq \frac{35L}{Gr_L^{1/4}}$
Horizontal cylinder 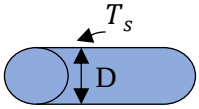	D	$Ra_D \leq 10^{12}$	$Nu = \left\{0.6 + \frac{0.387Ra_L^{1/6}}{[1+(0.559/Pr)^{9/16}]^{8/27}}\right\}^2$ (2.34)

Sphere 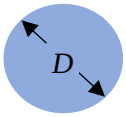	D	$Ra_D \leq 10^{11}$ ($Pr \geq 0.7$)	$Nu = 2 + \frac{0.589Ra_L^{1/4}}{[1+(0.469/Pr)^{9/16}]^{4/9}}$ (2.35)

When the average Nusselt number and hence the average convection coefficient is known, the rate of heat transfer by natural convection from a solid surface at a uniform temperature T_s to the surrounding fluid is described by Newton's law of cooling as

$$\dot{Q}_{conv} = hA_t(T_s - T_\infty) \quad (2.36)$$

where A_t is the heat transfer surface area and h is the average heat transfer coefficient on the surface.

Summary

It can be seen that different heat exchanger types are available depending on the purpose and applications to be used. For heat transfer enhancement in the heat exchanger, fins, plates are added to increase the heat transfer surface area. However, engineers and researchers utilized several heat exchangers designs according to their goals and applications. Moreover, natural convection is a heat transfer mode in which fluid motion results from the differences in density induced by thermal gradients, not external sources like fans or pumps. Hence, natural convection is heavily dependent on the temperature variations within the system.

Controlled greenhouse cultivation is famous for its benefits such as increased crop production and quality. On the other hand, the enormous energy consumption is a major drawback in greenhouse cultivation. Therefore, this thesis employed a simple shape serpentine heat exchanger for local climate control near the crops which is appropriate for greenhouse cultivation in humid areas. The serpentine heat exchanger is considered because it has a simple design, does not prevent sunlight, is easy to maintain, and is easy to handle near the crops for greenhouse cultivation.

References in chapter 2

[1] Yunus A. Cengel and Afshin J. Ghajar, Heat and mass transfer, McGraw Hill, 2015.

[2] Kuppan Thulukkanam, Heat Exchangers Classification, Selection, and Thermal Design, Taylor & Francis Group, 2024.

[3] M. Necati Özişik Heat transfer: a basic approach, McGraw Hill, 1985.

Chapter 3

Research methodology

3.1 Overall experimental procedure

This thesis focuses on periodic local climate control which is provided only near the crop area using serpentine copper tube heat exchanger. In particular, this thesis will evaluate the local air temperature near the crops as well as daily periodic temperature control. Furthermore, the theoretical energy requirements between the whole area control and local area control of the practical greenhouse will be addressed. The methodological flow chart of this thesis can be described as shown in Fig. 3.1.

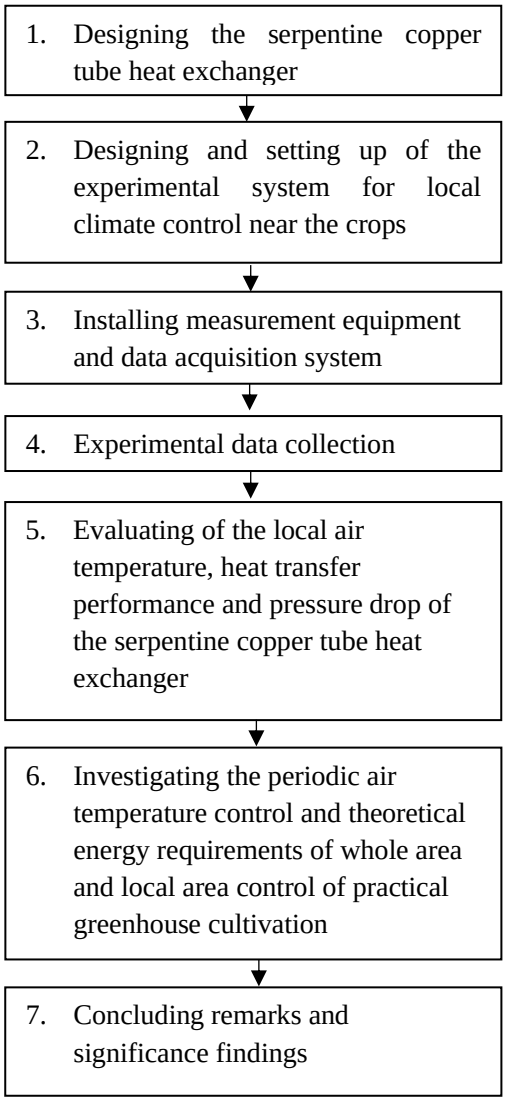

Figure 3.1. Methodological flow chart.

3.2 Overview concept of the experiment for temperature control in practical applications

The concept of the illustration for real greenhouse applications is shown in Fig. 3.2. For practical greenhouse applications in the future, heat exchangers can be installed both over and under the crop to provide cooling and heating alternately by switching the supplied fluid as shown in Fig. 3.2 (a) and Fig. 3.2 (b). In the cooling process, hot water is stored during the condensation stage. In contrast, cold water is stored during the evaporation stage of the refrigeration cycle. With reference to temperature control, hot and cold water are used as auxiliary sources for heating and cooling, respectively.

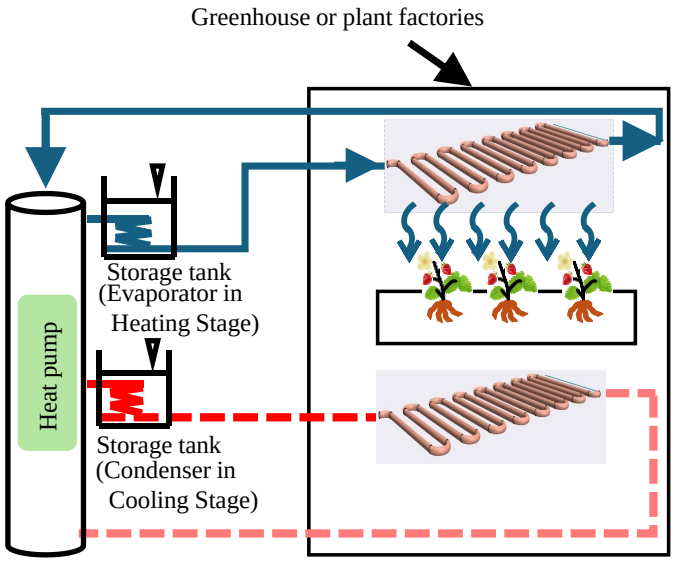

(a) Cooling

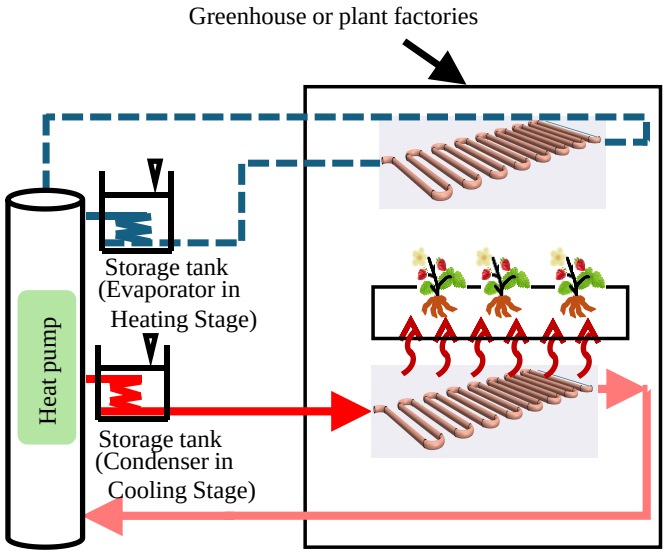

(b) Heating

Figure 3.2. Overview concept of periodic temperature control for cultivation.

3.3 Experiments in laboratory

As the goals of this thesis were to evaluate the local air temperature and periodic air temperature change using the serpentine heat exchanger near the crops, an experimental test rig was set up in the laboratory. Then, the experiments were performed in the laboratory.

3.3.1 Configuration of the heat exchanger

Figure 3.3 shows the arrangement of the copper tube heat exchanger. Copper tubes were arranged in a serpentine shape and used as a heat exchanger. Copper has been selected due to its excellent thermal conductivity. Moreover, it has better corrosion resistance than other metals. The outer diameter of the copper tube was 15.88 mm, with a thickness of 0.8 mm. The length and width of the heat exchanger were 700 and 253 mm, respectively, excluding the U-tube bends. The overall dimension of this heat exchanger can cover one small rectangular block area of the plantation. Moreover, this dimension is considered to be appropriate for creating low shade for the plants. The U-tube bends were insulated from the surrounding areas to evaluate the heat transfer exactly from the straight tubes.

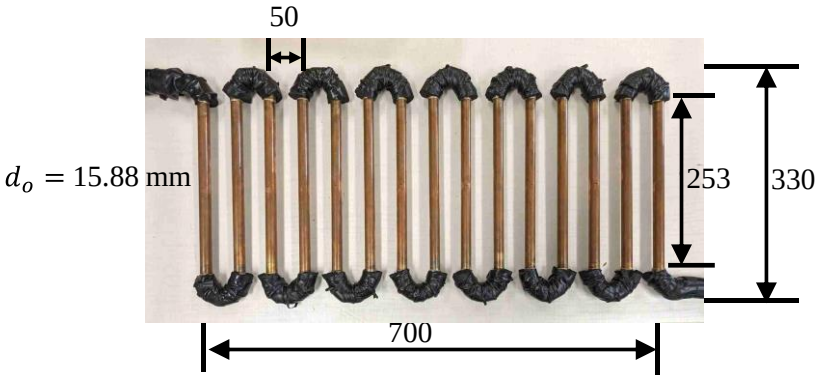

Figure 3.3. Serpentine copper tube heat exchanger (All units are in mm.).

3.3.2 Experimental system set-up

Figure 3.4 shows the experimental system setup. The dimensions of the experimental area are 1.4 m (W)× 0.7 m (D) × 1.0 m (H). In the experiments, the Shape 1 heat exchanger was set up at only one level, and the air temperatures at the area below and above the heat exchanger were evaluated. For this purpose, the aluminum frame was constructed and the heat exchanger was installed 0.5 m from the bottom surface of the experimental system. This experimental construction also considers for the replacement of other heat exchanger configurations in the same test section area so that different heat exchanger configurations can be replaced easily. The experimental system was enclosed in insulation foam, thereby reducing direct contact with the laboratory. The insulation foam is Styrofoam. The thermal conductivity of the Styrofoam is 0.036 W/m·K with 30 mm thickness.

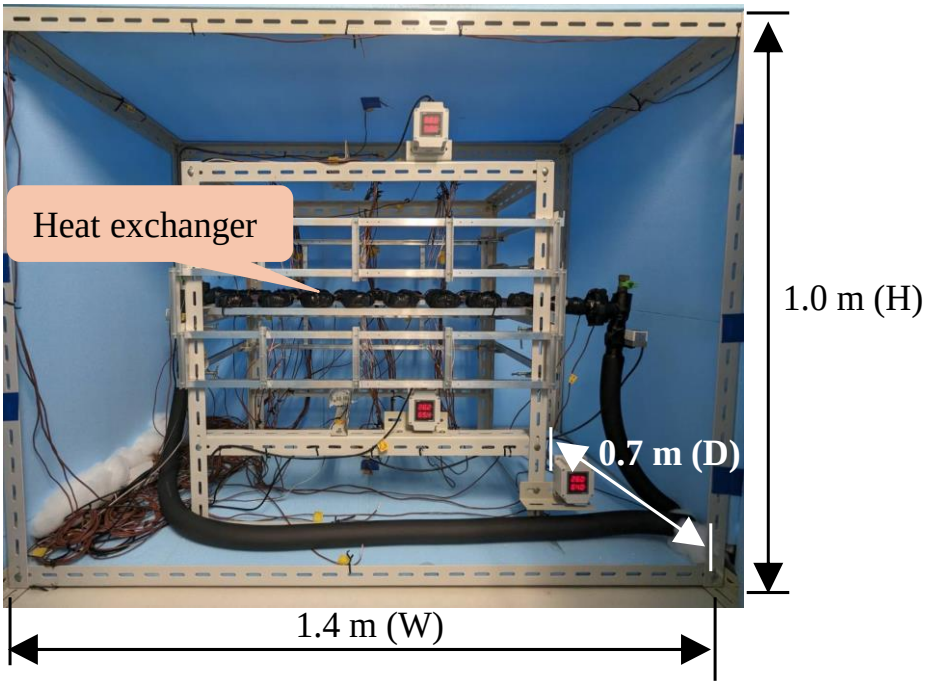

Figure 3.4. Overall dimension of the experimental system.

3.3.3 Data acquisitions

Figure 3.5 shows the local air temperature measurements at the area below and above the serpentine copper tube heat exchanger. The local air temperatures of the areas below and above the heat exchanger were measured by installing thermocouples in the vertical and horizontal planes. The positions of the thermocouples above the heat exchanger were indicated using (−) signs, whereas those below were indicated using (+) signs, because the airflow was downward owing to natural convection. Three layers each were considered above and below the heat exchanger. The layers below and above the heat exchanger were spaced at intervals of 50 mm, with the heat exchanger at the center. In total, 54 thermocouples were used, wherein nine thermocouples were positioned in each layer. The uncertainty in the vertical positions of the thermocouples was ±2 mm.

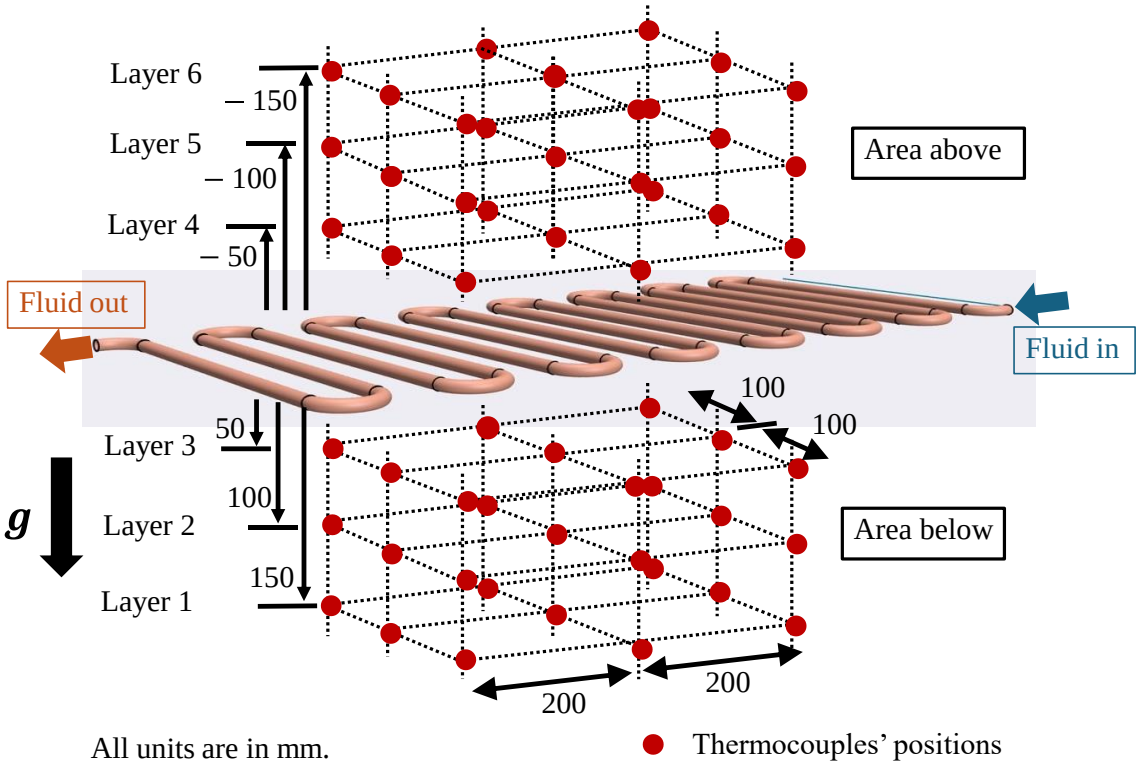

Figure 3.5. Schematic diagram of air temperature measurement are below and above the heat exchanger.

Figure 3.6 shows physical photos of thermocouples positions at the each vertical layer. Figure 3.6 (a) presents the thermocouples positions at the area below the heat exchanger and Fig. 3.6 (b) shows the thermocouples positions at the area above the heat exchanger. A detailed explanation of thermocouples' positions and installation is shown in the previous figure.

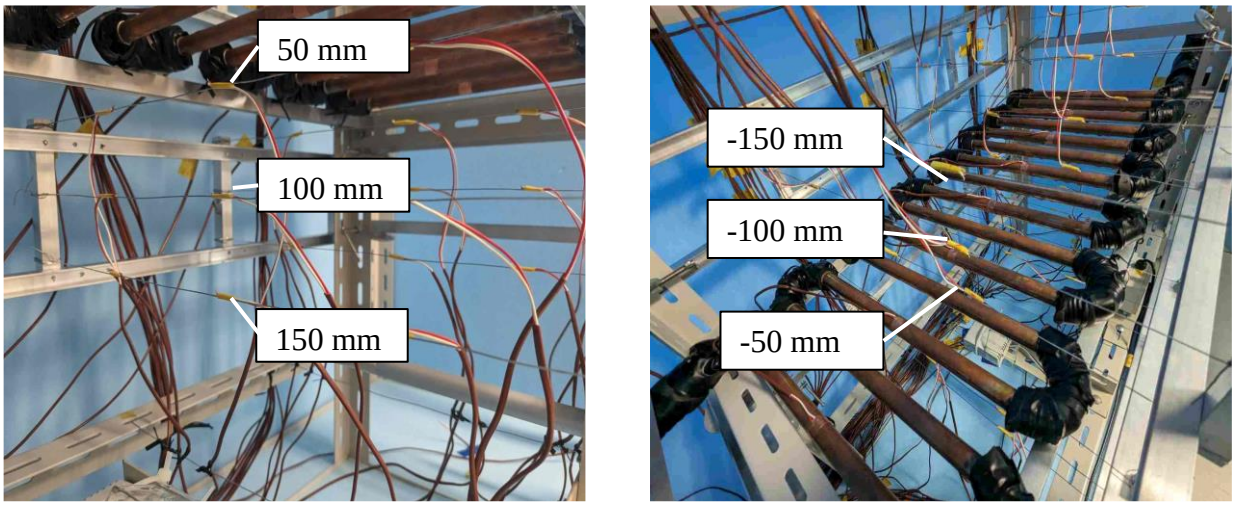

(a) Area below (b) Area above

Figure 3.6. Physical thermocouples setup and positioning at the area below and above the heat exchanger.

Figure 3.7 shows the upper and lower air temperature measurements in the experimental system. To monitor the air temperature far away from the heat exchanger, four thermocouples were placed near the ceiling

and floor area of the experimental system, respectively. The thermocouples are 450 mm vertically away from the heat exchanger for ceiling and floor area, correspondingly.

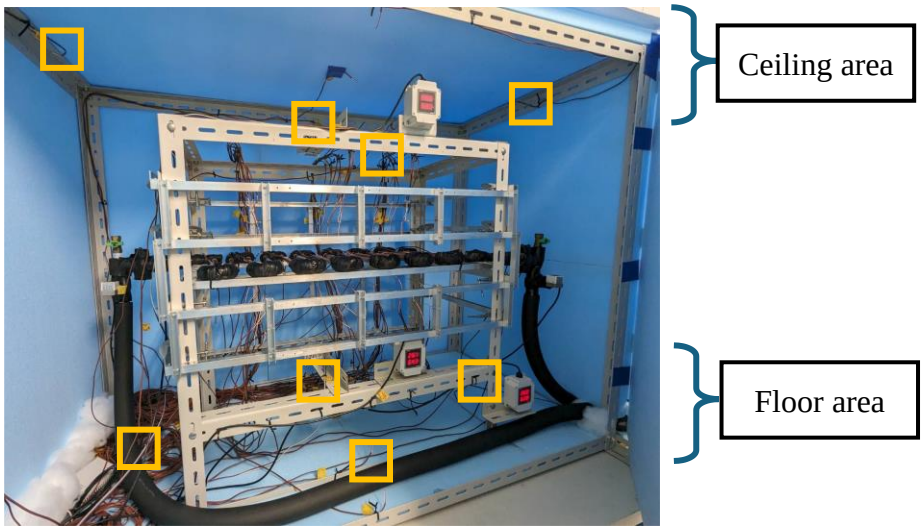

Figure 3.7. Upper area and lower area air temperature measurement in the experimental system.

A schematic diagram of the experimental system is shown in Fig. 3.8. The experimental system consists of a serpentine copper tube heat exchanger, a chiller to supply cool/hot fluid, a flow meter, a pressure difference sensor, thermocouples, and humidity sensors. A globe valve is used to adjust the flow rate. To reduce the water freezing temperature, ethylene glycol (40% by volume) was mixed into water (60% by volume). This water fluid was used as a working fluid in this thesis. Figure 3.9 shows the overall view photo of the experimental system including data loggers and the chiller.

Experimental data were collected using three data loggers. Because several thermocouples were used in this experiment, the temperatures were calibrated before the experimental period. This was done to reduce the inaccuracy of the temperature measurements. The reference thermocouple was carefully chosen and remained at a stable temperature. After that, the other thermocouples were calibrated based on the reference thermocouple.

The flowmeter was calibrated by manually weighing a precise amount of water and measuring the time required for the water to flow through the flowmeter.

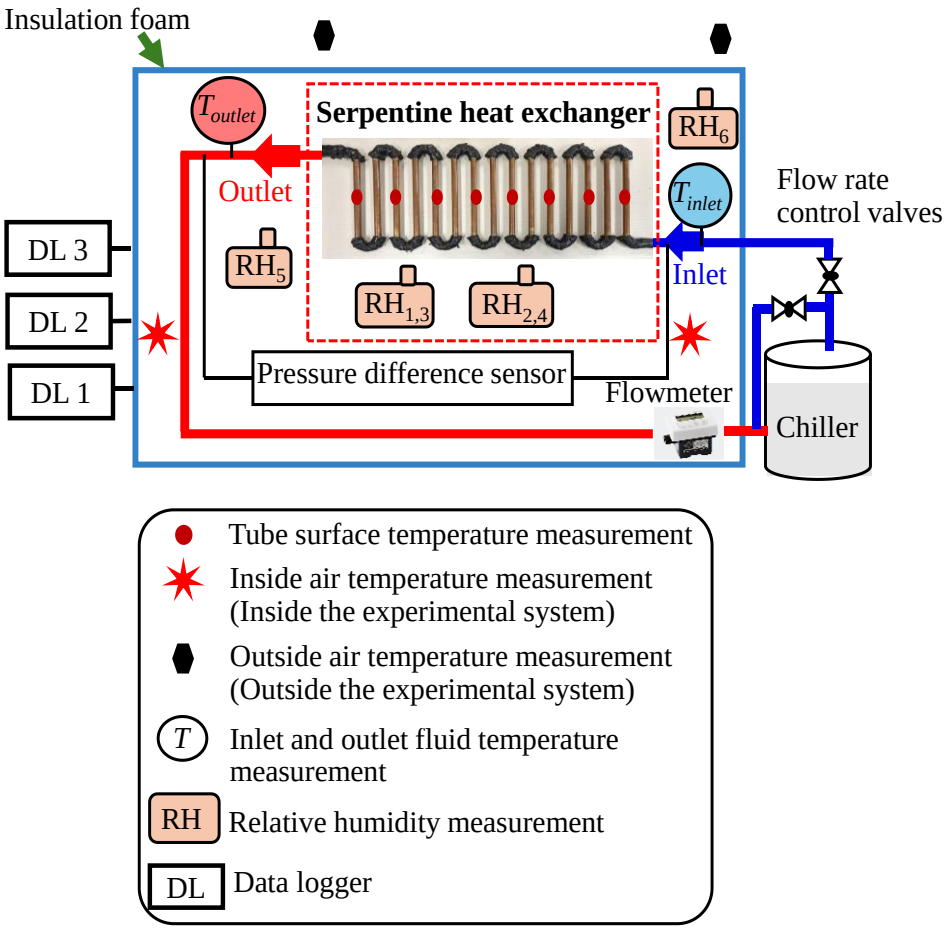

Figure 3.8. Layout of the experimental system.

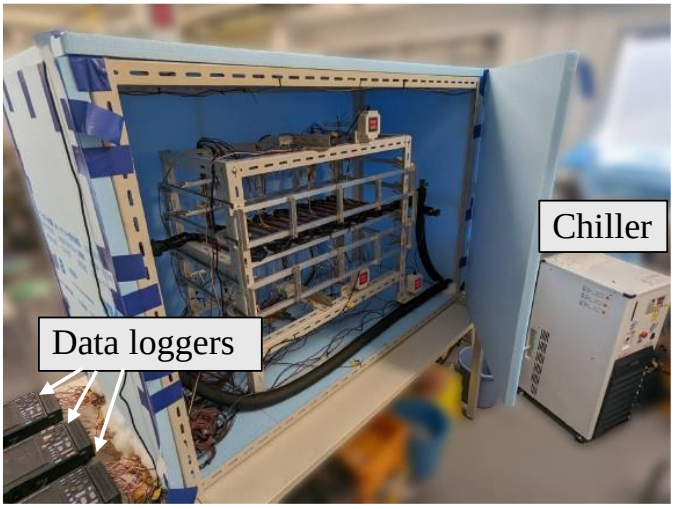

Figure 3.9. Overall view of the experimental system including data loggers and chiller.

Data loggers used in this thesis are Hioki 8422-50 data loggers and GL 840 WV data logger. Figure 3.10 shows the picture of Hioki 8422-50 data logger and Table 3.1 lists the specification of Hioki data logger. Hioki data logger allows for the measurement of temperature, voltage, pulse cumulation, rotations and humidity.

Input channels such as analog 32 channels and pulse inputs 4 channels are available. Many thermocouple types including type K, E, J, T, N, W (WRe5-26), R, S, and B can be measured.

Figure 3.10. Hioki 8422-50 data logger.

Table 3.1. Specifications of Hioki 8422-50 data logger.

Item	Description
Model	Hioki 8422-50
Measurement items	Temperature, voltage, pulse cumulation, rotations, humidity
Input channels	Analog 32 channels isolated PHOTO-MOS relays Pulse Inputs: 4 channels Logic Inputs: 16 channels (using the 8993 DIGITAL I/O UNIT)
Thermocouple types	K, E, J, T, N, W (WRe5-26), R, S, and B
Analog voltage input	4 ranges: 100 mV, 1 V, 10 V, 100 V and 1-5 V f.s.
Recording interval	100 ms to 1 hour (200 ms to 1 hour when using more then 17 channels). Note: All input channels are scanned at high speed during each recording interval.
Digital filter	Off /50 Hz/60 Hz (when set to 50 or 60 Hz), the appropriate digital filter is automatically set according to the recording interval
Memory capacity	Internal: 32 MB (16 MW data points) External: up to 528 MB (Flash ATA Card)
Power Supply	(1) 9418-15 AC ADAPTER

Item	Description
	(2) 9447 BATTERY PACK (NiMH, when used with AC adapter, the adapter has priority)

In this thesis, GL840 data logger is also employed to measure the fluid temperature with the Resistance thermal detectors (RTD). Figure 3.11 shows GL840-WV data logger and Table 3.2 shows the specifications of this data logger. This GL 840 data logger accommodates a wide variety of measurements. The GL840 is a compact, lightweight, multi-channel, and multi-purpose data logger with a 7-inch color display.20-channels measurements are available with the standard terminal or Withstand high-voltage high-precision terminal, and 200-channels measurements are available with the extension terminal base. In addition, when connecting various modules, the voltage, temperature and humidity as well as the acceleration, AC current, CO_2, and illuminance / ultraviolet etc. can be measured.

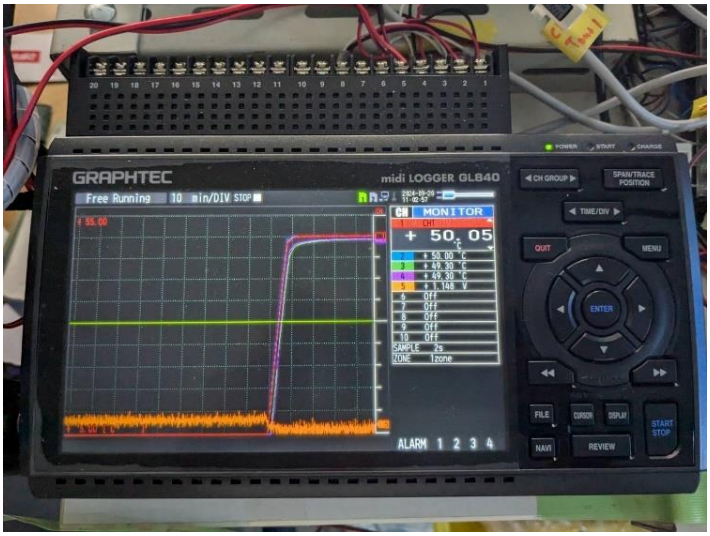

Figure 3.11. GL840-WV midi logger.

Table 3.2. Specifications of the GL 840 data logger.

Item	Description
Model	GL840-WV
Number of analog input channels	20 channels in standard configuration, Expandable up to 200 channels
Sampling interval	10 ms to 1 hour (10ms to 50ms: voltage only), External signal
Operating environment	0 to 45 ºC, 5 to 85 % RH (non condensed) (When operating with battery pack 0 to 40 ºC, charging battery 15 to 35 ºC)

Item		Description
Power source	AC adapter	100 to 240 V AC, 50/60 Hz (1 pc of adapter is attached as standard accessory)
	DC power	8.5 to 24 V DC (DC drive cable (option B-514) is required)
	Battery pack	Mountable battery pack (battery pack (option B-569): 7.2V DC, 2900mAh)
External dimensions (W × D × H in mm, Excluding projections)		Approximately 240 × 166 × 52.5 (Excludes AC adapter and battery pack)
Weight		Approximately 1035 g

3.3.4 Specifications of sensors and equipment

Table 3.3 lists the specifications of the measuring devices used in the study. Fundamental sensor specifications were employed to ensure accuracy during data collection. T-type thermocouples were used to measure the air temperatures and tube surface temperatures. Resistance thermal detectors (Pt 100) were used to measure the inlet and outlet fluid temperatures to obtain the fluid temperature difference. Since the heat flux of the heat exchanger was estimated from the fluid temperature difference, resistance thermal detectors are suitable to achieve reliable and accurate fluid temperature. Resistance thermal detectors were calibrated from the initial temperature difference before the experimental period. A differential pressure sensor (GC 50) was installed to measure the pressure drop in the system. Additionally, the flow rate was also measured. Relative humidity was monitored as a reference.

Table 3.3. Specifications of the measuring devices.

Parameters	Device	Accuracy	Measurement range
Air temperature	Thermocouple (T-type)	Class 2	−250 to 350 °C
Fluid temperature	Resistance thermistor (Pt 100)	JIS[*1] class A	−50 to 200 °C
Differential pressure	Pressure sensor (GC 50, Nagano Keiki)	±(1.0% FS[*2]+ 1 digit) at 23 °C	0 to 20 kPa
Flow rate	Flow meter (NW05- NTN, Aichi Tokei Denki)	±2% RS[*3]±0.05 L/min	0.3 to 3.0 L/min
Relative humidity (RH)	Humidity sensors THD-DD2-V, Autonics; THD-R-V, Autonics	±2% RH [*4]; ±3% RH [*4]	0 to 99%, 0 to 99%

*1 Japanese Industrial Standard.

*2 Full-scale.

*3 Reading scale.

*4 At room temperature 23°C±5°C.

3.3.4.1 Temperature measurement

As shown in Fig. 3.12, T-type thermocouples are used to measure the air temperatures and tube surface temperatures. One wire is made of copper, and the other is constantan (an alloy of copper and nickel). T-type thermocouples are suitable for measuring temperatures in the range of −250°C to 350°C.

Figure 3.12. T-type thermocouple.

Figure 3.13 shows the photos of resistance thermal detectors and their installation for measuring inlet and outlet fluid temperatures. Figure 3.13 (a) presents the Pt 100 resistance thermal detector. This sensor is used to measure the inlet and outlet fluid temperature of the heat exchanger. This sensor is a platinum resistance thermometer sensor with an extremely thin protective tube so it is suitable for precise temperature measurements such as minor temperature changes. Figures 3.13 (b) and (c) illustrate the physical photos of inlet and outlet fluid temperature measurements with resistance thermal detectors. Table 3.4 shows the general specifications of the resistance thermal detector.

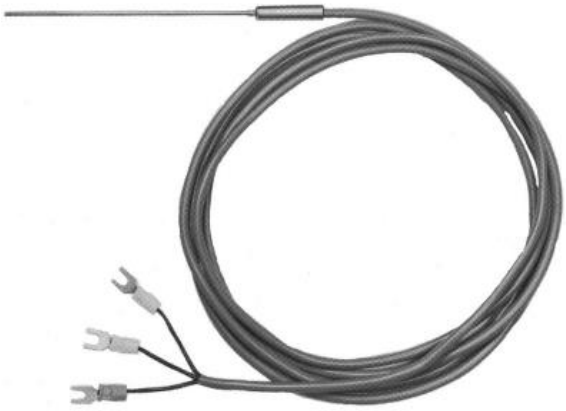

(a) Resistance thermal detector

(b) Physical photo of inlet fluid temperature measurement

(c) Physical photo of outlet fluid temperature measurement

Figure 3.13. Photos of resistance thermal detector.

Table 3.4. General specifications of resistance thermal detector.

Element	**Pt 100, three-wire type**
Rated current	2 mA
Class	JIS class A
Material of probe tube	SUS316
Response	Room temperature, Boiling water (100 °C) About 1.5 seconds

3.3.4.2 Pressure drop measurement

In this thesis, pressures difference sensor (GC 50) was used to measure the pressure drop in the heat exchanger. Figure 3.14 shows the GC 50 sensor and Table 3.5 list the specification of the GC 50 sensor. GC 50 is a multifunctional digital differential pressure gauge with a liquid-filled highly sensitive silicon capacitance sensor for detecting micro differential pressure featuring sensor module consisting of stainless diaphragm for wetted parts. This can be used for a variety of pressure media (gases and fluids).

Figure 3.14. GC 50 multifunctional digital differential pressure gauge.

Table 3.5. Specifications of GC 50 multifunctional digital differential pressure gauge.

Model	**GC 50 (Multifuctional digital differential pressure guage)**
Media	Gases and fluids (Not corrosive to the wetted material)
Differential pressure range	0 to 20 kPa
Indication accuracy	±(1% F.S.+1 digit) at 23 ºC
Power supply	24 V DC±10% Withstand voltage: 500V AC50/60 Hz
Model type	Current output (2 wire system)
Operating fluid temperature	−10 to 70 °C (Non-freezing)
Operating temperature and humidity	−10 to 50 °C, 10 to 85 % RH (Non-freezing and condensing)
Weight	Main display body only: Approximately 520 g

3.3.4.3 Volume flow rate monitoring

The fluid circulation was monitored with the flow meter sensor as the volume flow rate is one of the important parameters for evaluating the heat transfer rate. The flow meter sensor (NW05- NTN) was used in this thesis as shown in Fig.3.15. The sensor is a digital display and its flow rate range is 0.3 to 3.0 L/min. The detail of the specification of flow meter is shown in Table 3.6.

Figure 3.15. Flow meter sensor.
(Source: https://www.aichitokei.co.jp/products/flowsensor/nw/)

Figure 3.16 shows the globe valve used for the experimental system. The flow rate was controlled by using globe valve. The globe valve was installed near the chiller system so that it is easy for open/closed manually.

Figure 3.16. Globe valve for controlling flow rate.

Table 3.6. Specifications of flow meter sensor.

Model	**NW05-NTN**
Flow rate range	0.3 to 3.0 L/min
Accuracy	±2% RS±0.05 L/min (At the standard installation positions)

Model	NW05-NTN
Fluid viscosity range	0.5 to 1.5 mPa·s (equivalent to water)
Fluid temperature rage	0 to +60°C (should not get frozen)
Ambient temperature/ humidity	0 to +60 ºC/ 35 to 85%RH (No condensation)
Maximum working pressure	1 MPa (at the fluid temperature of 20 ºC)
Power supply	Lithium battery (Battery life: Approximately 4 years, battery not replaceable)
Output	Digital display
Weight	Approximately 280 g

3.3.4.4 Relative humidity monitoring

Relative humidity monitoring is captured by using THD series models in this thesis. One model is with display (THD-DD2-V) and another model is without display (THD-R-V) as shown in Figure 3.17. The humidity sensor with display was mounted in order to check the humidity during the experiments. Along with the air temperature, relative humidity is one of the crucial variables in crop cultivation. However, in this thesis, relative humidity is monitored as a reference. The relative humidity was monitored both in the area below and above the heat exchanger as shown in Figs. 3.17 (a) and (b). The positions of the humidity sensors were 300 mm away from the heat exchanger in the area below whereas that of the humidity sensors were 500 mm from the heat exchanger in the area above. The specifications of the humidity sensors are shown in Table 3.7. The humidity sensors have a range of 0.0 to 99.9% RH.

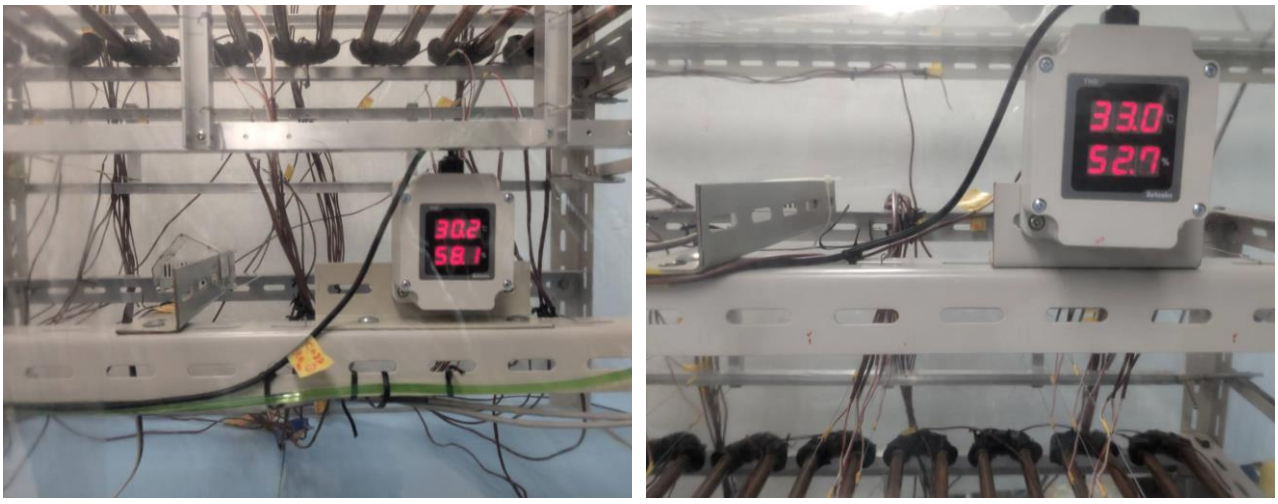

(a) Humidity sensors in the area below (b) Humidity sensors in the area above

Figure 3.17. Humidity sensors photo.

Table 3.7. Specifications of the humidity sensors.

Model	**THD-DD2-V**	**THD-R-V**
Power supply	24 VDC	
Power consumption	Maximum 2.4 Watts	
Display type	7 Segment LED display	Non-display
Measuring range	0.0 to 99.9%	
	±2% RH at room temperature	±3% RH at room temperature
Output	1-5 VDC	
Resolution	1/1000	
Environment (Ambient temperature)	−20 to 60 °C	
Weight	160 g	55 g

The chiller is used to produce cool or hot water fluid and circulate it in the experimental system. The chiller model is NCC-3000D and it is an EYELA product. This chiller can provide not only cooling but also heating conditions. The temperature range is from –10 to 80 °C. Figure 3.18 shows the chiller and the specifications of the chiller are shown in Table 3.8.

Figure 3.18. NCC-3000 D chiller.

Table 3.8. Specifications of NCC-3000 D chiller.

Product Name		**Chiller (Low temperature constant temperature water circulation device)**
Model		NCC-3000D
Circulation method		Closed system circulation
Temperature setting range/accuracy		−10 to 80 °C/±0.1 to 0.2 °C
Cooling capacity (at liquid temperature)	30°C	1680 W
	10°C	1240 W
	−10°C	600 W
External Circulation Nozzle		Outlet and return ports (Rc3/8 female thread) 14mm outer diameter hose port
Heater		2kW
Freezer/refrigerant		Water-cooled output 550W/R410A
Water tank capacity		3.5 L
Ambient temperature range		5 to 35 °C
External dimension (mm)		340 W × 440 D × 850 H,
Weight		Approximately 55 kg
Power-supply voltage		AC200V single phase 50/60Hz

3.4 Experimental conditions and procedure

Cooling experiments were performed at inlet fluid temperatures T_{inlet} of −5 to 10 °C, whereas heating experiments were performed at 30 to 50 °C. The flow rate $\dot{V}$ was varied from 0.3 to 3.0 L/min at each T_{inlet}. These experimental conditions are shown in Tables 3.9 (a) and (b). The Reynolds numbers were 50 < Re < 1,100 and 26 < Re < 3,480 for the cooling and heating processes, respectively. The ambient temperature was set to approximately 25 and 20 °C for cooling and heating, respectively. The fluid mixture in this thesis comprised 60% water and 40% ethylene glycol by volume to lower the freezing point under −20°C.

Based on a previous study, a flow rate lower than 3.0 L/min is sufficient because the local temperature profile does not markedly change at flow rates higher than 3.0 L/min [1].

When this heat exchanger is used in real greenhouse cultivation, several heat exchangers can be connected in parallel (parallel connection) and next to each other (series connection). Low flow rates ($\dot{V}$= 0.3 to 1.3 L/min) can be used for each heat exchanger when the heat exchangers are connected in parallel. High flow rates ($\dot{V}$ = 1.5 to 3.0 L/min) are considered suitable for the heat exchangers in series in real greenhouse cultivation, because the temperature drop in each section becomes low.

Table 3.9. Experimental conditions.

(a) Cooling conditions

Inlet fluid temperature −5 °C		**Inlet fluid temperature** 0 °C		**Inlet fluid temperature** 5 °C		**Inlet fluid temperature** 10 °C	
No.	**Fluid flow rate (L/min)**	**No.**	**Fluid flow rate (L/min)**	**No.**	**Fluid flow rate (L/min)**	**No.**	**Fluid flow rate (L/min)**
1	0.3	11	0.3	21	0.3	31	0.3
2	0.5	12	0.5	22	0.5	32	0.5
3	0.7	13	0.7	23	0.7	33	0.7
4	0.9	14	0.9	24	0.9	34	0.9
5	1.1	15	1.1	25	1.1	35	1.1
6	1.3	16	1.3	26	1.3	36	1.3
7	1.5	17	1.5	27	1.5	37	1.5
8	2.0	18	2.0	28	2.0	38	2.0
9	2.5	19	2.5	29	2.5	39	2.5
10	3.0	20	3.0	30	3.0	40	3.0

(b) Heating conditions

Inlet fluid temperature 30 °C		**Inlet fluid temperature** 40 °C		**Inlet fluid temperature** 50 °C	
No.	**Fluid flow rate (L/min)**	**No.**	**Fluid flow rate (L/min)**	**No.**	**Fluid flow rate (L/min)**
1	0.3	11	0.3	21	0.3
2	0.5	12	0.5	22	0.5
3	0.7	13	0.7	23	0.7
4	0.9	14	0.9	24	0.9
5	1.1	15	1.1	25	1.1
6	1.3	16	1.3	26	1.3
7	1.5	17	1.5	27	1.5
8	2.0	18	2.0	28	2.0
9	2.5	19	2.5	29	2.5
10	3.0	20	3.0	30	3.0

Reynolds number Re was calculated using Eq. 3.1.

$$Re = \frac{\rho_{fluid}\, v\, d_{inner}}{\mu} \tag{3.1}$$

where, ρ_{fluid} denotes the fluid mixture density (kg/m^3), v denotes the fluid velocity (m/s), d_{inner} denotes inner copper tube diameter (m) and μ denotes the dynamic viscosity of the fluid (Pa·s).

The experimental procedures are as follows:

(1) Before the experimental days, the laboratory room temperature was set at 25 and 20 °C for cooling and heating conditions, respectively but for periodic air temperature experiments the laboratory temperature was setup at 25 °C during the experimentation period.
(2) Later, the chiller was turned on.
(3) The chiller temperature is then setup to obtain the inlet fluid temperature.
(4) Then, flow rate is adjusted by using the globe valve.
(5) After the fluid temperature and flow rate were reached at the desired experimental set point, the data were collected.
(6) The evaluation of the experimental data was performed under the steady state conditions.

Heat flux in the heat exchanger

To estimate the heat flux in the heat exchanger, the temperature gradient close to the heat transfer surface of the copper tube should be measured at the exact position. However, copper tube diameter is quite small, and it may bring inaccurate temperature gradient measurement. And the heat flux in this serpentine copper tube heat exchanger comes only from natural convection. Moreover, the overall heat transfer from the copper tubes possibly be uniform since the inlet and outlet temperature difference is small in this heat exchanger. Thus, the heat flux was estimated from the fluid temperature difference ΔT_f between the inlet T_{inlet} and outlet T_{outlet} under steady-state conditions by following Eq. 3.2.

$$\dot{q}_a = \frac{\rho_{fluid}\ \dot{V} c_{pf}\ \Delta T_f}{A_s} \tag{3.2}$$

where $\dot{q}_a$ denotes the heat transfer from the copper tube surfaces (W/m^2), $\dot{V}$ denotes the volumetric flow rate of the fluid mixture (m^3/s), c_{pf} denotes the specific heat of the fluid mixture [J/(kg·K)], A_s denotes the outer surface area of the copper tube, except for U-bends (m^2) and $\Delta T_f = |T_{outlet} - T_{inlet}|$ is the absolute fluid temperature difference in the heat exchanger (°C). The tube surfaces at the U-bends were covered with insulation material.

From the experiments, the T-type thermocouple has uncertainty of ±0.2 °C while resistance thermal detector has uncertainty of ±0.02 °C. The thermal detector uncertainty is taken into account when the heat flux was evaluated.

External convective heat transfer coefficient (natural convection)

The external convective heat transfer coefficient over the surface of the horizontal cylinder can be calculated as Eq. 3.4.

$$Nu = \left\{0.6 + \frac{0.387Ra_L^{1/6}}{[1 + (0.559/Pr)^{9/16}]^{8/27}}\right\}^2 \tag{3.3}$$

$$h_a = \frac{Nu\ k}{d_{outer}} \tag{3.4}$$

where, Nu is the Nusselt number of natural convection (dimensionless), Ra_L is the Rayleigh number (dimensionless), is the Prantl number (dimensionless), h_a is the external convective heat transfer coefficient (W/m^2·K), k is the thermal conductivity of air at film temperature (W/m·K) and d_{outer} is the outer diameter of the tube (m).

Internal convective heat transfer coefficient

The internal convective heat transfer coefficient in a straight tube was calculated using Eq. 3.6.

$$Nu_i = 3.66 + \frac{0.065\left(\frac{d_{inner}}{L}\right)Re\ Pr}{1 + 0.04[\left(\frac{d_{inner}}{L}\right)Re\ Pr]^{2/3}} \tag{3.5}$$

$$h_f = \frac{Nu_i\ k_f}{d_{inner}} \tag{3.6}$$

where, Nu_i is the Nusselt number of internal force convection (dimensionless), L is the length of the tube (m), h_f is the internal convective heat transfer coefficient (W/m^2·K) and k_f is the thermal conductivity of working fluid (W/m·K).

References in chapter 3

[1] N. Khammayom, N. Maruyama, C. Chaichana, M. Hirota, Experimental analysis of local air temperature and thermal performance of a serpentine copper pipe, Energy Report, pp .653–661, 2023.

Chapter 4

Results and discussion

In control environment agriculture, greenhouse and plant factory cultivations are well-known because the high quality and quantity of crops can be obtained. Environmental control systems such as cooling /heating systems are required to control the desirable climate for crops in greenhouse cultivation. These environmental control systems are employed and control the environment especially the air temperature for the overall area of the greenhouse. In terms of energy consumption, the energy use is enormous when the environmental control systems are used in the agricultural greenhouse section. The huge energy consumption is still an issue.

Many technologies and approaches are innovated to solve the high energy consumption for cultivating in the greenhouse. One method for reducing energy consumption is to provide local climate control near the crop areas. This thesis introduces a simple design, easy-maintenance, easy-to-handle, and low-cost serpentine copper tube heat exchanger. Copper tubes are assembled in the shape of serpentine and used as a heat exchanger. The serpentine copper tube heat exchanger will not prevent the sunlight for the crops. The serpentine heat exchanger is considered for installation near the crop area. This means the environment far away from the crop remains constant since the environment near the crops is important for the crops.

In this chapter, first, the local air temperature profile of the serpentine copper tube heat exchanger for cooling and heating, respectively was investigated. Moreover, the heat exchanger's performance is important. Thus, the heat flux and pressure drop in the heat exchanger were examined for cooling and heating correspondingly.

The main objective of this thesis is to evaluate the periodic air temperature field control for local climate area crop cultivation. At last, the energy requirement was theoretically estimated for the whole area and local area control of greenhouse crop cultivation. Then, the theoretical energy requirements of the whole area and local area control crop cultivation were analyzed and compared.

4.1 Local air temperature

The thermocouple positions in each layer are shown in Fig 4.1. The local air temperature contour for each vertical layer horizontally was plotted based on the area marked in Fig 4.1. A total of six layers were installed where three layers for the area above and below the heat exchanger, correspondingly.

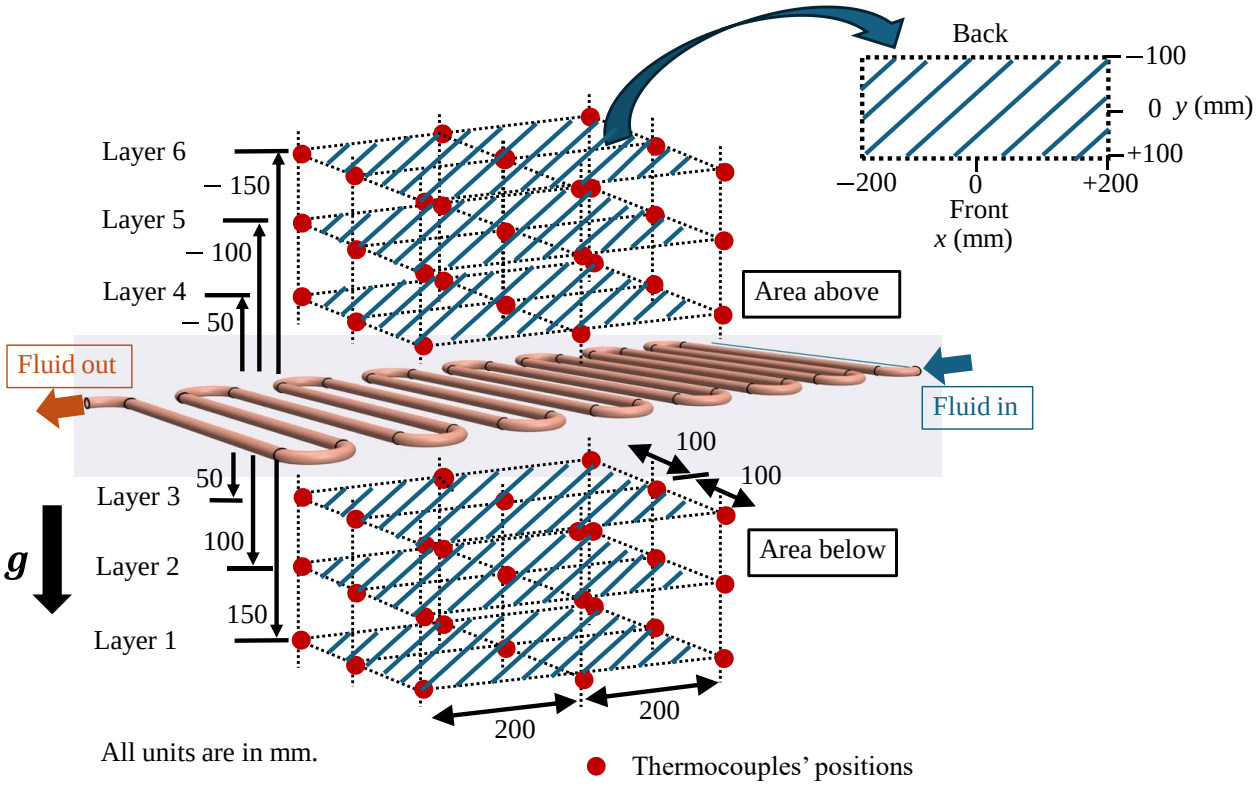

Figure 4.1. Configuration for air temperature measurements in each layer around the heat exchanger.

4.1.1 Local air temperature profile (cooling)

Contour graphs are used to visualize the local air temperature profile. The contours are plotted according to the area marked in Fig. 4.1, that is, the horizontal plane in the vertical direction of the heat exchanger. Figure 4.2 depicts the local air temperature contours for each layer at all experimental cooling conditions under steady state. The initial air temperature is approximately 22 °C. The color gradients illustrate the variations in the local air temperatures of all layers. At T_{inlet}= −5 °C, the local air temperature of all three layers color at the area below the heat exchanger is blue approximately 13°C. When T_{inlet} increases from −5 to 0, 5, and 10 °C, the contour color gradually changes from blue to green and orange for the area below the heat exchanger. The contour color gradually changes from green to red for the area above the heat exchanger as well. A cooler color can be found below the area of the heat exchanger, indicating an effective cool air temperature distribution around the heat exchanger. This indicates that the local air temperatures decrease vertically with decreasing T_{inlet}. Moreover, the temperature profile of each layer is moderately stable. In terms of flow rate, the contour color of six layers at all inlet fluid temperatures was not significantly changed after $\dot{V}$ = 0.9 L/min.

The contour plot visualization highlights the effectiveness of the heat transfer from the heat exchanger to the area below and above. The detailed numerical discussion will be explained in the next section.

The relative humidity around the heat exchanger is between 65% and 80% at T_{inlet} = −5, 0, 5, and 10 °C and $\dot{V}$ = 0.3 to 1.3 L/min. Fungal outbreaks can be prevented when the relative humidity is approximately 60–80%.

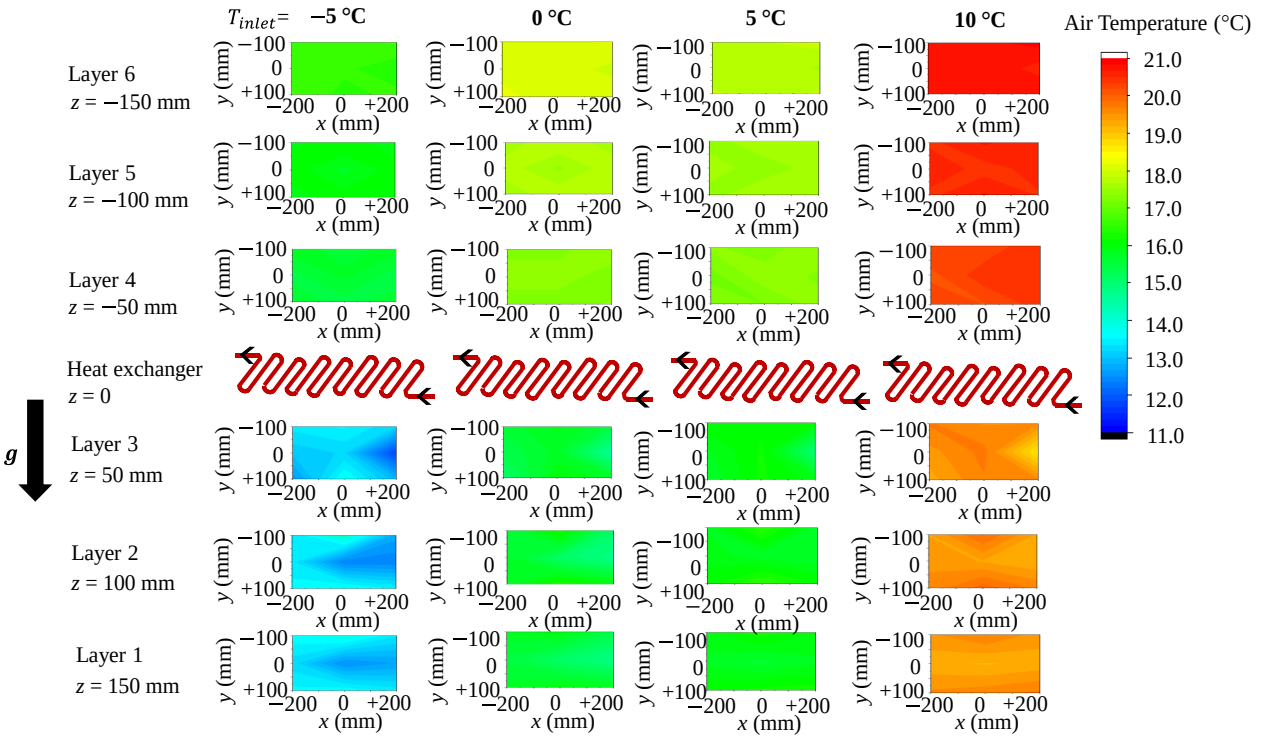

(a) $\dot{V}$ = 0.3 L/min

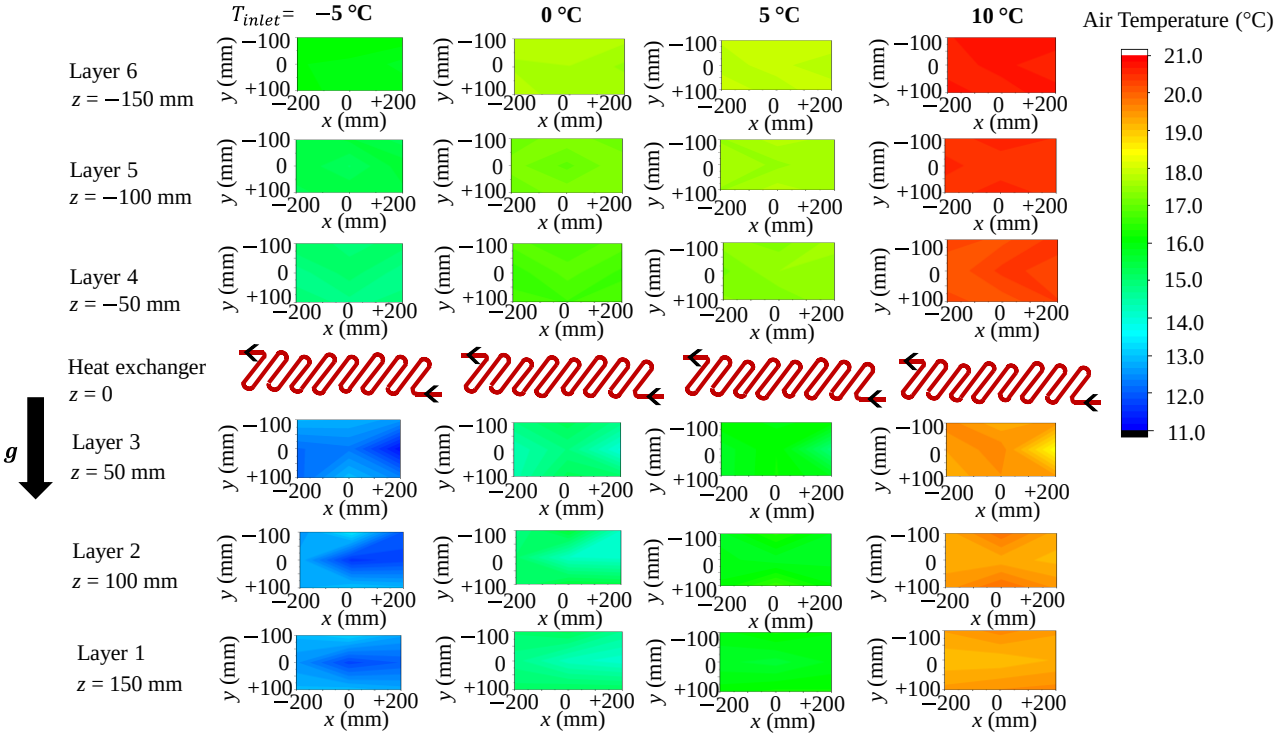

(b) $\dot{V}$ = 0.5 L/min

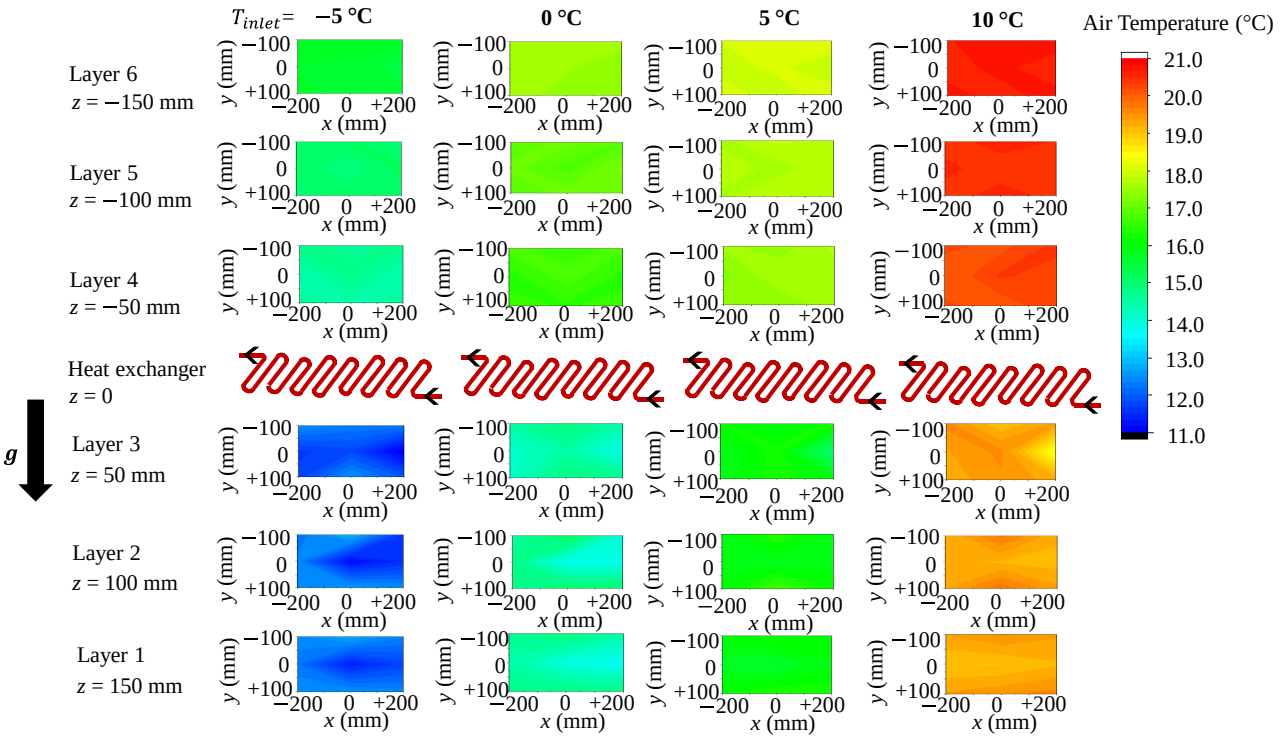

(c) $\dot{V}$ = 0.7 L/min

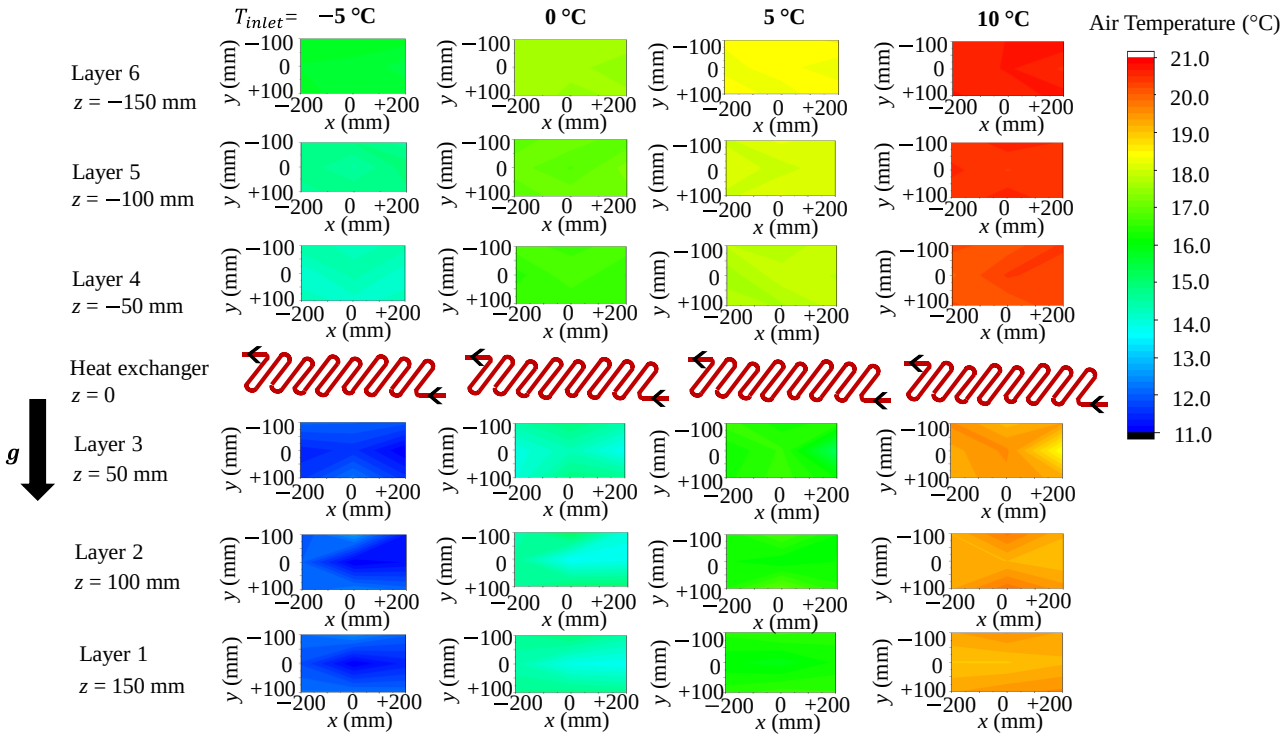

(d) $\dot{V}$ = 0.9 L/min

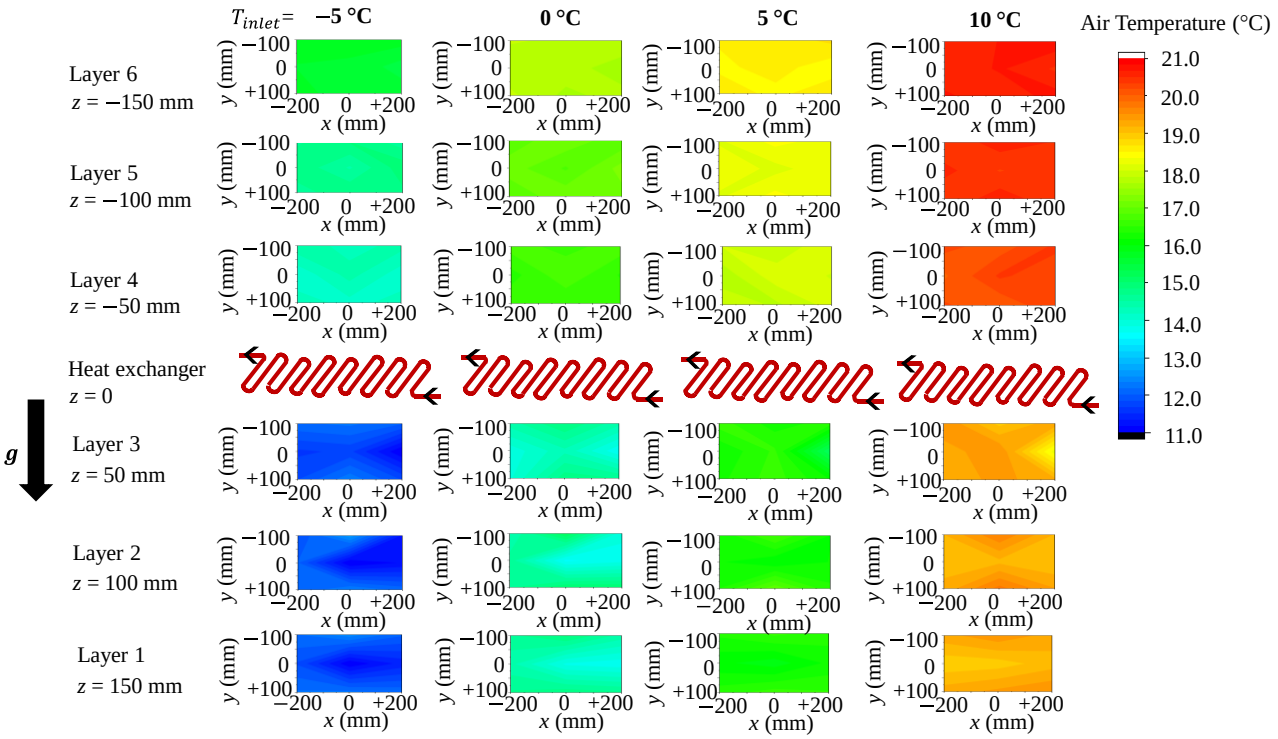

(e) $\dot{V}$ = 1.1 L/min

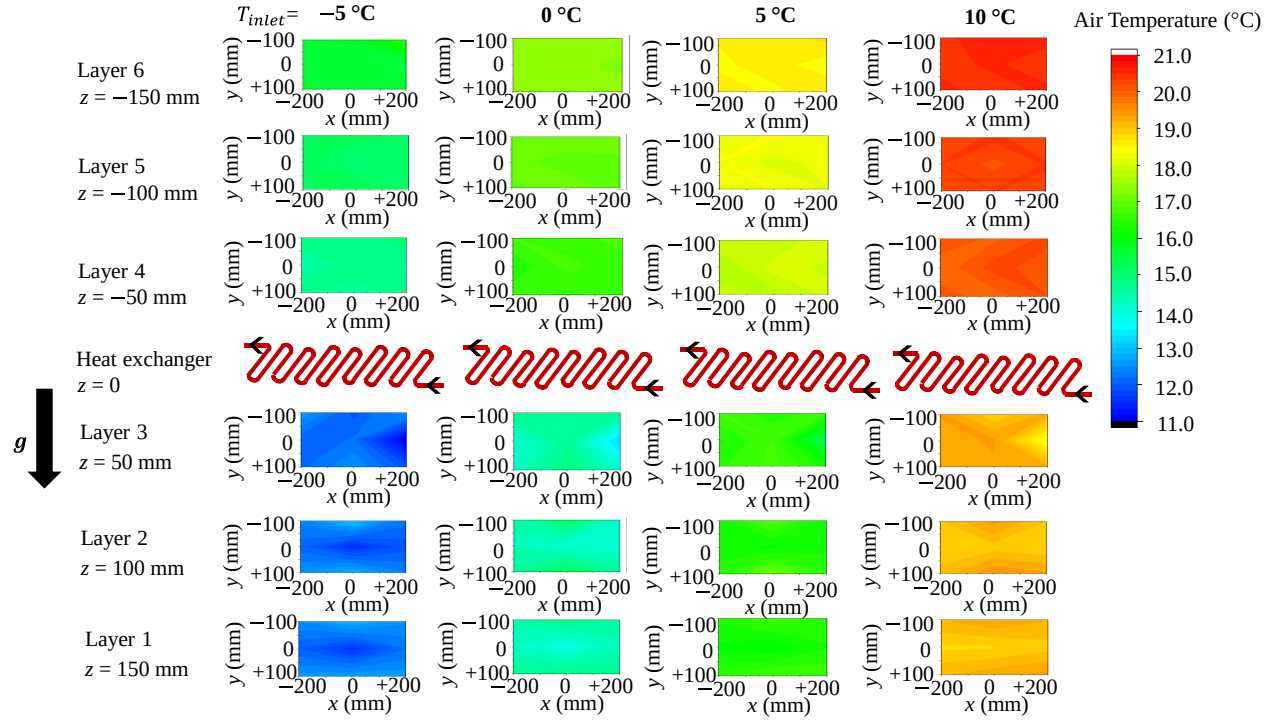

(f) $\dot{V}$ = 1.3 L/min

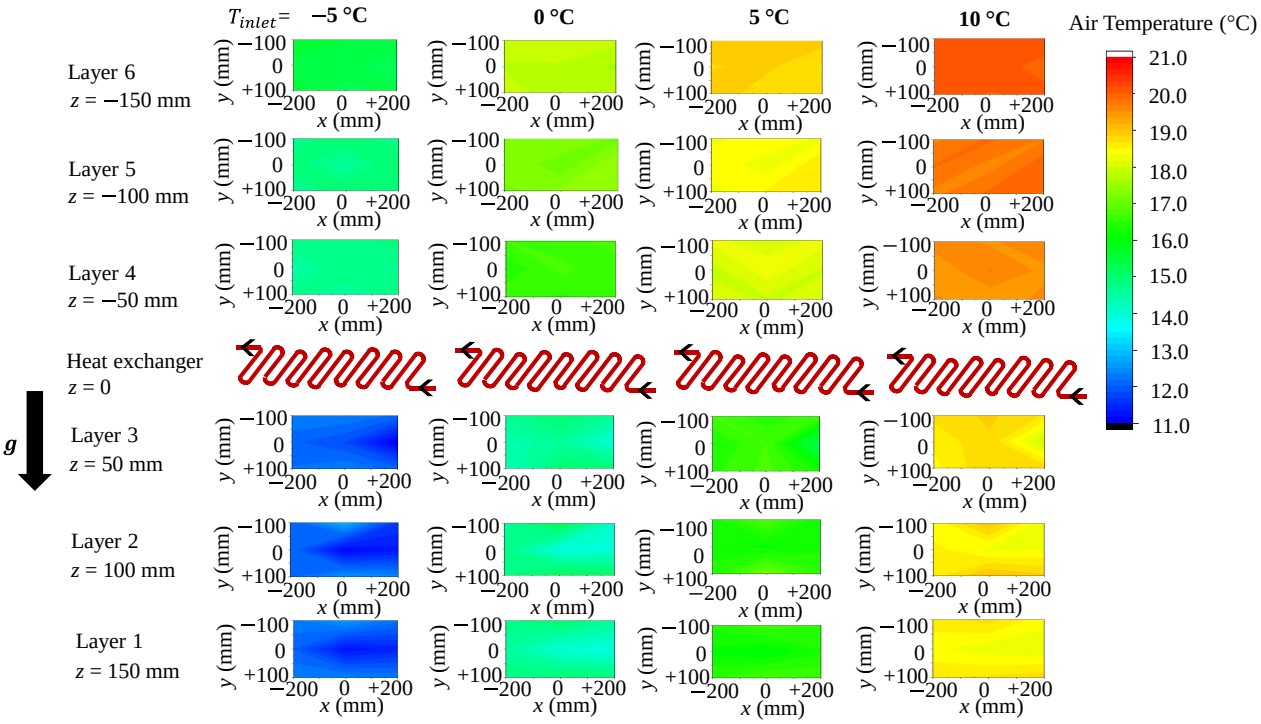

(g) $\dot{V}$ = 1.5 L/min

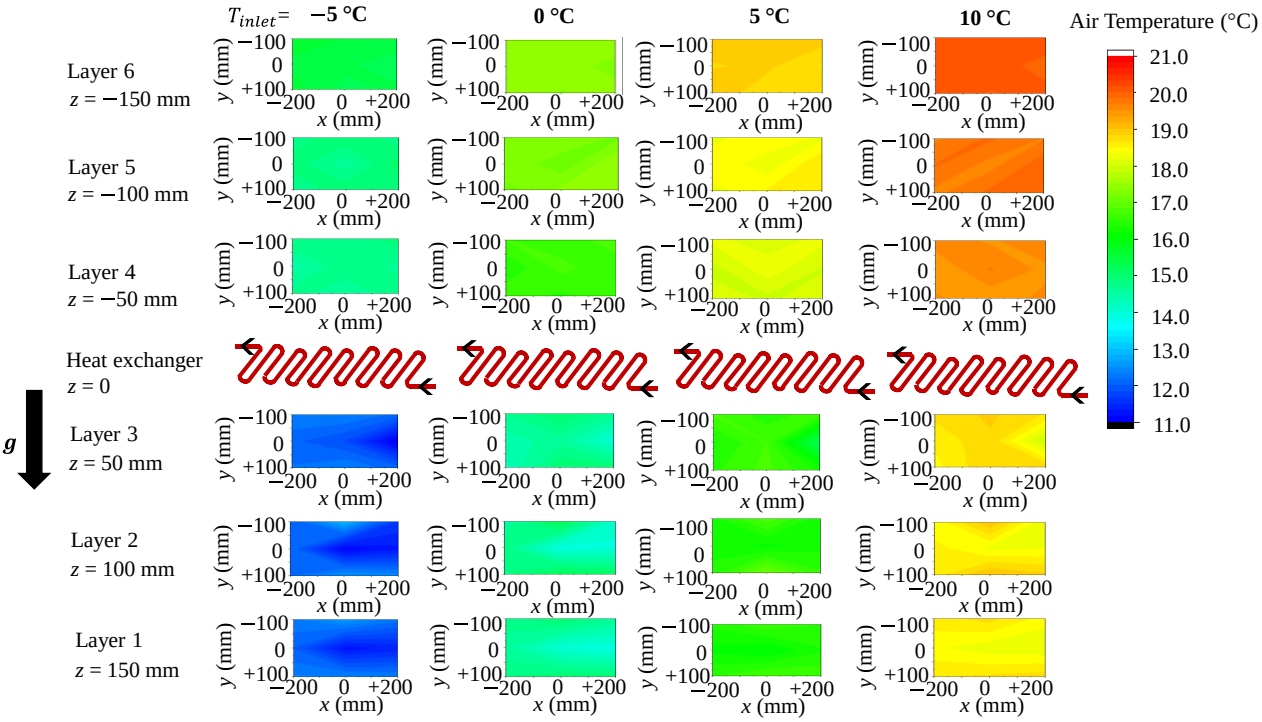

(h) $\dot{V}$ = 2.0 L/min

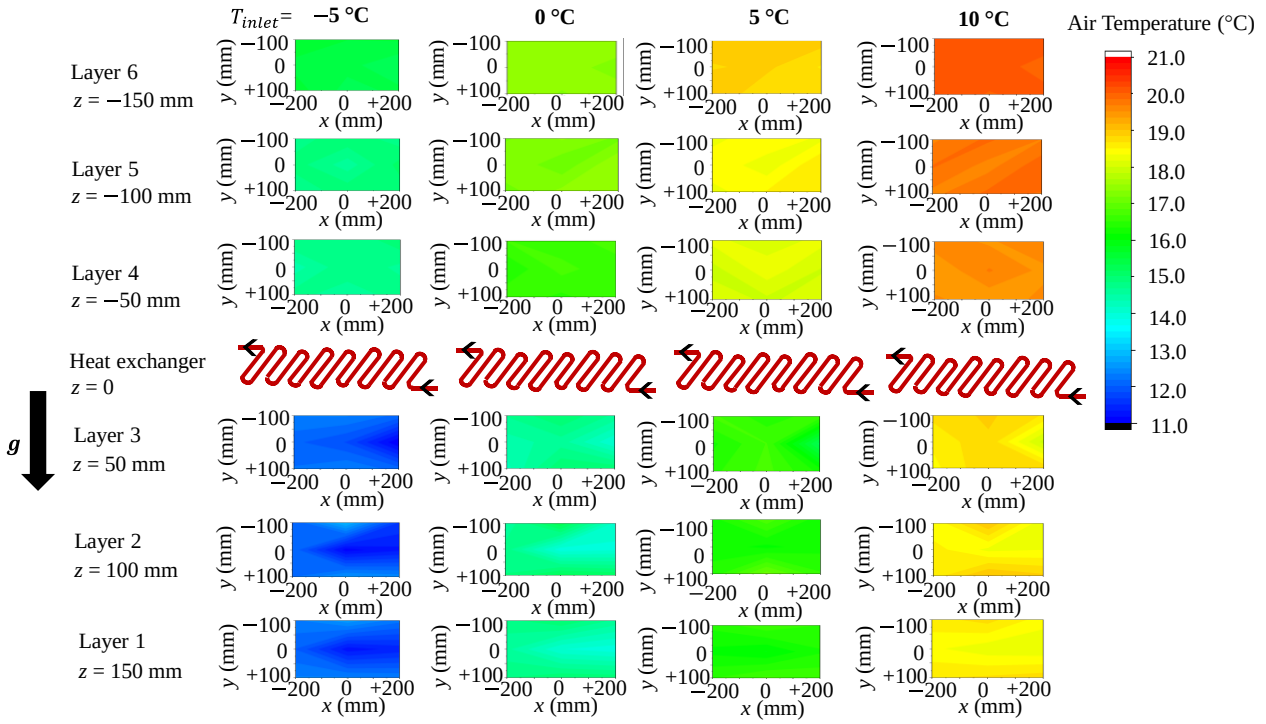

(i) $\dot{V}$ = 2.5 L/min

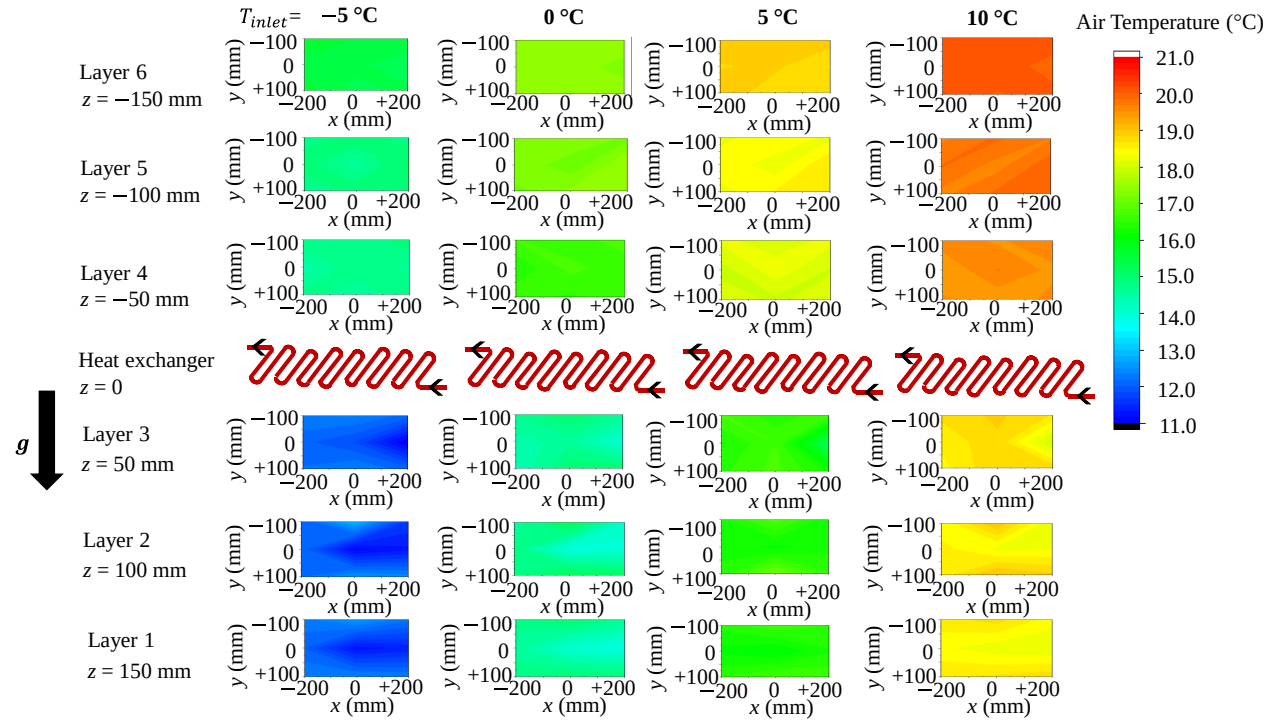

(j) $\dot{V}$ = 3.0 L/min

Figure 4.2. Air temperature contour of the area below and above the heat exchanger for all flow rates under steady state condition (cooling).

Local air temperatures were investigated vertically, both below and above the heat exchanger. The local air temperatures at the nine points in each layer were averaged. Figure 4.3 shows the average local air temperature of six layers for $\dot{V}$ = 0.3 to 3.0 L/min, under cooling conditions. The layers are indicated in the vertical direction as follows: z = −50, −100, and −150 mm for the area above and z = 50, 100, and 150 mm for the area below the heat exchanger.

When $\dot{V}$ is increased from 0.3 to 3.0 L/min, the average local air temperatures of the area below T_{l,be_avg} the heat exchanger gradually decrease for all T_{inlet}. When $\dot{V}$ exceeds 0.9 L/min, the average local air temperatures above T_{l,ab_avg} and below T_{l,be_avg} the heat exchanger are not markedly changed.

As shown in Figure 4.3, T_{l,ab_avg} and T_{l,be_avg} are highest at T_{inlet} = 10 °C for all layers. T_{l,ab_avg} and T_{l,be_avg} gradually decrease for all layers when T_{inlet} is decreased from 10 to 5, 0, and −5 °C. T_{l,be_avg} is approximately 19.0 °C for the three layers below the heat exchanger (z = 50, 100, and 150 mm) at T_{inlet} = 10 °C. However, T_{l,ab_avg} is approximately 20.5 °C for the three layers above the heat exchanger (z = −50, −100, and −150 mm). At T_{inlet} = −5 °C, the minimum T_{l,be_avg} reaches approximately 12 °C at z = 50, 100, and 150 mm. Furthermore, T_{l,ab_avg} is approximately 15 °C at z = −50, −100, and −150 mm. For all values of T_{inlet} and $\dot{V}$, the T_{l,ab_avg} values increase slightly at z = −100 and −150 mm, that is, at an increasing vertical distance from the heat exchanger. In addition, these average local air temperatures are lower than the initial air temperature of approximately 22 °C.

For all conditions, T_{l,be_avg} is approximately 2.0 °C lower than T_{l,ab_avg} of the heat exchanger. This indicates that the area below the heat exchanger is slightly cooler than that above it.

Moreover, T_{l,be_avg} can be decreased up to 7.0 °C by decreasing T_{inlet} from 10 to −5 °C. The local air temperature is observed to decrease with decreasing T_{inlet}. This is due to the downward airflow generated by buoyancy forces with decreasing T_{inlet}.

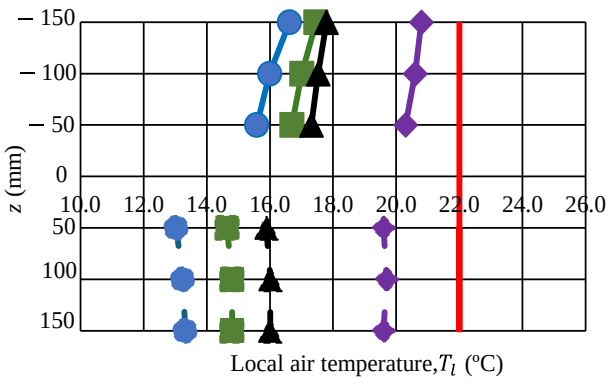

(a) $\dot{V}$ = 0.3 L/min

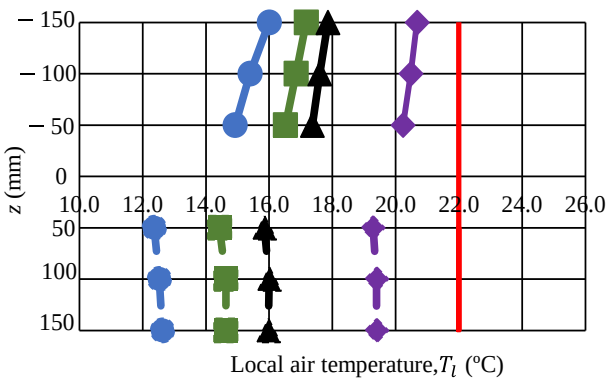

(b) $\dot{V}$ = 0.5 L/min

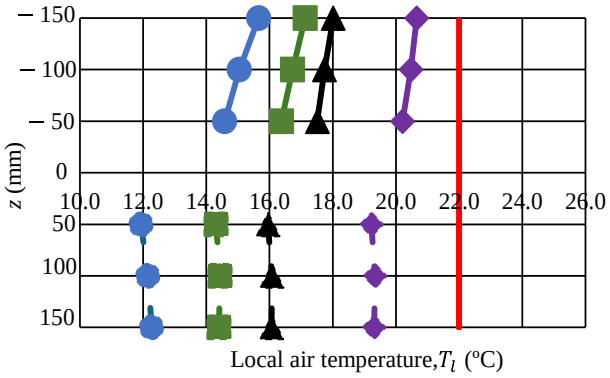

(c) $\dot{V}$= 0.7 L/min

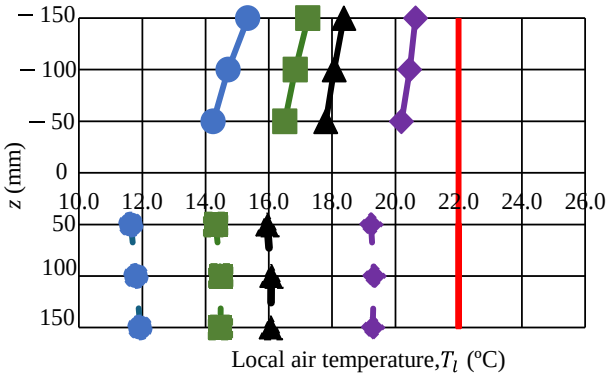

(d) $\dot{V}$= 0.9 L/min

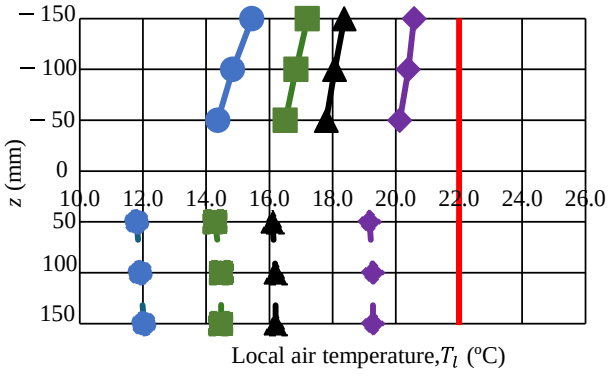

(e) $\dot{V}$= 1.1 L/min

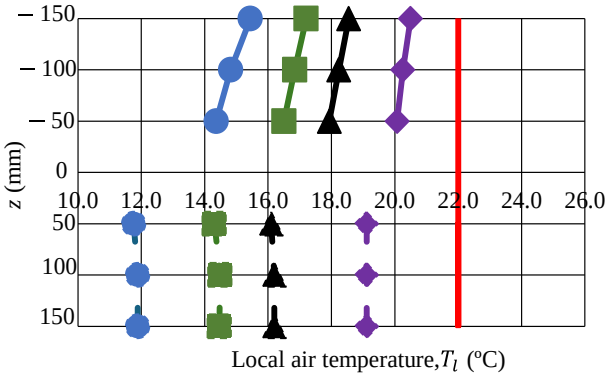

(f) $\dot{V}$= 1.3 L/min

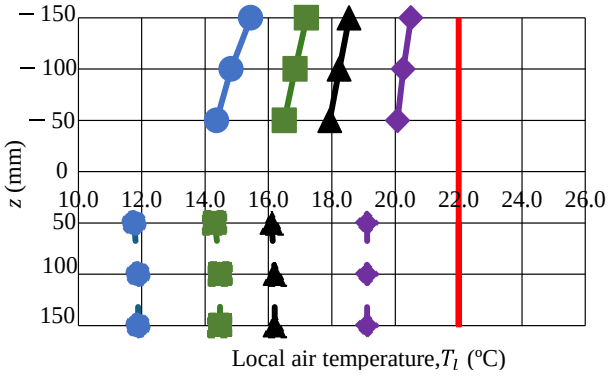

(g) $\dot{V}$= 1.5 L/min

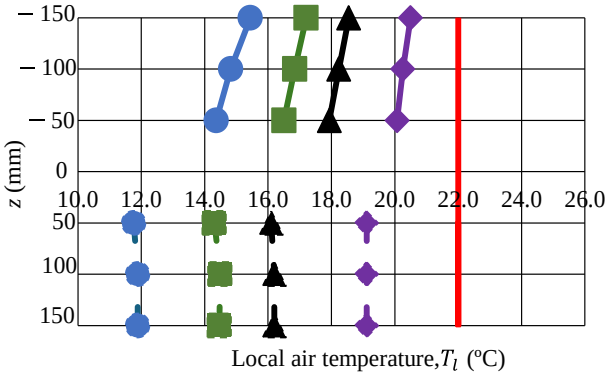

(h) $\dot{V}$= 2.0 L/min

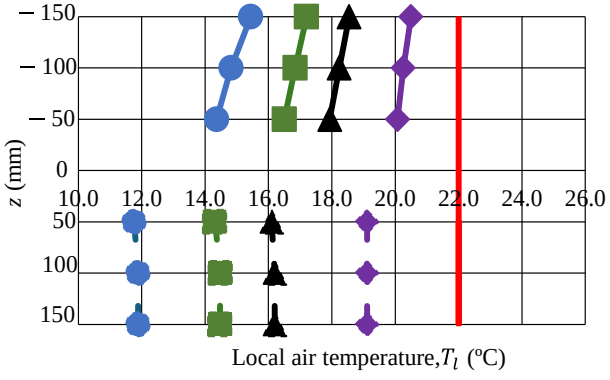

(i) $\dot{V}$= 2.5 L/min

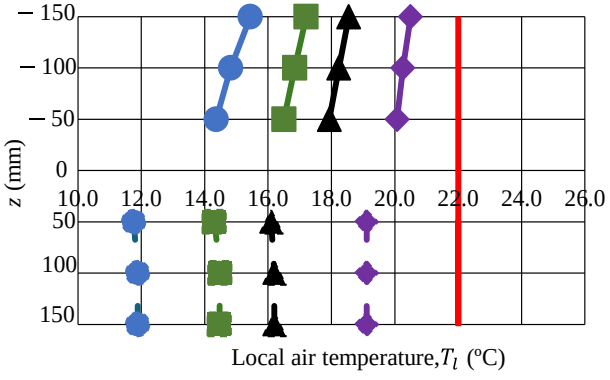

(j) $\dot{V}$= 3.0 L/min

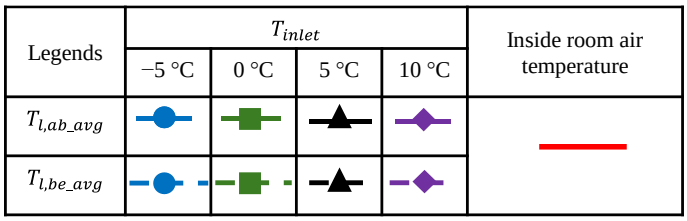

Figure 4.3. Average local air temperatures at all flow rates (cooling).

4.1.2 Local air temperature profile (heating)

Figure 4.4 presents the local air temperature contours for each layer at all heating experimental conditions under steady state. The color difference indicates the variations in the local air temperatures in different layers. The initial air temperature is approximately 22 °C. At T_{inlet}= 50 °C, the local air temperature of all three layers color at the area above the heat exchanger is orange approximately 35°C. When T_{inlet} decreases from 50 to 30 and 40 °C, the contour color gradually changes from orange to green and blue for the area above the heat exchanger. The contour color also steadily changes from yellow to blue for the area below the heat exchanger.

A warmer color can be observed both above and below the heat exchanger, indicating an effective warm air temperature distribution around the heat exchanger. This reveals that the local air temperatures increase vertically with increasing T_{inlet}. Additionally, the temperature profile of each layer is moderately stable. When $\dot{V}$= 0.3 L/min of T_{inlet}= 50 °C, the contour color of the above three layers is light orange which is about 34 °C. The contour color of the above three layers gradually change to orange with the increases of $\dot{V}$. However, the contour color of six layers at all inlet fluid temperatures do not significantly change after $\dot{V}$=0.9 L/min.

The temperature gradient between the above and below areas increases with increasing T_{inlet}, suggesting a more efficient air distribution to the air above the heat exchanger. Higher inlet temperatures result in significant increases in air temperature, particularly above the heat exchanger, where heat rises and accumulates more efficiently. The air temperature below the heat exchanger, however, remains relatively cooler, even with higher inlet temperatures. This implies that increasing inlet fluid temperature has a great effect on the local air temperatures for heating. The comprehensive numerical analysis will be elucidated in the subsequent section.

The relative humidity ranges between 30% and 50% around the heat exchanger for T_{inlet} = 30, 40, and 50 °C and $\dot{V}$ = 0.3 to 3.0 L/min. The humidity is low when the air temperature is relatively warm.

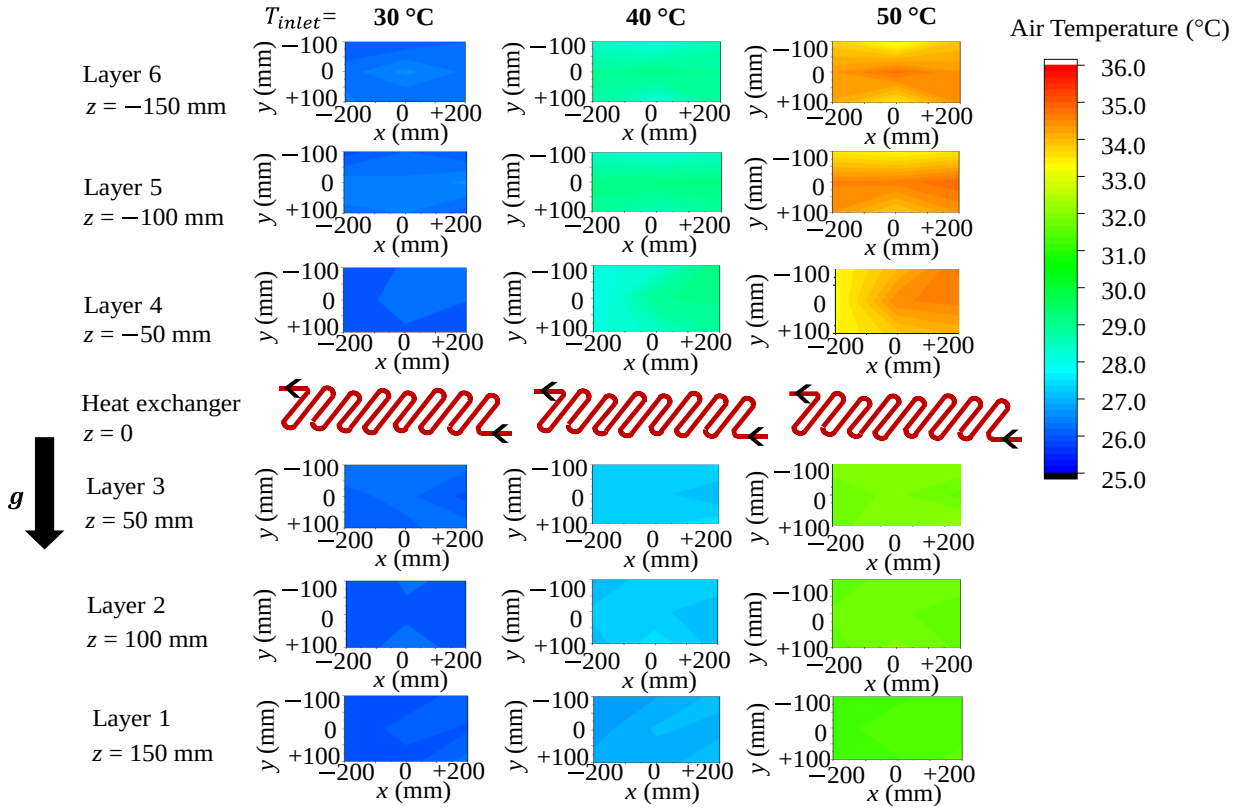

(a) $\dot{V}$ = 0.3 L/min

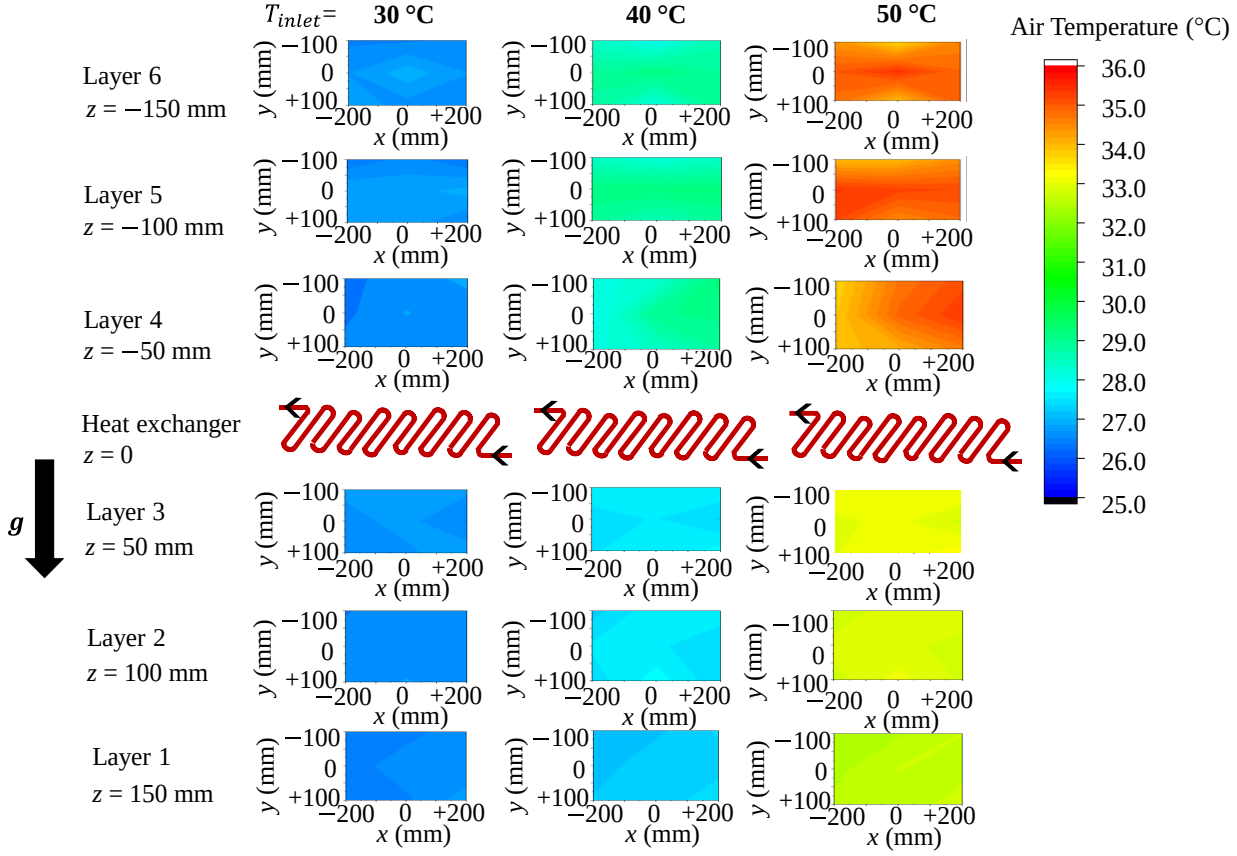

(b) $\dot{V}$ = 0.5 L/min

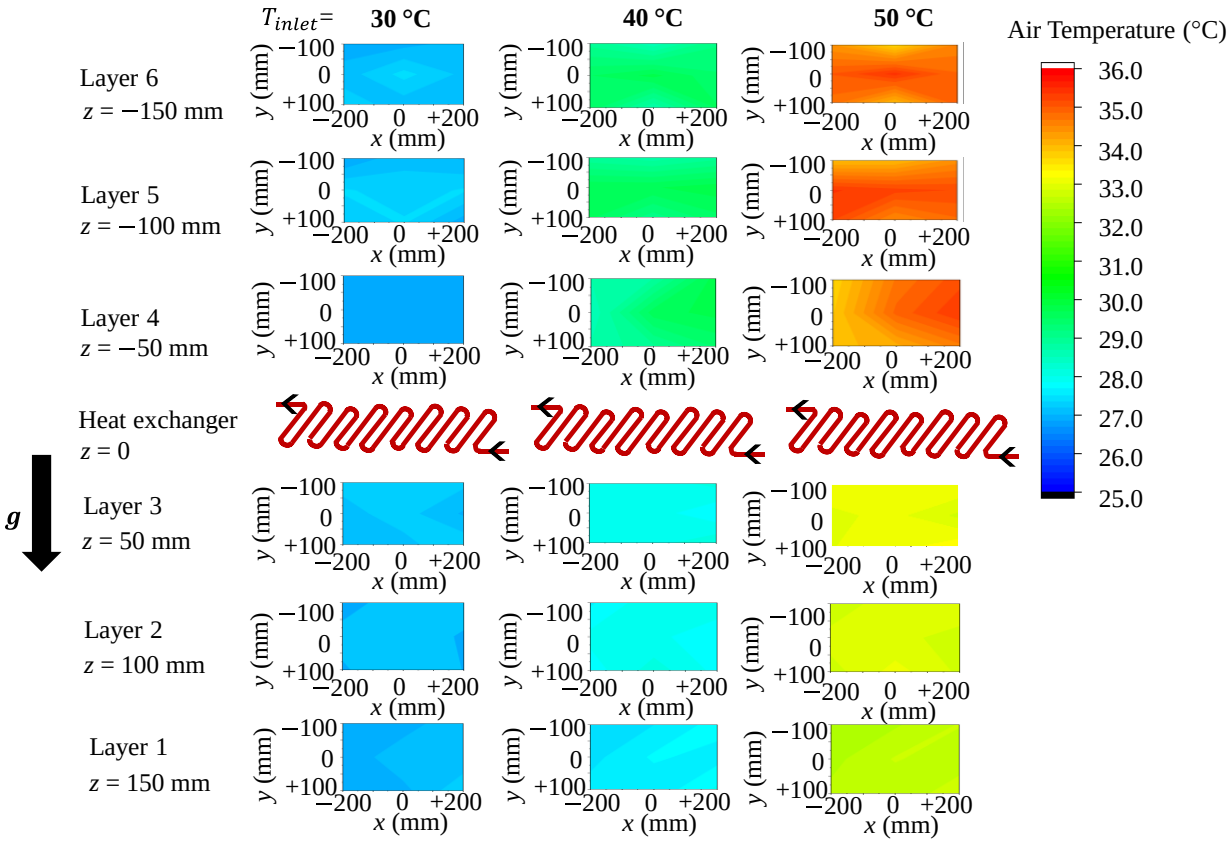

(c) $\dot{V}$ = 0.7 L/min

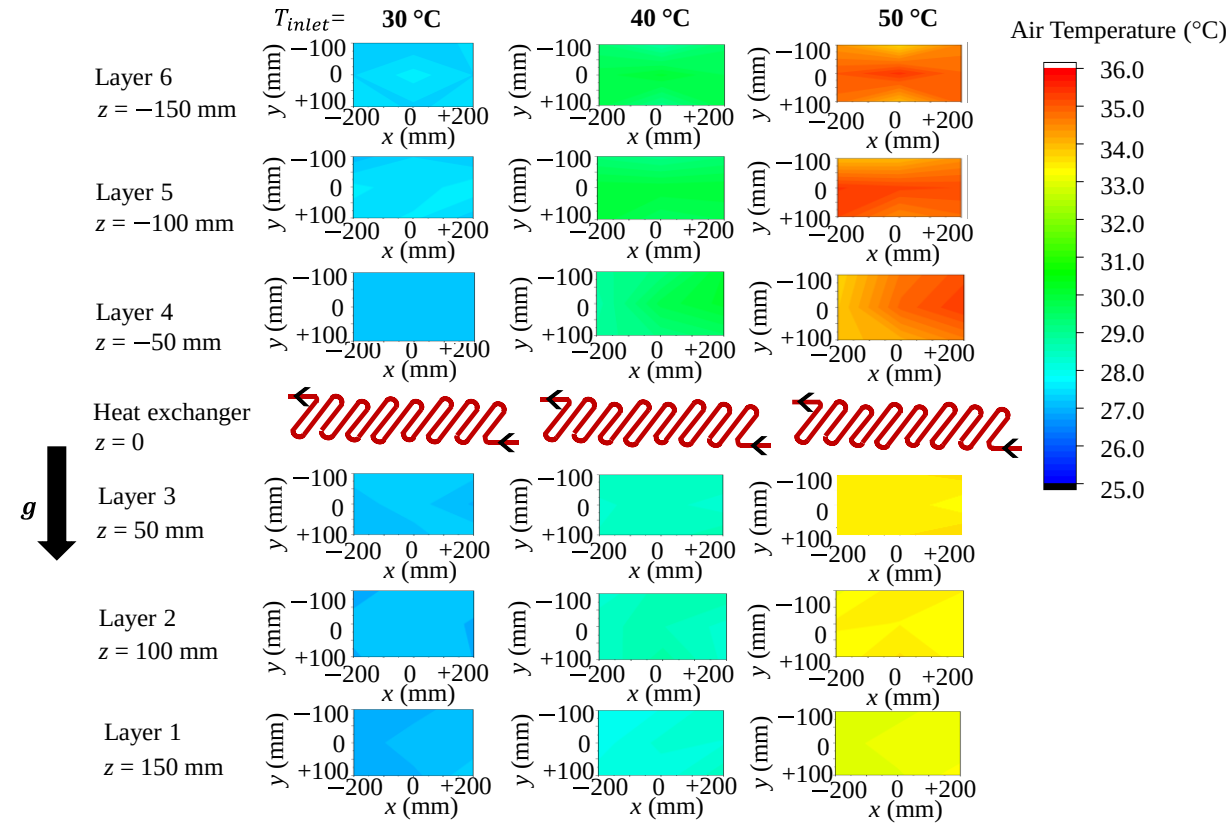

(d) $\dot{V}$ = 0.9 L/min

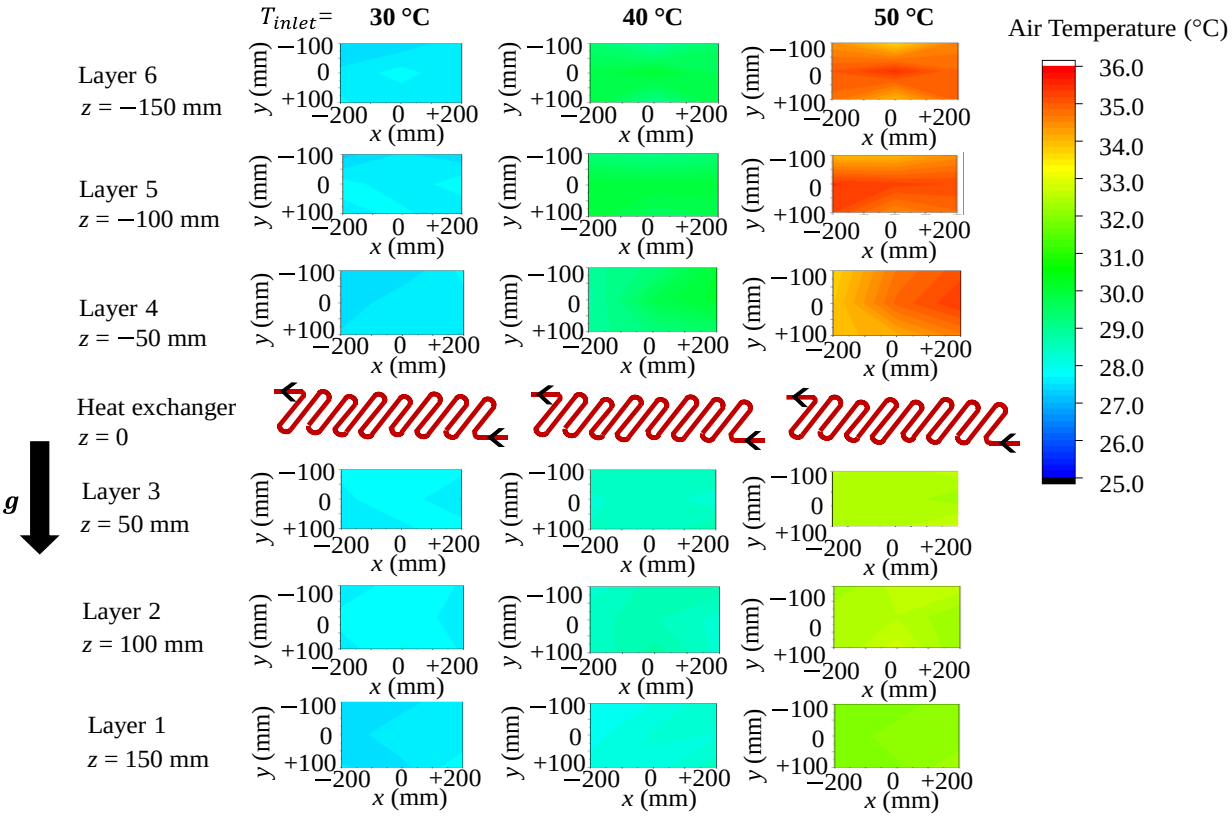

(e) $\dot{V}$ = 1.1 L/min

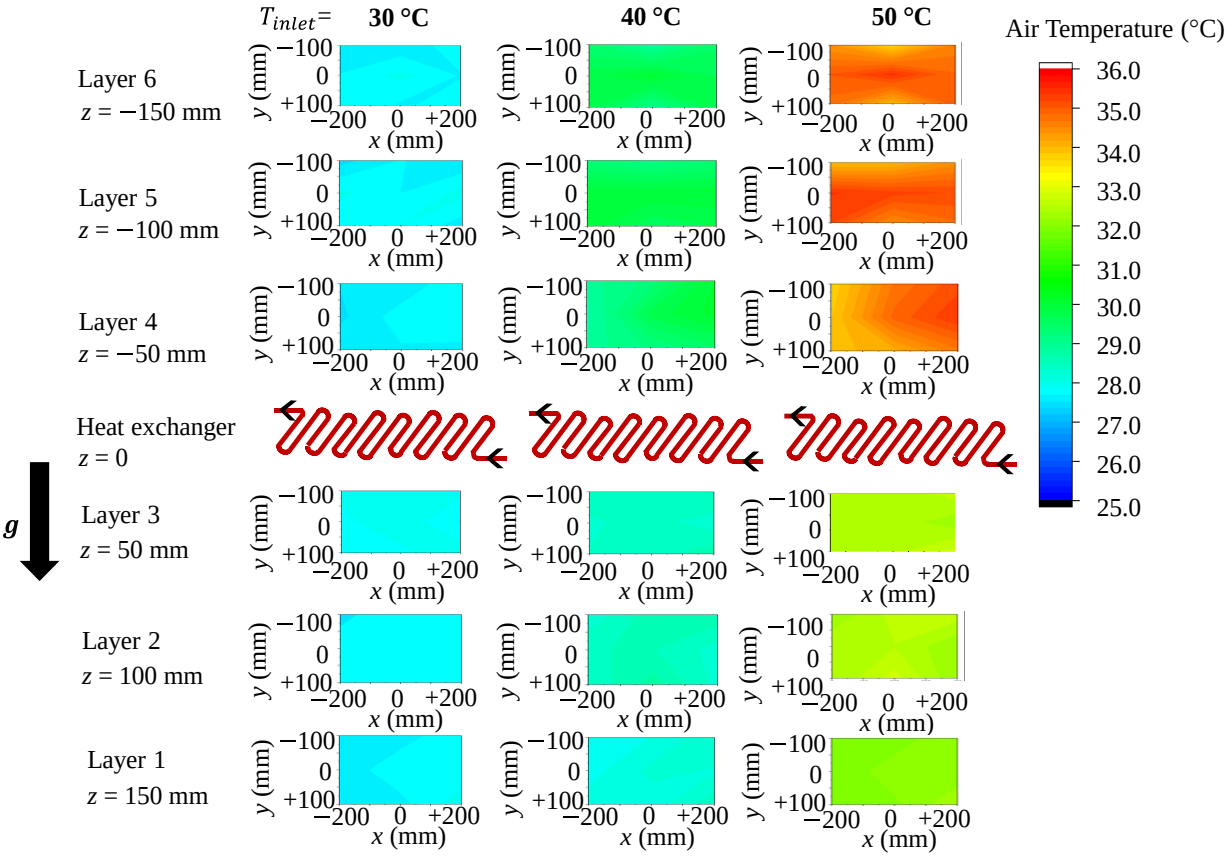

(f) $\dot{V}$ = 1.3 L/min

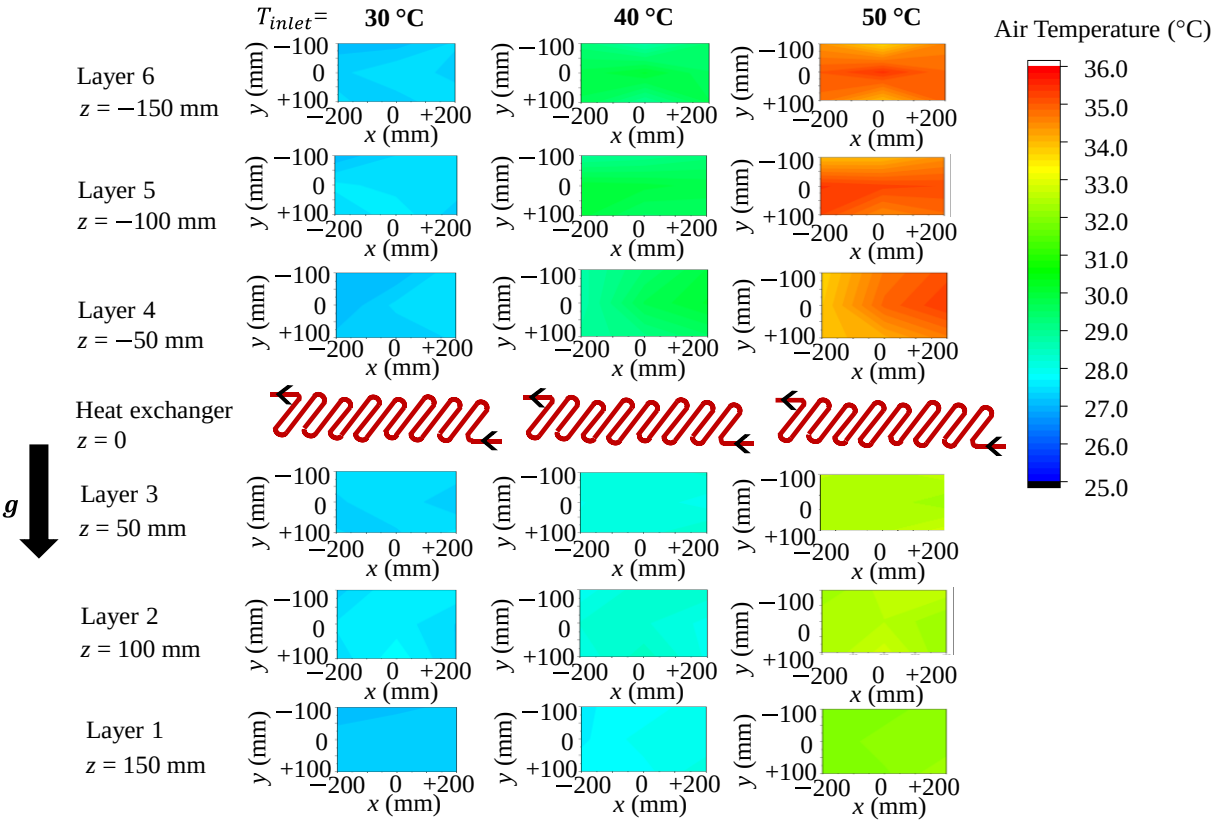

(g) $\dot{V}$ = 1.5 L/min

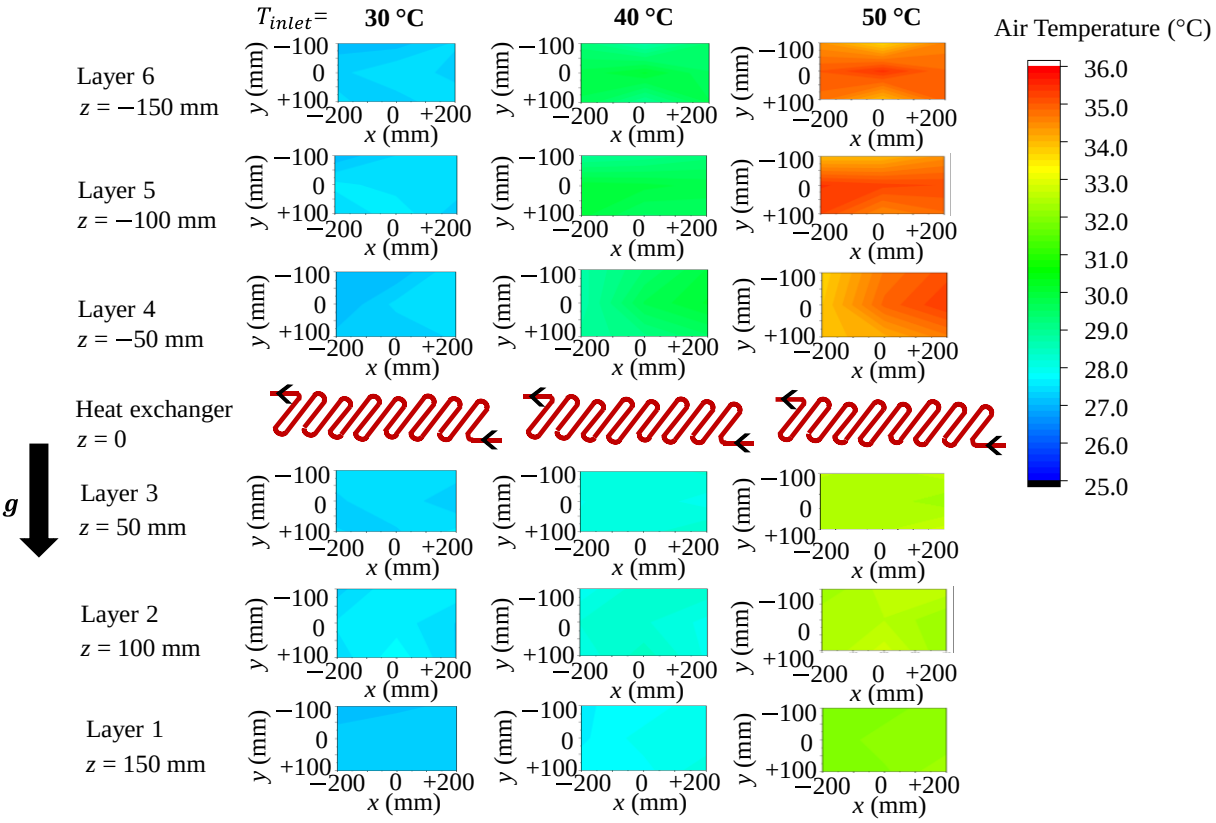

(h) $\dot{V}$ = 2.0 L/min

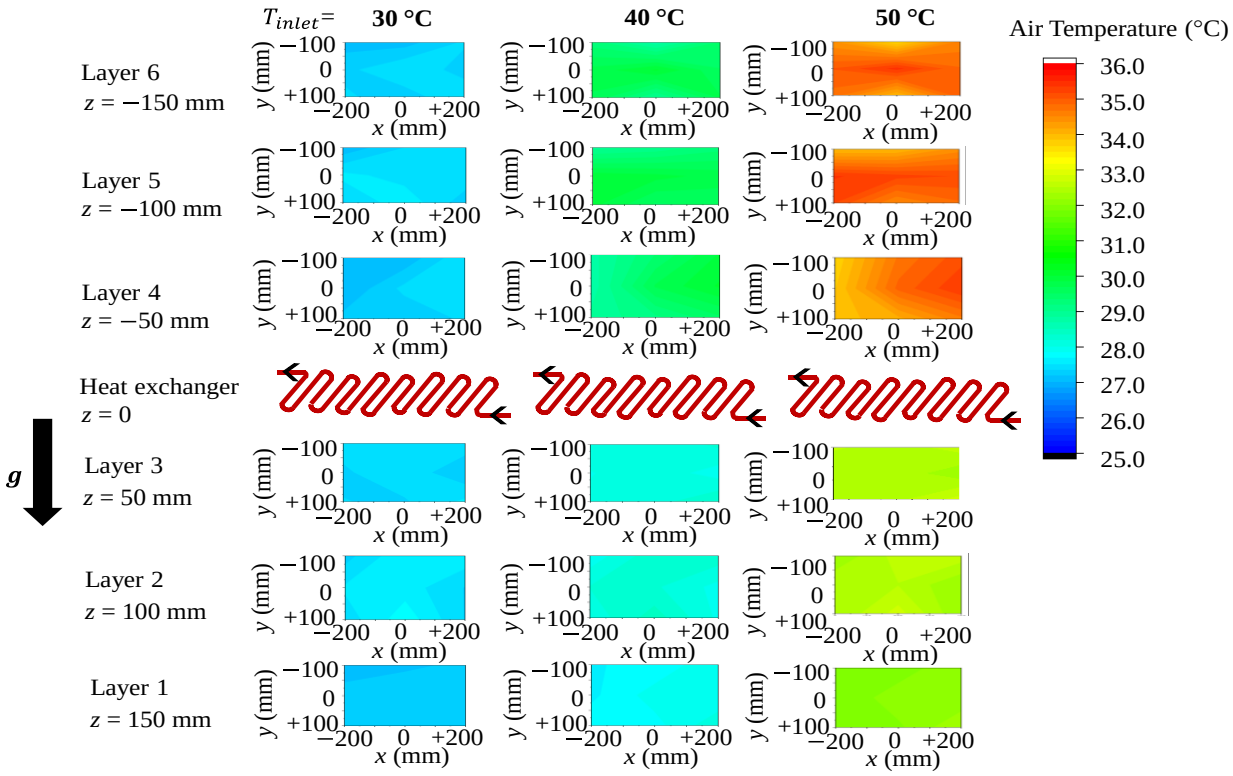

(i) $\dot{V}$ = 2.5 L/min

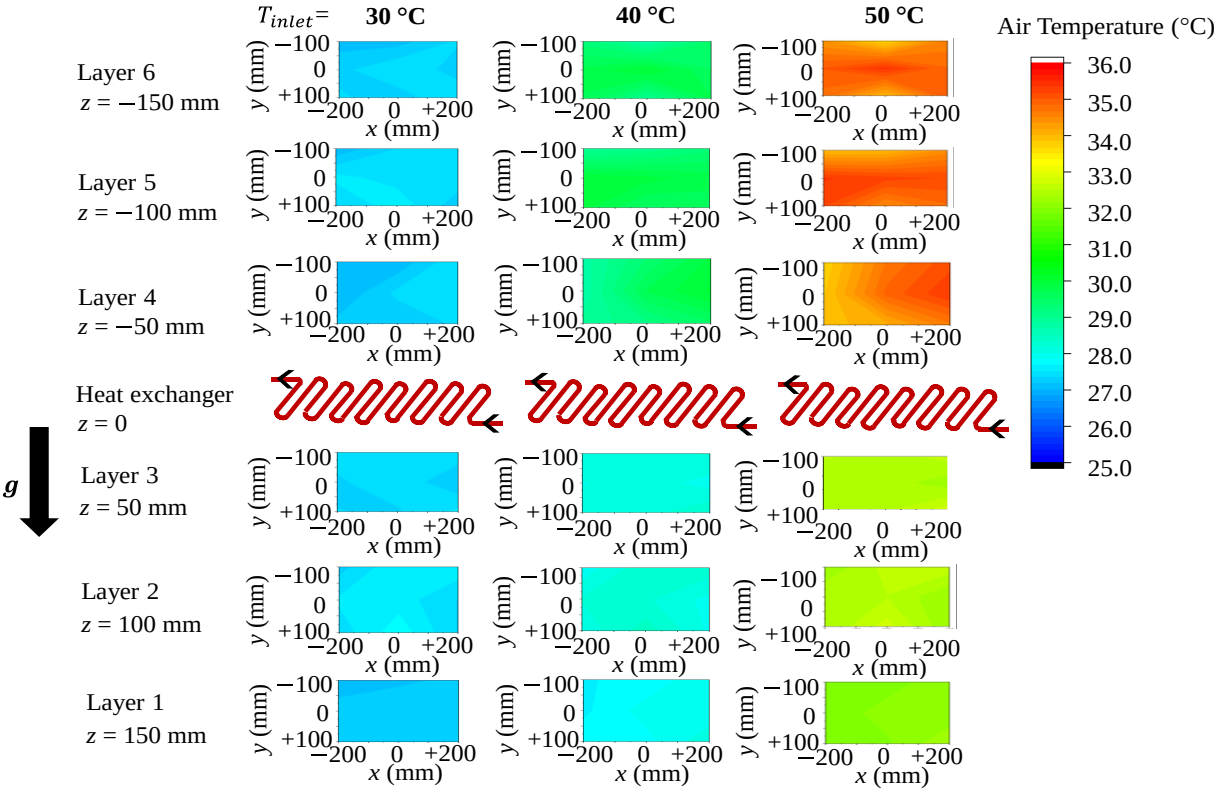

(j) $\dot{V}$ = 3.0 L/min

Figure 4.4. Air temperature contour of the area below and above the heat exchanger for all flow rates under steady state condition (heating).

Figure 4.5 shows the average local air temperature of six layers (both above and below) for $\dot{V}$ = 0.3 to 3.0 L/min, under heating conditions. The local air temperatures at the nine points in each layer are averaged. The average local air temperatures above T_{l,ab_avg} and below T_{l,be_avg} the heat exchanger are slightly increased as $\dot{V}$ is increased from 0.3 to 3.0 L/min for all T_{inlet} .

T_{l,ab_avg} and T_{l,be_avg} are approximately 27 °C for all layers when T_{inlet} = 30 °C. T_{l,be_avg} reaches approximately 28 °C for the three layers below the heat exchanger (z = 50, 100, and 150 mm), and T_{l,ab_avg} is approximately 30 °C for the three layers above the heat exchanger (z = −50, −100, and −150 mm) when T_{inlet} = 40 °C. At T_{in} = 50 °C, T_{l,be_avg} is approximately 33 °C for the three layers below the heat exchanger, and T_{l,ab_avg} is approximately 35 °C for the three layers above the heat exchanger. The initial air temperature is approximately 22 °C. These local air temperatures are higher than the initial air temperature, implying that the air becomes warm.

T_{l,ab_avg} and T_{l,be_avg} are not considerably different at T_{inlet} = 30 °C. However, at T_{inlet} = 40 and 50 °C, T_{l,ab_avg} is approximately 2.5 °C higher than T_{l,be_avg}. This is caused by the upward airflow generated by buoyancy force with the increase of T_{inlet}.

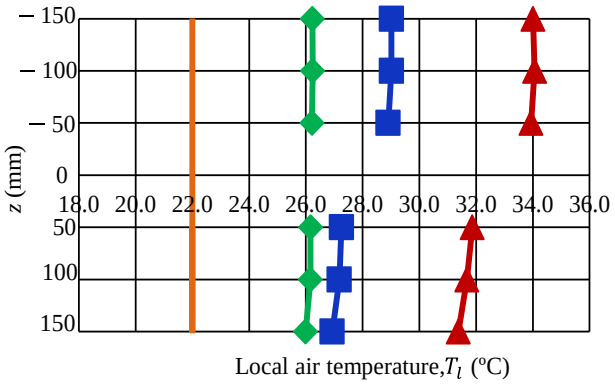

(a) $\dot{V}$= 0.3 L/min

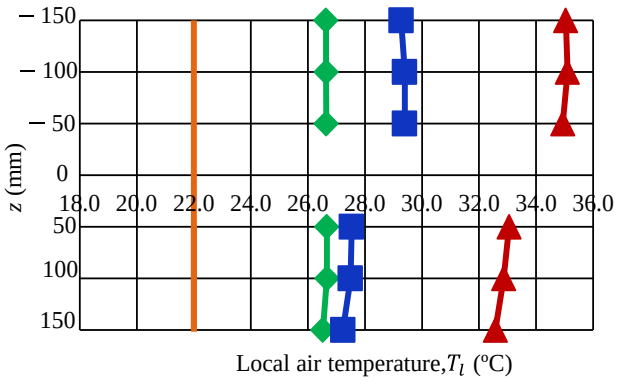

(b) $\dot{V}$= 0.5 L/min

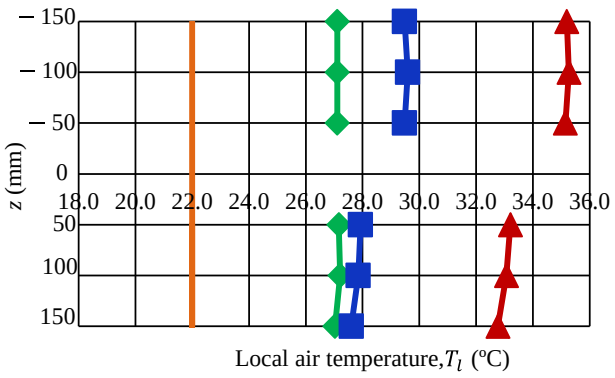

(c) $\dot{V}$= 0.7 L/min

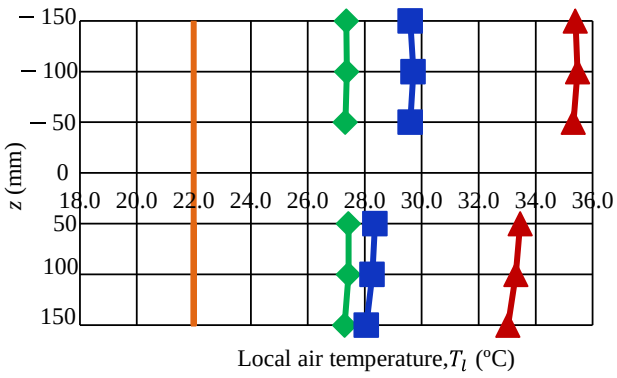

(d) $\dot{V}$= 0.9 L/min

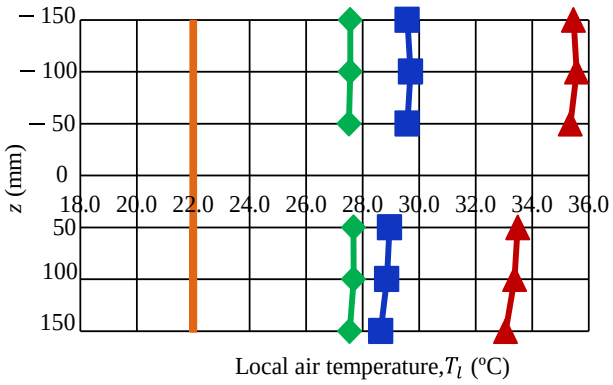

(e) $\dot{V}$= 1.1 L/min

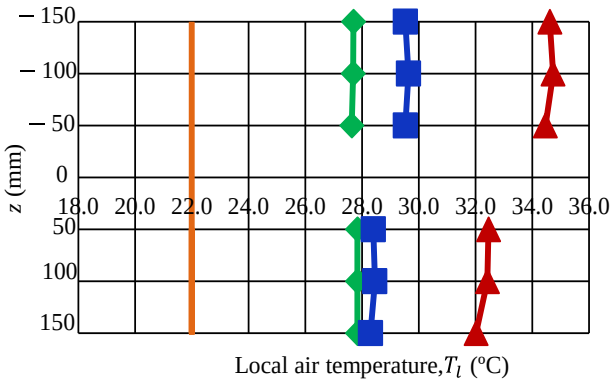

(f) $\dot{V}$= 1.3 L/min

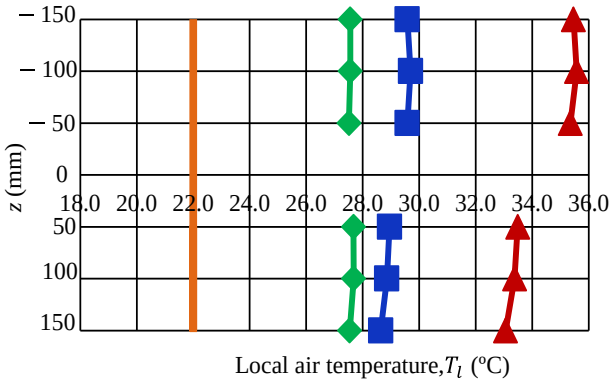

(g) $\dot{V}$= 1.5 L/min

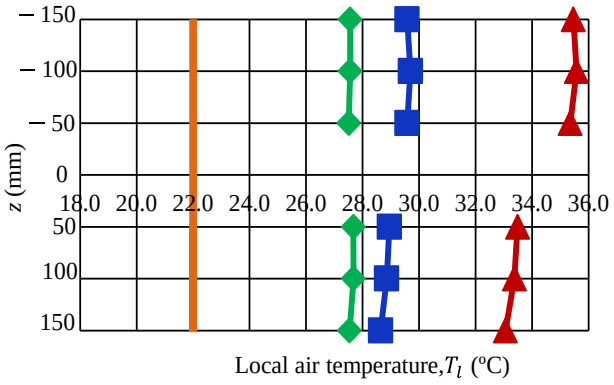

(h) $\dot{V}$= 2.0 L/min

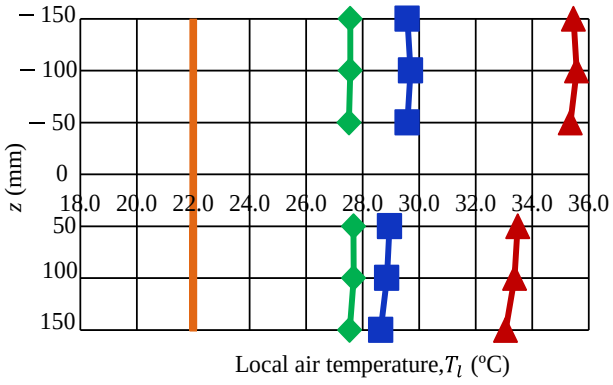

(i) $\dot{V}$= 2.5 L/min

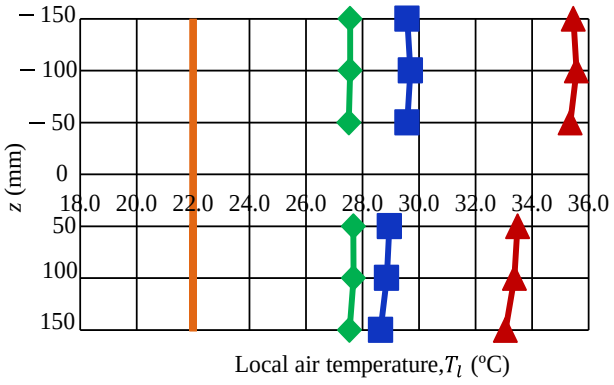

(j) $\dot{V}$= 3.0 L/min

Legends	T_{inlet}			Inside room air temperature
	30 °C	40 °C	50 °C	
T_{l,ab_avg}				
T_{l,be_avg}				

Figure 4.5. Average local air temperatures at all flow rates (heating).

According to Figs. 4.3 and 4.5, local air temperature profiles do not significantly change more than flow rate 0.9 L/min. This means the air temperature profiles depend on $\dot{V}$ when $\dot{V}$ is less than 0.9 L/min. Hence, 0.9 L/min flow rate is sufficient and can be selected to control the local air temperature for reducing the pumping power as well.

External and internal convective heat transfer coefficient on the surface of heat exchanger

The experiments are conducted in the laboratory. Moreover, the experimental system was covered with the insulation board to avoid the influence from the laboratory. Thus, the heat transfer mechanism is considered natural convection during experiments. The external convective heat transfer coefficient was estimated using Eq. 3.4. Figure 4.6 shows the external convective heat transfer coefficient on the surface of the heat exchanger with the various flow rates for all inlet fluid temperatures. When the flow rates increase, the heat transfer coefficient remains relatively stable. However, when the inlet fluid temperatures change, the heat transfer coefficient significantly changes. At T_{inlet} = −5 °C and 50 °C, the heat transfer coefficients were the highest about 7 W/m^2·K. The heat transfer coefficient value is the lowest which is about 4.5 W/m^2·K at T_{inlet} = 30 °C. This is because the temperature difference between the surface and surroundings is small.

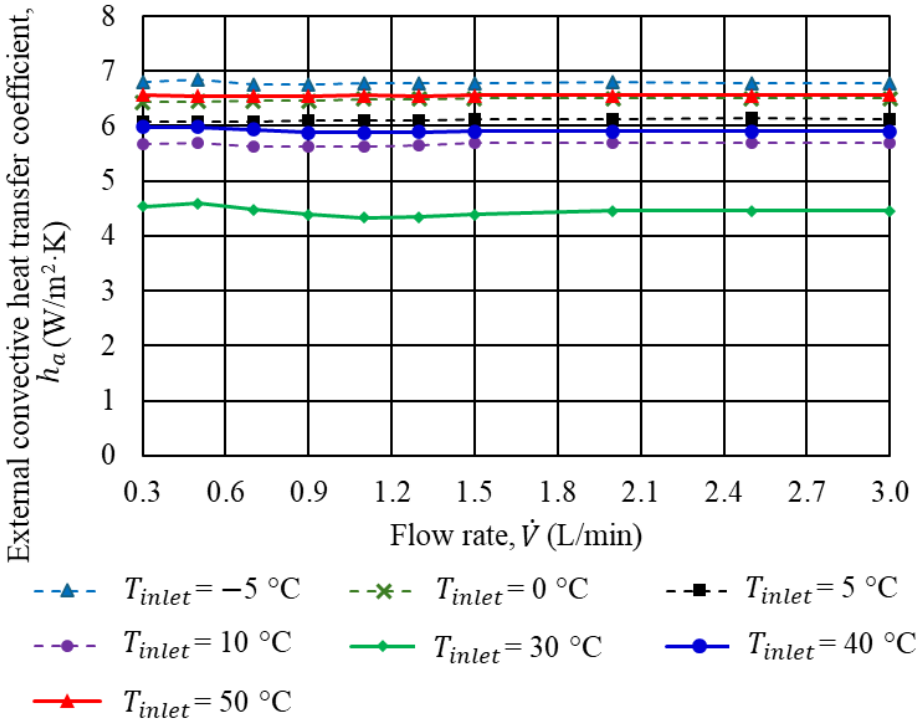

Figure 4.6. External convective heat transfer coefficient with different flow rates for all inlet fluid temperatures.

The internal heat transfer coefficient was estimated using Eq. 3.6. Figure 4.7 shows the internal fluid heat transfer coefficient, h_f in a tube of the heat exchanger for varying flow rates at all inlet fluid temperatures. At all inlet fluid temperatures, h_f shows an initial increase with flow rate, reaching a peak at lower flow rates (approximately 0.7–1.1 L/min). Beyond this point, h_f decreases gradually with increasing flow rate,

suggesting a non-linear relationship between flow dynamics and heat transfer. However, h_f values at T_{inlet} = 50 °C is the highest than other inlet fluid temperatures.

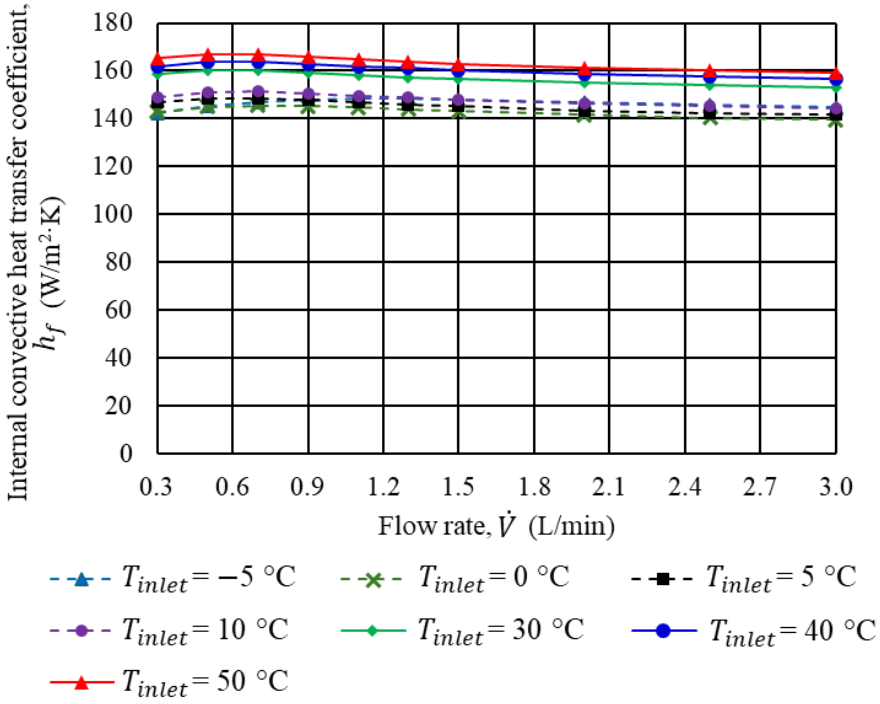

Figure 4.7. Internal convective heat transfer coefficient with different flow rates for all inlet fluid temperatures.

Plant environmental conditions play a crucial role in modern agriculture. The air temperature is a major environmental factor. Understanding the air temperature requirements of specific crops is essential for their successful cultivation and optimal yield. For example, crops such as lettuce and fruits, including cucumbers and strawberries, are extensively cultivated. The optimal air temperature range for lettuce is approximately 20–24 °C [1]. For the growth of cucumbers, the optimal temperature is 25–30 °C during the day and 18–21 °C at night [2]. Periodic air temperature control is required for strawberries. Warm and cool air are frequently required each day during vegetative growth, flowering, and fruiting stages. The air temperature ranges for strawberries are 20–25 °C and 10–12 °C during daytime and nighttime, respectively [3]. Other factors such as humidity, sunlight intensity, water, and fertilizer are also important.

Based on the experimental results, the average local air temperature of the area below the heat exchanger can reach a minimum of 12 °C and a maximum of 19 °C during cooling. In contrast, the average local air temperature of the area above the heat exchanger can be increased to a minimum of 28 °C and a maximum of approximately 35 °C during heating.

Higher energy is consumed when cooling/heating is provided to an entire greenhouse or plant factory for crop cultivation. However, the proposed heat exchanger is designed to provide local air temperature control only around the plantation area. In terms of air temperature, this heat exchanger can satisfy the air temperature

requirements of the abovementioned crops. This implies that the heat exchanger can control a sufficiently local air temperature around the heat exchanger.

The local air temperatures are sufficiently cool and warm around the area of the heat exchanger during cooling and heating operations, respectively. This indicates that the heat exchanger can provide periodic air temperature control, with alternate cooling and heating. Most crops require warm air during the day. For example, heating may be required for approximately 10 hours during the day, whereas approximately 14 hours of cooling may be required during the night. However, these are estimated times, and it is not necessary to provide the time when the air temperature is suitable for crop growth.

4.2. Heat flux in the heat exchanger

The heat flux $\dot{q}_a$ in the heat exchanger was evaluated for $\dot{V}$ = 0.3 to 1.3 L/min. The heat flux evaluation for $\dot{V}$ higher than 1.5 L/min was not considered owing to the low measurement accuracy of fluid temperature difference ΔT_f.

4.2.1 Fluid temperature difference and heat flux in the heat exchanger (cooling)

Figure 4.8 presents the values of ΔT_f between the inlet and outlet and $\dot{q}_a$ in the heat exchanger under cooling conditions. Under all conditions, ΔT_f steadily decreases when $\dot{V}$ is increased. ΔT_f ranges between 0.1 and 2.3 °C under all cooling conditions. ΔT_f is high at $\dot{V}$ = 0.3 L/min. This is possibly because the fluid remains in the tubes for a slightly longer duration at a low $\dot{V}$ (0.3 L/min). This prolonged contact time between the fluid and tube walls results in a higher ΔT_f than that at other values of $\dot{V}$.

Notably, $\dot{q}_a$ depends on both $\dot{V}$ and ΔT_f. The $\dot{q}_a$ values are calculated using Eq. 3.2. Additionally, the estimated $\dot{q}_a$ values are calculated using approximate ΔT_f values based on Eq. 3.2. In theory, $\dot{q}_a$ increases with an increase in $\dot{V}$. $\dot{q}_a$ has a minimum of 1% and a maximum of 8 % uncertainty. These are shown as an error bar in the figure. These error bars are estimated by considering the Resistance Thermal Detectors measurement accuracy of ± 0.02 ºC. In this thesis, the $\dot{q}_a$ values are observed to fluctuate slightly although $\dot{V}$ is increased. This can be attributed to the decrease in ΔT_f. The average $\dot{q}_a$ is approximately 100 W/m^2 at T_{inlet} = 10 °C. The average $\dot{q}_a$ increases with a decrease in T_{inlet}. The average $\dot{q}_a$ values at T_{inlet} = 5, 0, and −5 °C are approximately 150, 230, and 270 W/m^2, respectively. Compared with the average $\dot{q}_a$ at T_{inlet} = 10 °C, the average $\dot{q}_a$ values at T_{inlet} = 5, 0, −5 °C are enhanced by 55%, 120%, and 170%, respectively, for all values of $\dot{V}$. Based on these results, both T_{inlet} and $\dot{V}$ are considered to affect $\dot{q}_a$. However, $\dot{q}_a$ is more strongly affected by T_{inlet} than by $\dot{V}$.

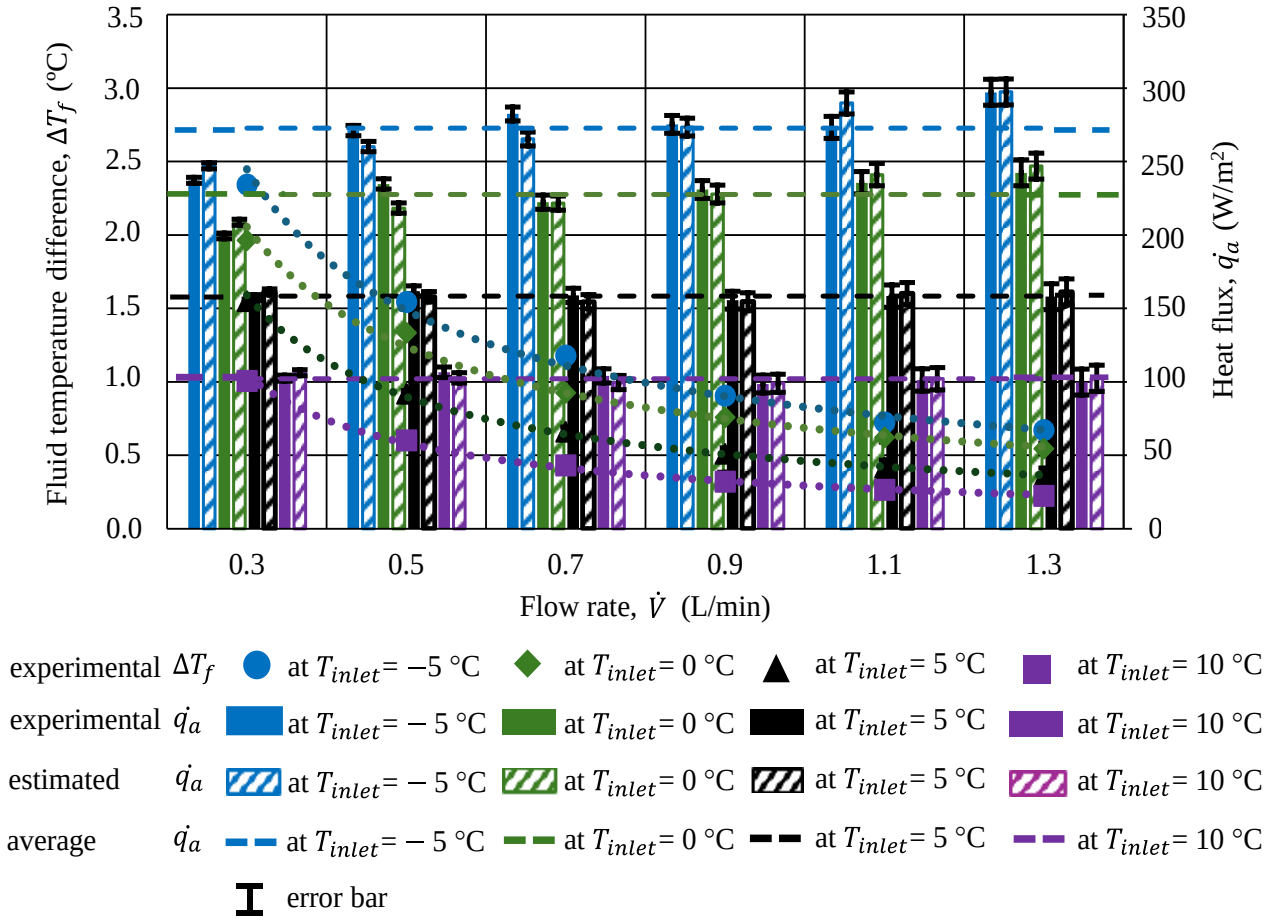

Figure 4.8. Fluid temperature difference and heat flux for all conditions (cooling).

It can be noticed that $\dot{q}_a$ increases with T_{inlet} decreases. This could be due to the temperature gradient between T_{inlet} and surrounding air temperature becomes larger, leading to $\dot{q}_a$ increases. Moreover, $\dot{q}_a$ increases with the flow rate increases and ΔT_f decreases. When the flow rate increases, the surface temperature of the tube is close to the value of the inlet fluid temperature. As a result, $\dot{q}_a$ increases at higher flow rates, due to temperature difference between the surrounding air and the copper tube surface becoming high.

4.2.2 Fluid temperature difference and heat flux in the heat exchanger (heating)

Figure 4.9 presents the values of ΔT_f and $\dot{q}_a$ in the heat exchanger under heating conditions. ΔT_f is between 0.2 and 2.6 °C for all heating conditions. Notably, ΔT_f decreases with an increase in $\dot{V}$. At a low $\dot{V}$ (0.3 L/min), ΔT_f is substantially higher than at other values of $\dot{V}$. This is possibly because the fluid spends a longer duration within the tube, thereby promoting heat exchange between the fluid and tube walls. Consequently, ΔT_f is higher at lower values of $\dot{V}$. Additionally, ΔT_f at T_{inlet} = 50 °C is the highest for all values of $\dot{V}$. This is attributed to the considerable difference between the inlet fluid and ambient temperatures.

In this thesis, $\dot{q}_a$ is considered to be a function of $\dot{V}$ and ΔT_f. The $\dot{q}_a$ values are calculated using Eq. 3.2. Moreover, the estimated $\dot{q}_a$ values are calculated using the approximate ΔT_f values based on Eq. 3.2. $\dot{q}_a$ has a minimum of 1% and a maximum of 8 % uncertainty. These are shown as an error bar in the figure. These error bars are estimated by considering the Resistance Thermal Detectors measurement accuracy of ± 0.02 ºC. A slight fluctuation is observed in the $\dot{q}_a$ values although $\dot{V}$ is increased at all values of T_{inlet}. This is possibly because of the decrease in ΔT_f. The average $\dot{q}_a$ values at T_{inlet} = 30, 40, and 50 °C are approximately 100, 190, and 280 W/m^2, respectively. This indicates that the average $\dot{q}_a$ values at T_{inlet} = 40 and 50 °C are enhanced by 100% and 197%, respectively, compared with that at T_{inlet} = 30 °C, for all values of $\dot{V}$.

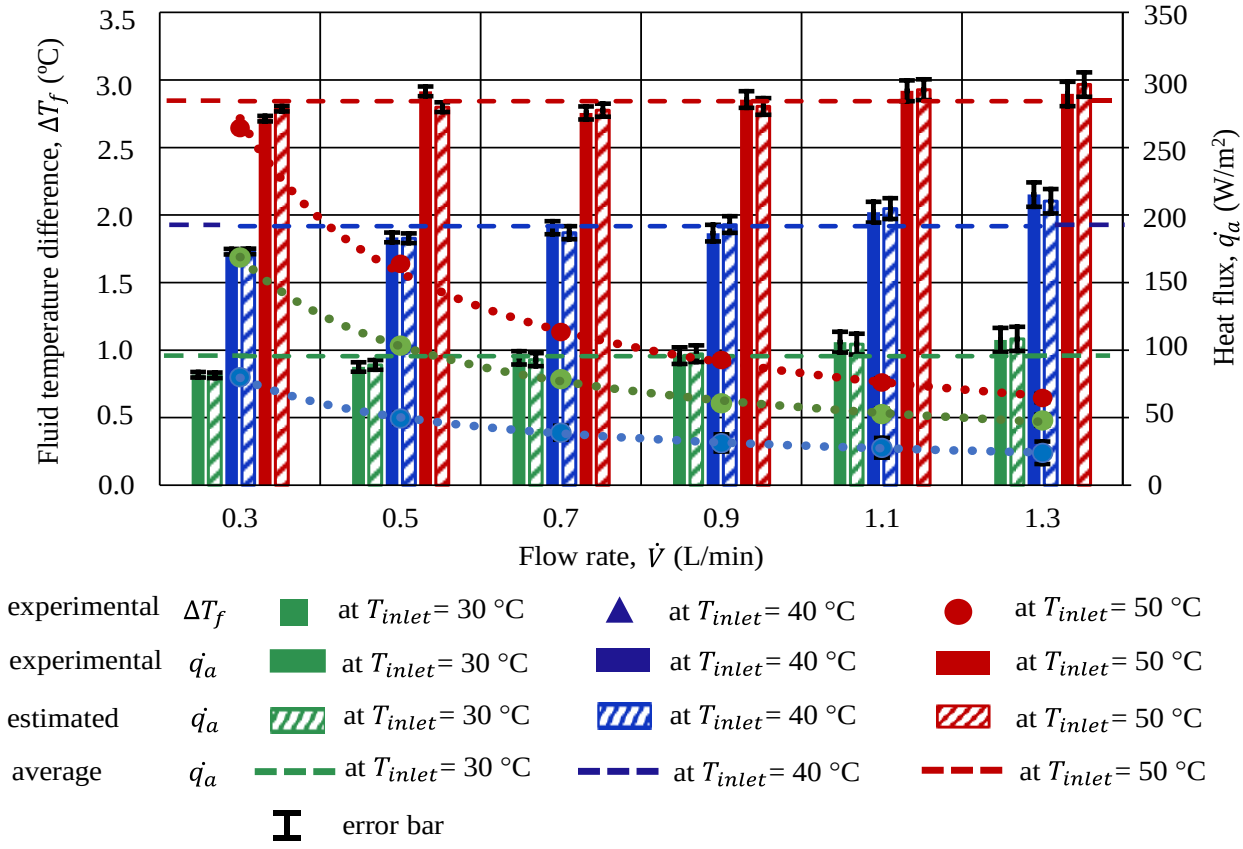

Figure 4.9. Fluid temperature difference and heat flux for all conditions (heating).

As already mentioned in the cooling, T_{inlet} influence on the $\dot{q}_a$ more than $\dot{V}$. Moreover, the similar $\dot{q}_a$ trend can be seen for both cooling and heating experimental conditions as shown in Figs. 4.6 and 4.7. This is due to the temperature difference between T_{inlet} and surrounding air temperature is almost equivalent during cooling and heating, respectively. In the cases of T_{inlet} are –5 and 50 ºC, the temperature difference between T_{inlet} and their surrounding air temperature has a similar temperature difference approximately of 30 ºC. It is also same in the cases of T_{inlet} are 0, 5 and 40 ºC, as well as T_{inlet} are 10 and 30 ºC.

4.3 Pressure drop in the heat exchanger

Figure 4.10 shows the pressure drop in the heat exchanger for all values of T_{inlet} at $\dot{V}$ = 0.3 to 3.0 L/min. Theoretically, the pressure drop increases with increasing $\dot{V}$. It also depends on the fluid temperature, density, and viscosity. The pressure drop decreases with an increase in the fluid temperature. When the T_{inlet} increases, the viscosity of the fluid decreases causing the pressure drop to be decreased. For $\dot{V}$ = 0.3 to 3.0 L/min, the pressure drop in the heat exchanger shows a minimum of 0.3 kPa and a maximum of approximately 5.0 kPa at T_{inlet} = −5 to 50 ºC. At $\dot{V}$ = 3.0 L/min, the pressure drop decreases from 5.0 to 1.8 kPa as T_{inlet} is increased from −5 to 50 ºC. The pressure drop is less than 2 kPa, which is small. This aspect is expected to be useful when this heat exchanger is applied to actual greenhouse cultivation.

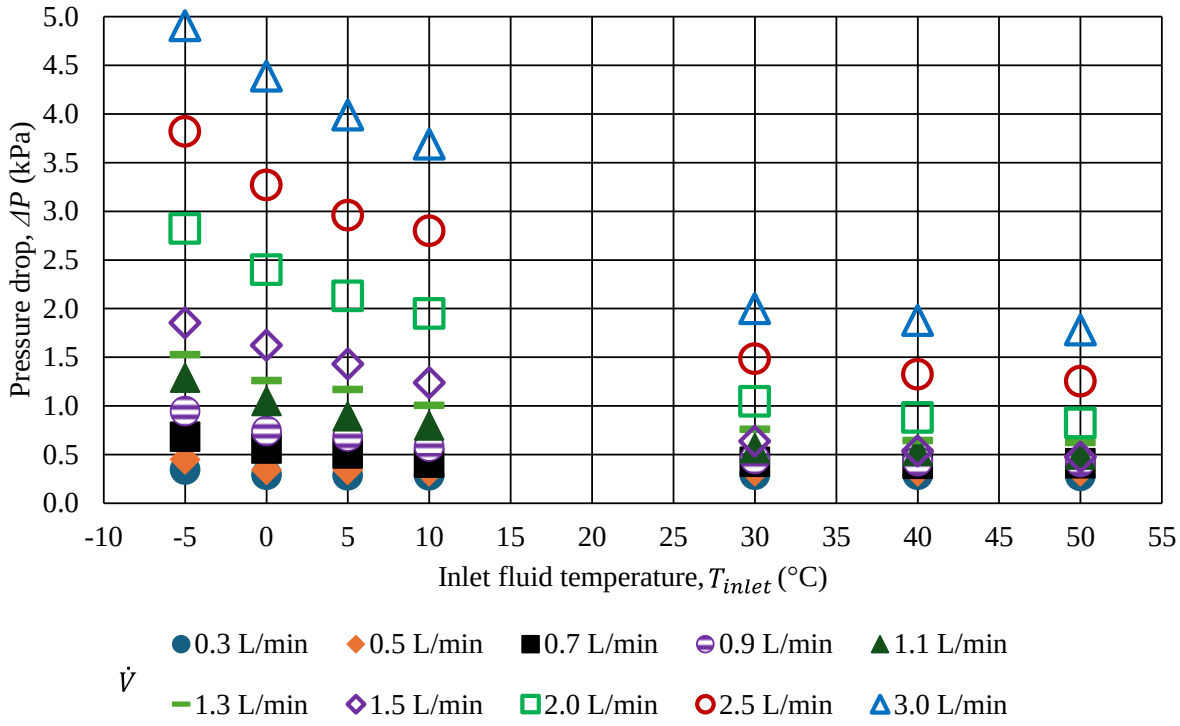

Figure 4.10. Pressure drop in the heat exchanger under cooling and heating conditions.

4.4 Periodic air temperature

The experimental system was enclosed in insulation foam, thereby reducing direct contact with the laboratory. Experiments for periodic air temperature were performed longer hours which takes about a day. However, the local air temperatures and the ceiling and floor area air temperatures in the experimental system almost become the same value when the experiment is conducted for a longer duration. This is due to the well-insulation of the experimental system from the laboratory. Thus, the insulation foam for the experimental system was removed and the experimental system was enclosed in a thin polyvinyl chloride transparent film instead of insulation foam as shown in Fig. 4.11. The polyvinyl chloride transparent film thickness is 0.07 mm. Then, the experiments for evaluating the periodic air temperature change were performed with the transparent film covered experimental system.

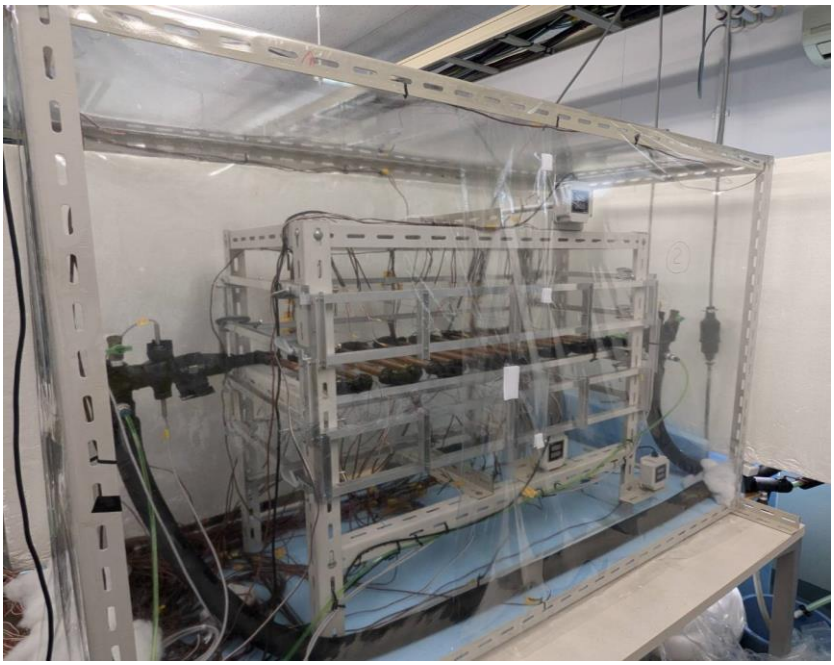

Figure 4.11. Experimental system enclosed with polyvinyl chloride transparent film.

The transition time of the heat exchanger system is important because the longer the duration the higher the energy is consumed. It takes time to reach the steady state of local air temperature when the cooling process is switched to heating and vice versa. This time is called the transition time. Moreover, three states of the transition time are defined for the heating and cooling transition as shown in Fig 4.12. τ_1 denotes the quick-change state, which is 90% change, τ_2 is the moderate change state and τ_3 is the steady state of heating transition. τ_4, τ_5 and τ_6 are defined for the cooling transition the same as the heating.

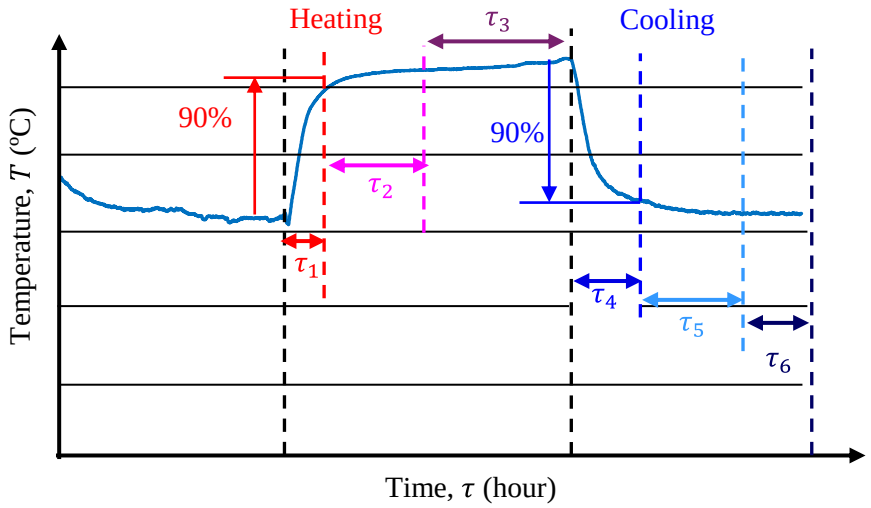

Figure 4.12. Schematic diagram of showing duration of time for transition.

Figure 4.13 shows the periodic air temperature change according to the cooling and heating process. For cooling and heating, T_{inlet} = −5 °C whereas T_{inlet} = 50 °C was chosen to examine periodic air temperature as these inlet temperatures can obtain the highest air temperature difference. Figures 4.13 (a) – (j) present the

change in periodic air temperature with $\dot{V} = 0.3$ to 3.0 L/min. The average local air temperatures of each layer and the air temperatures near the upper area and lower area in the experimental system were plotted. $T_{i,up}$ means the average upper air temperature inside the experimental system which is 450 mm far from the heat exchanger. $T_{i,lo}$ indicates the average lower air temperature inside the experimental system which is 450 mm far from the heat exchanger.

For cooling, the local air and air temperatures of the area below the heat exchanger are important while for heating that of the area above are essential. According to Fig. 4.13, the average local air temperatures at each layer of the area below $T_{l,avg,50\text{ mm}}$, $T_{l,avg,100\text{ mm}}$ and $T_{l,avg,150\text{ mm}}$ are almost identical during the cooling process in which their values are approximately 17 ºC. On the other hand, the average local air temperatures at each layer of the area above $T_{l,avg,-50\text{ mm}}$, $T_{l,avg,-100\text{ mm}}$ and $T_{l,avg,-150\text{ mm}}$ are similar during the heating process. The values are about 32 ºC. In the case of changing periodic air temperature field, the air temperature difference between the area below and the area above of the heat exchanger is important for crops. During the cooling process, $T_{i,lo}$ is approximately 16.5 ºC whilst $T_{i,up}$ is about 25 ºC. During the heating process, $T_{i,up}$ can reach about 33 ºC whereas $T_{i,lo}$ is around 27 ºC. Therefore, the temperature difference $T_{i,lo}$ and $T_{i,up}$ is approximately 15 ºC. This temperature difference would be sufficient for the strawberry crops because strawberry crops require air temperature difference of around 15 ºC. As explained earlier, inlet fluid temperature has more impact on the local air temperature than the flow rate. Variation flow rate has small impact on the local air temperature. However, the flow rate could have effect on the transition time between cooling and heating processes and vice versa.

Transition time

The transition time is investigated by varying $\dot{V} = 0.3$ to 3.0 L/min. However, the experimentation period was around 10 hours a day. Therefore, in practical case, the steady state, τ_3 of the heating transition is considered subtraction from 12 hours of $(\tau_1 + \tau_2)$ heating transition. The steady-state, τ_6 of the cooling transition was defined in the same way as the heating transition.

When $\dot{V} = 0.3$ to 1.3 L/min, the quick change state,τ_1 and moderate change state,τ_2 from cooling to heating (heating transition) take approximately twenty minutes and two hours, respectively. On one hand, the quick change state,τ_4 take around forty-nine minutes and moderate change state,τ_5 take about one hour and forty minutes from the heating to cooling process (cooling transition).

When $\dot{V} = 1.5$ to 3.0 L/min, τ_1 and τ_2 of heating transition take about eighteen minutes and one hour, respectively. On the other hand, τ_4 and τ_5 of cooling transition take approximately forty minutes and one hour, correspondingly.

The details of the periodic air temperature change including the temperature difference between heating and cooling processes and the heating and cooling transition time are elucidated in Table 4.1.

The quick change state of both the heating and cooling remains unchanged. However, the moderate change state of both the heating and cooling gradually decreases with the increase of the flow rate. When the

flow rate increases, the tube surface temperature becomes close to the value of T_{inlet}. Consequently, the moderate change state reduces because of the temperature difference between the copper tube surface and the surrounding air becoming high.

From the results, the cooling transition seems to be more gradual compared to the heating transition, indicating that while the system heats up quickly, it cools down more slowly. This means cooling is more difficult than heating. And cooling time longer than the heating. This could be because the internal heat transfer coefficient of cooling is lower than that of heating.

A quick switch could be great between cooling and heating or heating and cooling processes for crops to reduce energy consumption. However, a sudden temperature change may lead to stress for crops such as damage or slow growth of crops. Gradual transitions would be better for reducing plant stress.

According to the results, the system will be operated for twelve hours for cooling and heating, respectively within a day for crops. However, when the air temperature is suitable for crop growth, cooling or heating will not be necessary to be provided constantly.

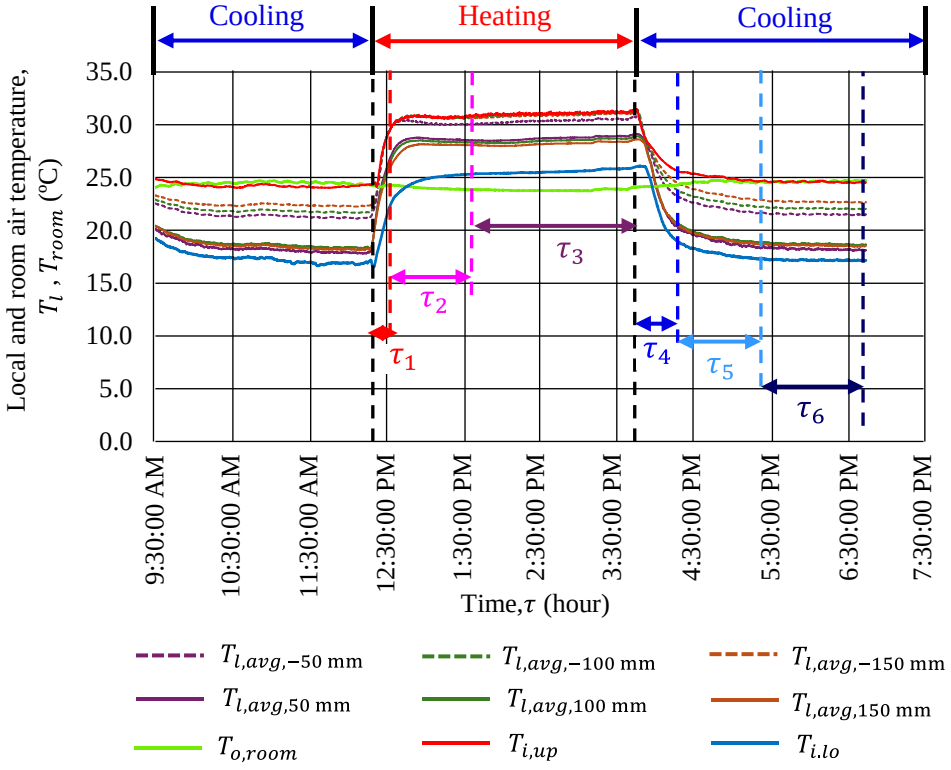

(a) $\dot{V}$ = 0.3 L/min

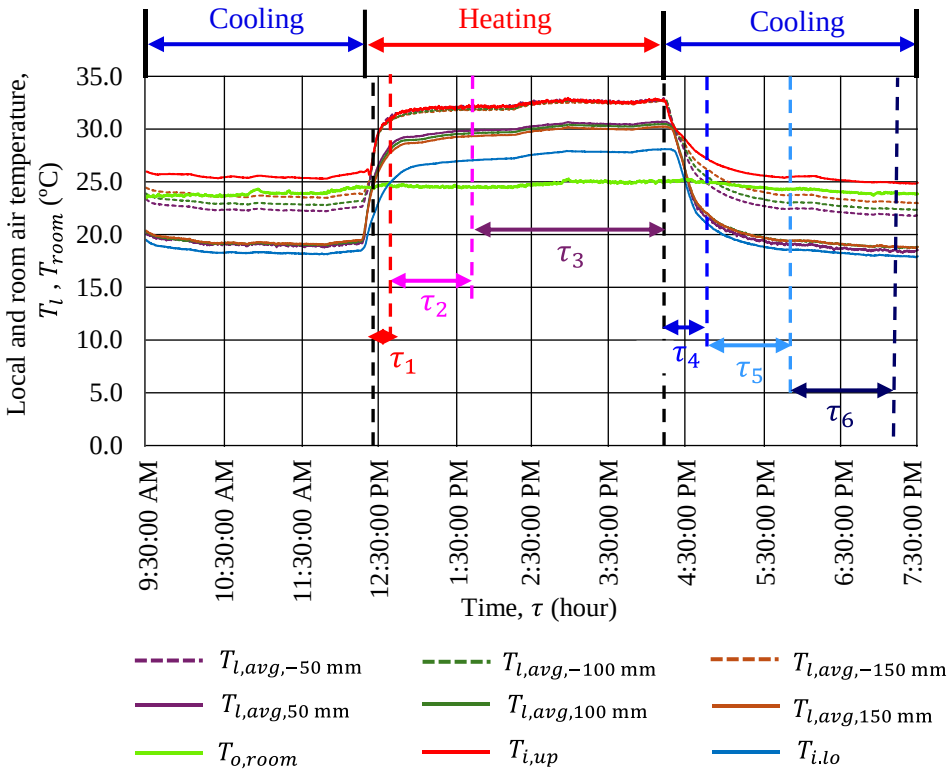

(b) $\dot{V}$ = 0.5 L/min

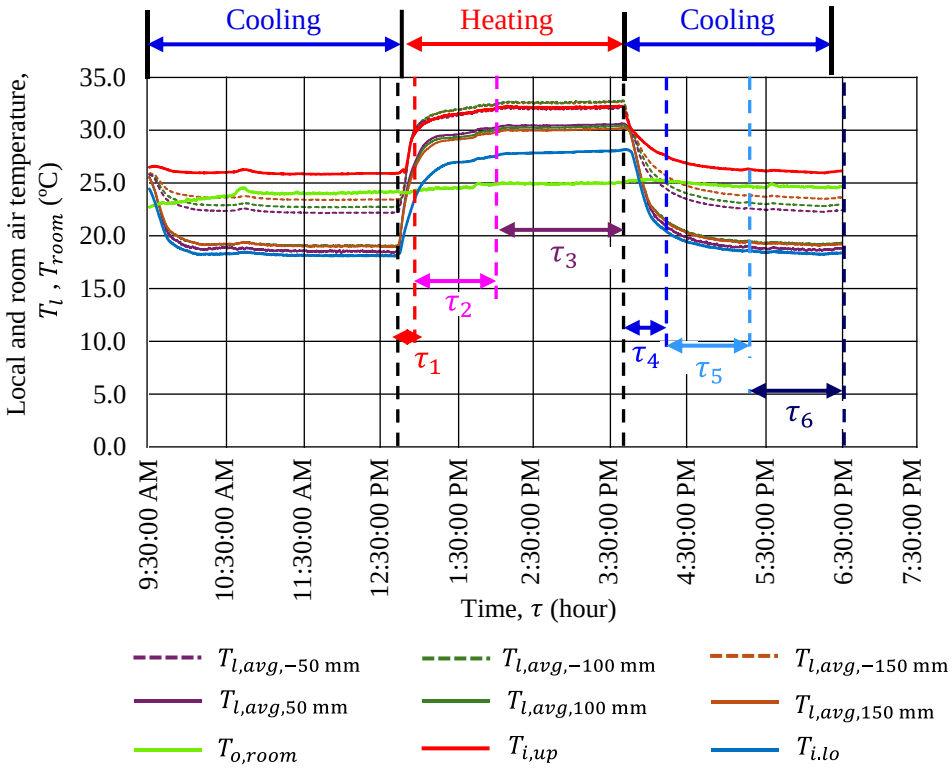

(c) $\dot{V}$ = 0.7 L/min

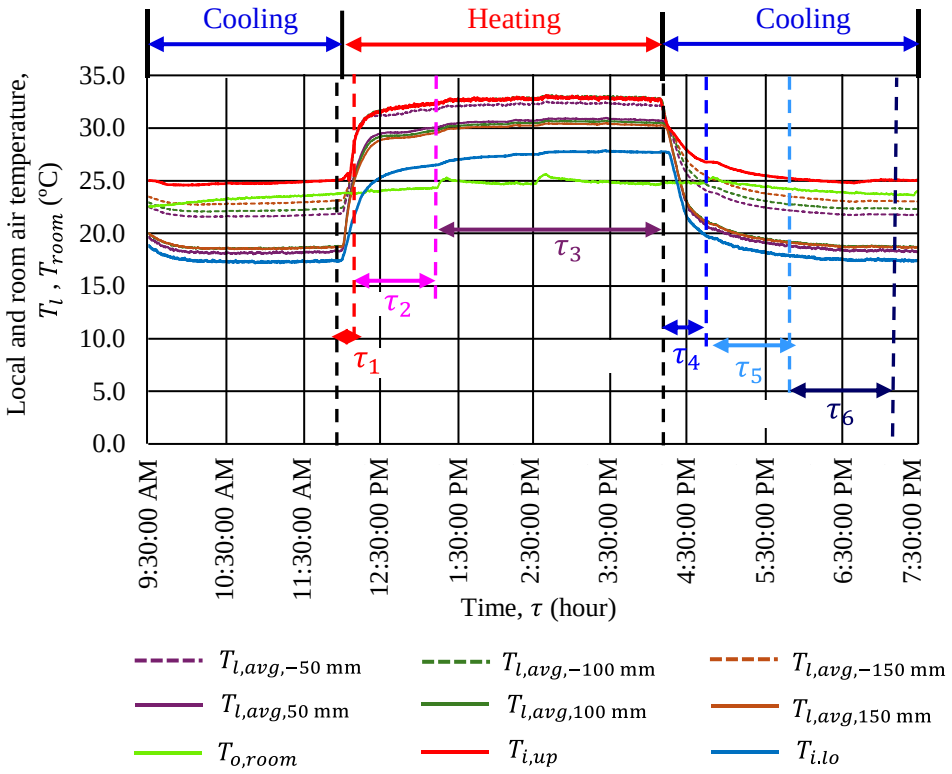

(d) $\dot{V}$ = 0.9 L/min

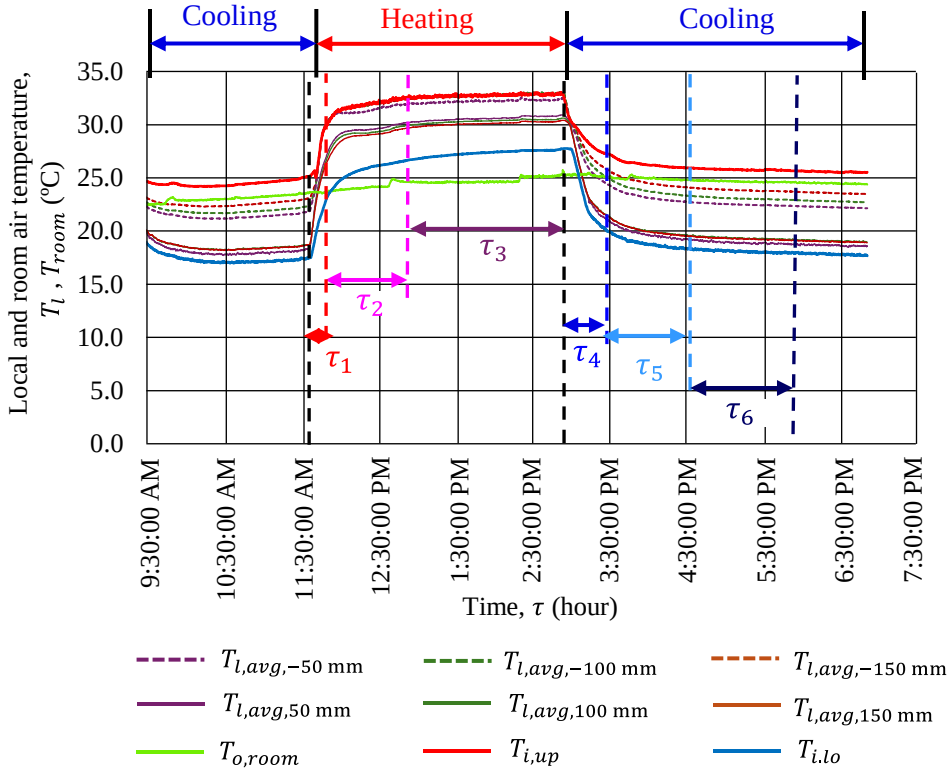

(e) $\dot{V}$ = 1.1 L/min

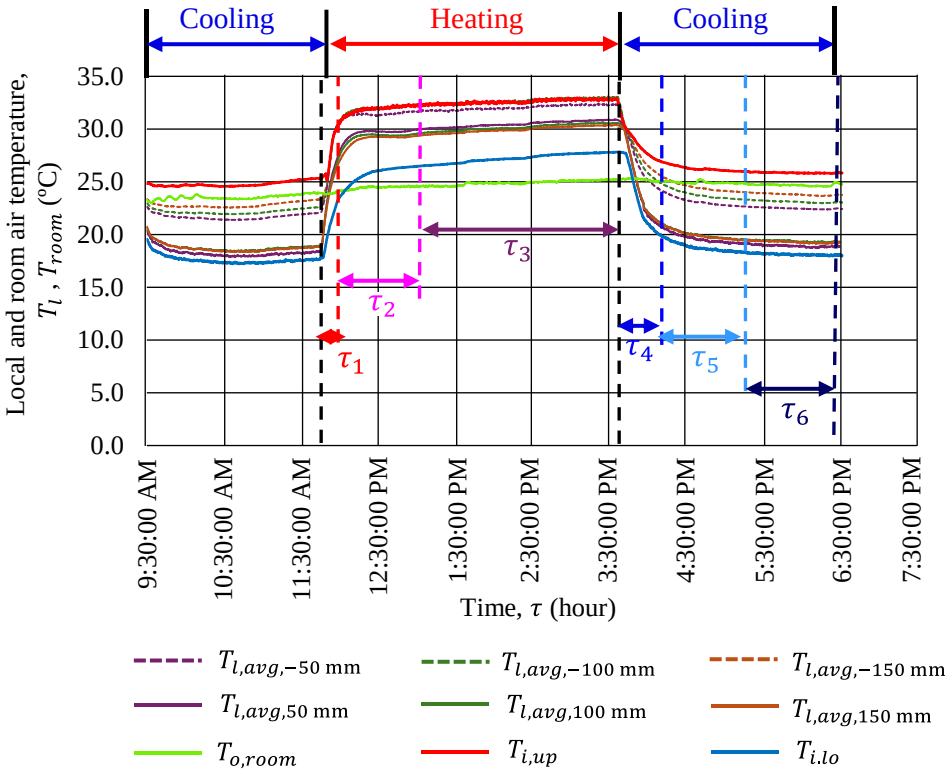

(f) $\dot{V}$ = 1.3 L/min

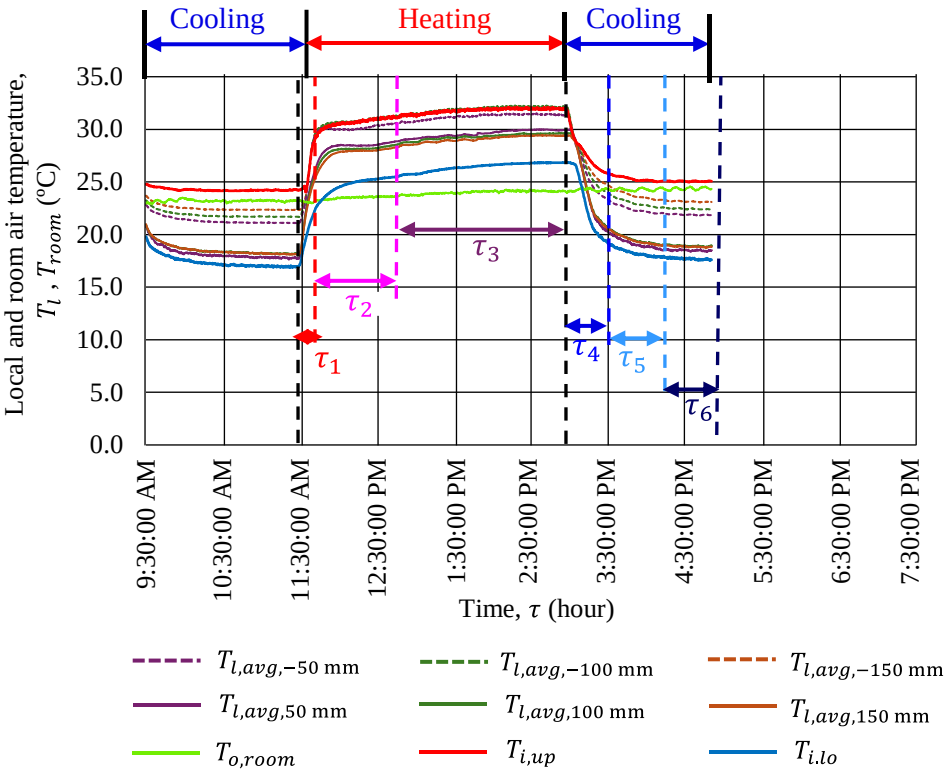

(g) $\dot{V}$ = 1.5 L/min

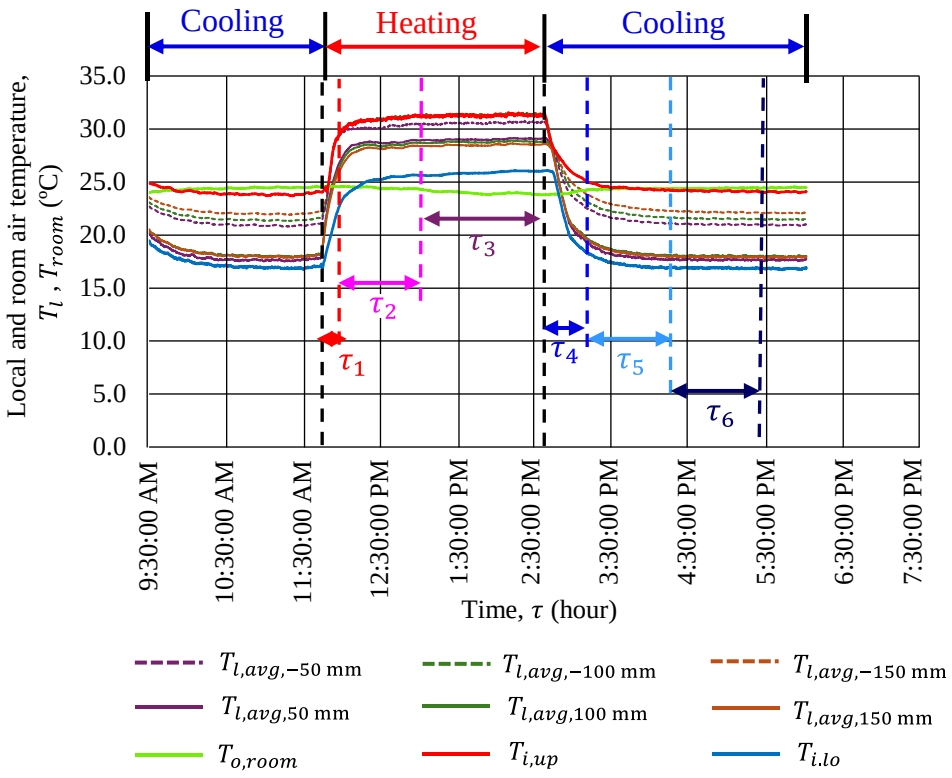

(h) $\dot{V}$ = 2.0 L/min

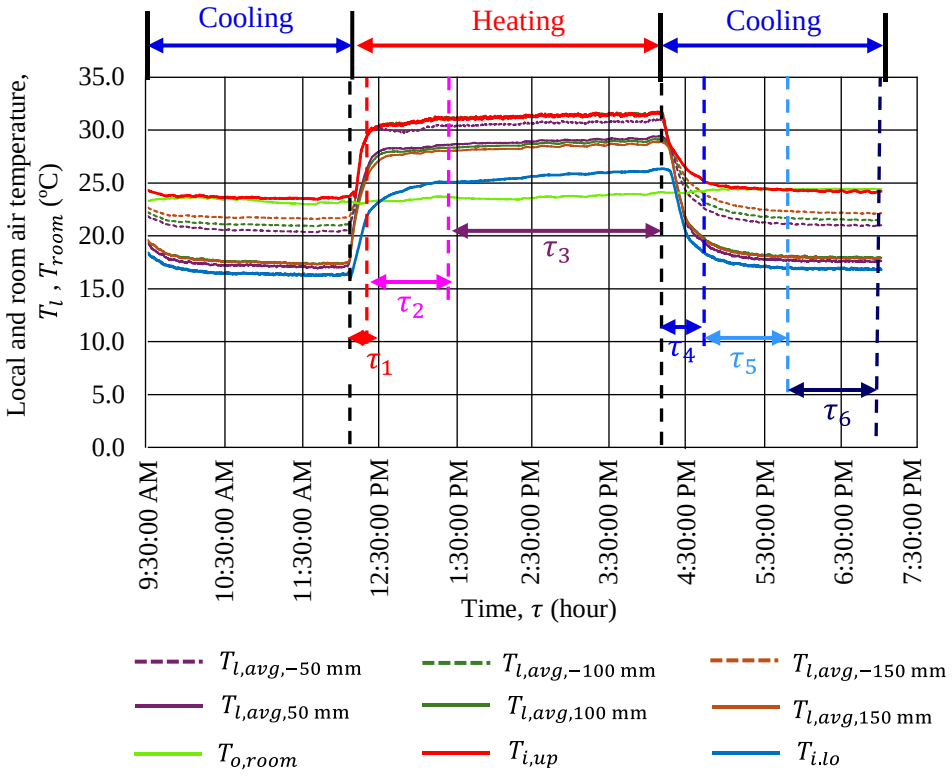

(i) $\dot{V}$ = 2.5 L/min

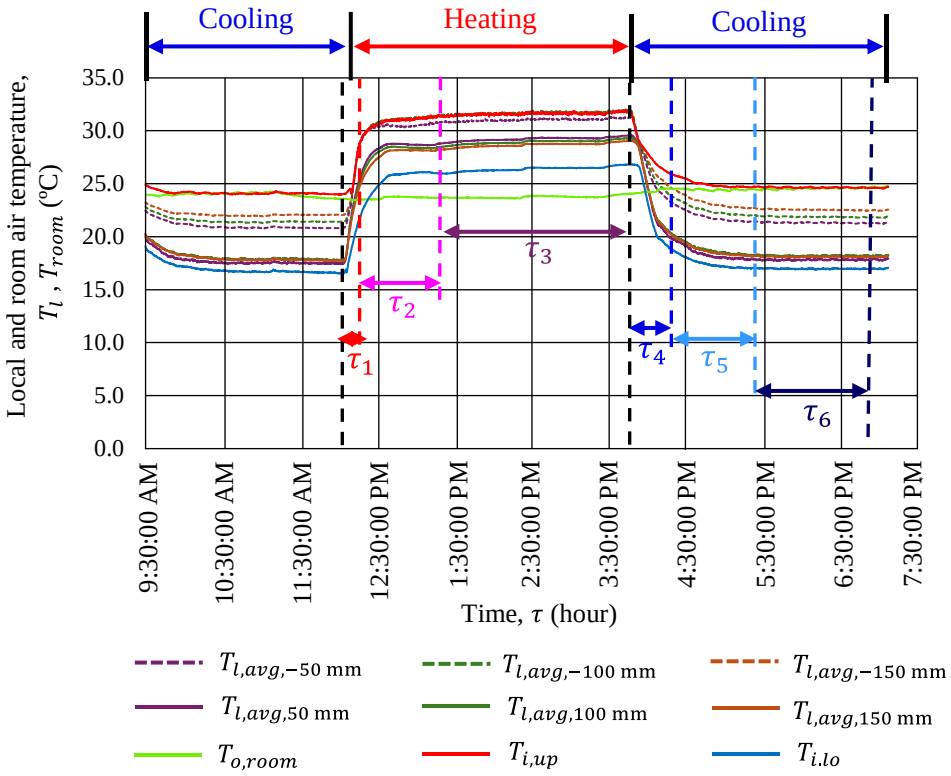

(j) $\dot{V}$ = 3.0 L/min

Figure 4.13. Periodic air temperature changes for conditions of T_{inlet} = −5 and 50 ºC with all flow rates.

Table 4.1. The characteristic of periodic air temperature change.

Flow rate (L/min)	**Air temperature difference between heating and cooling processes (ºC)**	**Transition time**					
		Heating			**Cooling**		
		τ_1	τ_2	τ_3	τ_4	τ_5	τ_6
0.3	13.7	20 min.	2 h 5 min.	9 h 35 min.	49 min.	1 h 51 min.	9 h 20 min.
0.5	14.4	24 min.	1 h 53 min.	9 h 43 min.	45 min.	1 h 44 min.	9 h 31 min.
0.7	14.6	20 min.	1 h 49 min.	9 h 51 min.	44 min.	1 h 32 min.	9 h 44 min.
0.9	15.2	21 min.	1 h 47 min.	9 h 52 min.	47 min.	1 h 32 min.	9 h 41 min.
1.1	15.3	23 min.	1 h 42 min.	9 h 55 min.	46 min.	1 h 30 min.	9 h 44 min.
1.3	15.3	18 min.	1 h 50 min.	9 h 52 min.	50 min.	1 h 23 min.	9 h 47 min.
1.5	15.1	18 min.	1 h 45 min.	9 h 57 min.	45 min.	58 min.	10 h 17 min.
2.0	15.1	18 min.	1 h 2 min.	10 h 40 min.	46 min.	45 min.	10 h 29 min.

Flow rate (L/min)	Air temperature difference between heating and cooling processes (ºC)	Transition time					
		Heating			Cooling		
		τ_1	τ_2	τ_3	τ_4	τ_5	τ_6
2.5	15.2	18 min.	1 h 1 min.	10 h 41 min.	44 min.	51 min.	10 h 25 min.
3.0	15.1	18 min.	1 h 4 min.	10 h 38 min.	32 min.	1 h.	10 h 28 min.

4.5 Theoretical estimation of energy consumption

Figure 4.14 shows schematic greenhouse dimension taking into consideration the practical greenhouse cultivation. The height of the greenhouse is 2.5 m and the width is 5.2 m. Here, it is considered length as a unit length. This greenhouse dimension is taken into account when energy requirement is estimated theoretically. Three crop rows are inside the greenhouse. During both summer and winter time, the air temperature difference between the outside and inside of the greenhouse was assumed to be about 15 ºC. Figure 4.15 shows the photo of the practical greenhouse strawberry cultivation.

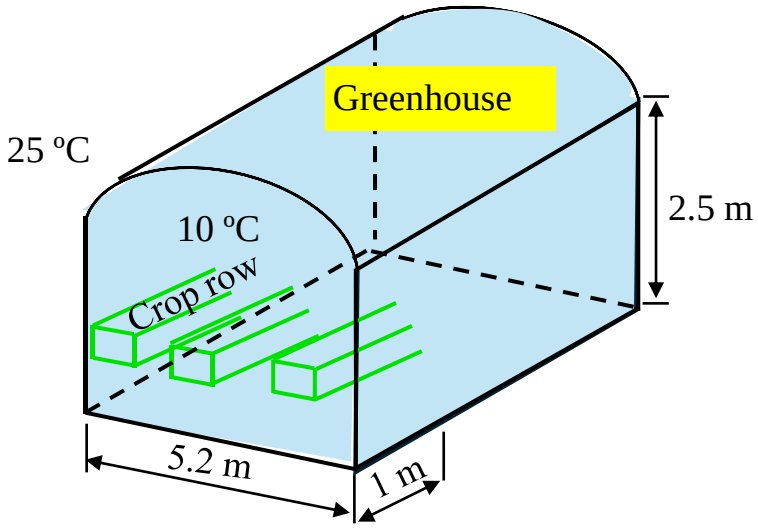

Figure 4.14. The schematic structure of the greenhouse with whole area control.

Figure 4.15. Photo of the strawberry crop rows in greenhouse [4].

For the local climate control, only the area near the strawberry crops will be considered. The whole area of the greenhouse does not require to be considered. Therefore, the experimental heat exchanger system area will be covered near the crops. The width and height near the crops are 0.7 m and 1.0 m as shown in Fig. 4.16. The unit length is considered for the volume. This local area dimension is taken into account when energy requirement is estimated theoretically. Moreover, the strawberry crops will be grown on the shelves in order to install the heat exchanger.

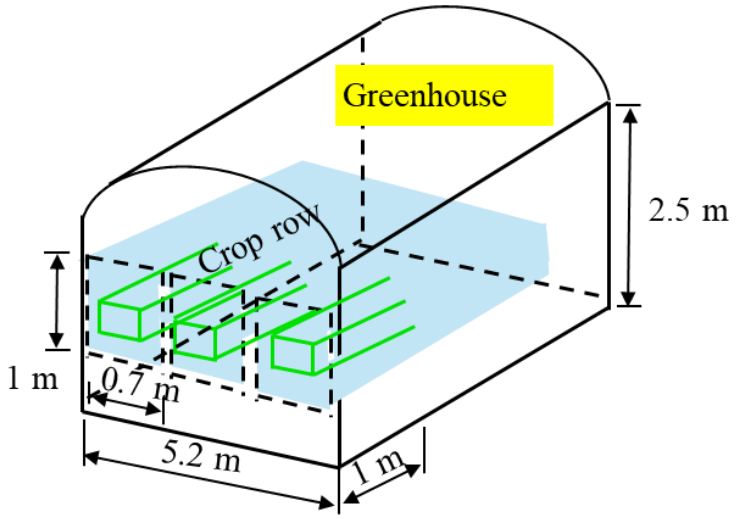

Figure 4.16. The schematic structure of the greenhouse with local area control.

The cooling/heating systems are employed to remove/add the heat load in the greenhouse area. In this case, the whole area air volume in the greenhouse is required to cool down/heat up to create a suitable climate for the crops. For simple calculation, the heating and cooling amount in the greenhouse can be estimated by Eq. 4.1.

$$Q = V\,\rho_a\,c_{pa}\,\Delta T_a \tag{4.1}$$

where Q is the heat amount to be removed/added with unit length (kJ/m), V is the volume of the control area (m^3/m), ρ_a is the density of air at a certain temperature (kg/m^3), c_{pa} is the specific heat capacity of air at a certain temperature (kJ/kg·K) and ΔT_a is the air temperature difference between heating and cooling processes (°C).

The heat diffusion from the local area to the nearby surroundings is calculated using Eq. 4.2.

$$Q_{loss} = k_{air}\, A \frac{\Delta T}{\Delta z} \tag{4.2}$$

where Q_{loss} is the heat diffusion from the local area to the near surroundings (W), k_{air} is the thermal conductivity of air at the certain air temperature (W/m·K), A is the area of the below and above the heat exchanger (m^2) for cooling and heating, respectively, ΔT is the air temperature difference between two vertical layers of heat exchanger (°C) and Δz is the vertical distance (m) ($\Delta z = 50\times10^{-3}$ m).

The heat amount to be removed/added with unit length considering the transition time was calculated by using Eq. 4.3.

$$P = \frac{Q}{\tau} \tag{4.3}$$

where P is the heat amount to be removed/added with unit length considering the transition time (kW/m), and τ is the transition time (second).

The coefficient of performance COP is the heat amount divided by the required input energy. The system capacity can be calculated from the heat amount and COP of the heat pump using the following equation.

$$S = \frac{P}{K} \tag{4.4}$$

where S is the system capacity (kW/m), and K is the coefficient of performance of the heat pump (dimensionless).

Eventually, the energy requirement can be estimated by Eq. 4.5.

$$E = S \times \tau \tag{4.5}$$

where E is the energy requirement (kJ/m).

Table 4.2 shows theoretical considerations for the energy requirements of the whole area and local area control for greenhouse crop cultivation at different states of the transition time at $\dot{V}$ = 0.9 L/min as an example. The volume of the whole area is 13 m^3/m while the volume for the local area is 2.1 m^3/m which includes three crop rows. The volume of the local area is reduced compared to that of the whole area.

By using Eq. 4.1, the heating and cooling amount of the whole area and local area control is calculated. During the steady state of heating and cooling for the whole area control, the heat amount becomes zero. This is due to there being no heat loss to the surroundings (adiabatic). However, the heat loss from the local area to the nearby surroundings should be considered during these steady states. This heat loss was estimated by using Eq. 4.2.

The COP of the heat pump is assumed to be about 3.3 and 4.2 heating and cooling, correspondingly. The system capacity of the whole area and local area control was estimated with COP value by using Eq. 4.4. Then, the energy requirement was calculated by multiplying the system capacity and transition time. Subsequently, the total energy requirement for the whole area control and local area control is summed up of the heating and cooling, correspondingly.

Table 4.3 shows the maximum system capacity requirements and total energy requirements of the whole area and local area control. The maximum system capacity requirement of the whole area control is around 62 W/m whereas that of the local area control is approximately 10 W/m which is more than 80% reduction compared to the whole area control. Moreover, the total energy requirement of the whole area control is approximately 152 kJ/m. On one hand, the total energy requirement of the local area control is about 37 kJ/m. Comparing the total energy requirement of the local area control with that of the whole area control of greenhouse cultivation, the total energy requirement of the local area control was more than 70% reduced. This theoretical calculation is simple and takes into account some assumptions to show the advantage of the local climate control heat exchanger system over the whole area control.

Table 4.2. Calculation of heating and cooling amount and energy requirements of the different states for the whole area and local area control in greenhouse cultivation. ($\dot{V}$ = 0.9 L/min)

Parameters	**Whole area**		**Local area**	
	Heating	**Cooling**	**Heating**	**Cooling**
Length (m)	1.0		1.0	
Width (m)	5.2		0.7	
Height (m)	2.5		1.0	
Crop rows	**3**		**3**	
V, volume (m^3/m)	**13**		**2.1**	
ρ_a, air density (kg/m^3)	1.46	1.36	1.46	1.36
c_{pa}, specific heat of air (kJ/kg·K)	1.006		1.006	

Parameters	Whole area						Local area					
	Heating			Cooling			Heating			Cooling		
ΔT_a, air temperature difference (ºC)	13.4	1.8	Adiab-atic	13.4	1.8	Adiab-atic	13.4	1.8	(ΔT =0.2)	13.4	1.8	(ΔT =0.2)
Transition state (second)	τ_1= 1,260	τ_2= 6,420	τ_3= 35,520	τ_4= 2,820	τ_5= 5,520	τ_6= 34,860	τ_1= 1,260	τ_2= 6,420	τ_3= 35,520	τ_4= 2,820	τ_5= 5,520	τ_6= 34,860
Q, heat amount (kJ/m)	255.9	34.4	0	238.5	32.0	0	41.3	5.6	3.3	38.5	5.2	8.0
P, heat amount considering time (kW/m) ($\times 10^{-3}$)	203.1	5.4	0	84.6	5.8	0	32.8	0.9	0.1	13.7	0.9	0.2
COP	3.3			4.2			3.3			4.2		
S, system capacity (kW/m) ($\times 10^{-3}$)	61.5	1.6	0	20.1	1.4	0	9.9	0.2	0.03	3.3	0.2	0.05
E, energy requirement (kJ/m)	77.5	10.3	0	56.7	7.7	0	12.5	1.5	1.0	9.3	11.0	1.9
E_{total}, total energy requirement (kJ/m)	152						37.2					

Table 4.3. Maximum system capacity and total energy requirements for the whole and local area control for greenhouse cultivation.

Parameters	Whole area		Local area	
	Heating	Cooling	Heating	Cooling
Maximum system capacity (W/m)	61.5		9.9	
Total energy requirement (kJ/m)	152		37.2	

Summary

This chapter discusses the periodic local climate control for strawberry crop cultivation. The serpentine copper tube heat exchanger experimental system was constructed in the laboratory and experiments were performed. First, the performance of the heat exchanger such as the local air temperature profiles near the crops, the heat flux, and the pressure drop in the heat exchanger were investigated. The local air temperature profiles were analyzed by the color contour plot and numerical graphs. During cooling, the color contour plots significantly change from light orange to blue in the area below the heat exchanger when T_{inlet} decreases from 10 to 5,0 and -5 ºC. On the other hand, during heating, the color contour plots considerably change from blue to dark orange in the area above the heat exchanger with T_{inlet} increases from 30 to 40, 50 ºC. When increasing the flow rate after $\dot{V}$= 0.9 L/min, the local air temperatures were not substantially changed. The heat flux also increases when T_{inlet} increases. Additionally, the heat flux increases steadily with the increase in $\dot{V}$. For both cooling and heating, T_{inlet} has a huge impact on the local air temperatures and heat flux than $\dot{V}$. In terms of pressure drop, the pressure drop increases with $\dot{V}$ increases. Nonetheless, the pressure drop decreases when T_{inlet} increases. This is due to the fluid viscosity decreases with the increasing T_{inlet}.

The periodic air temperature change was evaluated at T_{inlet}= -5 and 50 ºC for all flow rates. It was found that the air temperature difference between the areas below and above the heat exchanger of cooling and heating processes is approximately 15 ºC. Increasing flow rate does not notably change the air temperature at the areas below of cooling and above of heating the heat exchanger. After $\dot{V}$= 0.9 L/min, the local air temperatures and air temperatures in the experimental system were not substantially changed. Regarding the transition time, the cooling transition seems to be more gradual compared to the heating transition, indicating that while the system heats up quickly, it cools down more slowly. The transition time reduces with $\dot{V}$ increases. When the flow rate increases, the tube surface temperature becomes close to the value of T_{inlet} enhancing the heat exchange between the tube wall and surroundings.

The maximum system capacity requirement of the whole area control is around 62 W/m whereas that of the local area control is approximately 10 W/m which is more than 80% reduction compared to the whole area control. The total energy requirement of the whole area control was about 152 kJ/m. On the other hand, the total energy requirement of the local area control was approximately 37 kJ/m. The total energy requirement of

the local area control was more than 70% reduced compared to that of the whole area control of the practical greenhouse crop cultivation.

References in chapter 4

[1] J.F. Hancock, Strawberries,2nd Ed., Crop production science in horticulture series CABI, 2021.

[2] M. P. N. Gent, Effect of temperature on composition of hydroponic lettuce, Acta Horticulturae, pp. 95–100, 2016.

[3] Aparna, A. Skarzyńska, W. Pląder, M. Pawełkowicz, Impact of Climate Change on Regulation of Genes Involved in Sex Determination and Fruit Production in Cucumber, Plants, Vol.12, pp. 1–21, 2023.

[4] N. Khammayom, N. Maruyama, C. Chaichana, M. Hirota, Experimental analysis of local air temperature and thermal performance of a serpentine copper pipe, Energy Report, pp. 653–661, 2023.

Chapter 5

Conclusions

To examine the periodic local air temperature control, an experimental study was conducted in a laboratory. The experimental conditions were altered by varying T_{inlet} and $\dot{V}$ in the serpentine copper tube heat exchanger for cooling and heating. The main findings of this thesis are summarized as follows.

In terms of cooling, the local air temperature can be reduced by 4–10 °C from the initial air temperature of 22 °C in the area below the heat exchanger at a distance of 150 mm. In terms of heating, the local air temperature can be increased by 6–13 °C from the initial air temperature of 22 °C in the area above the heat exchanger at a distance of 150 mm. For cooling, the average $\dot{q}_a$ values in the heat exchanger at T_{inlet} = 5, 0, and −5 °C are enhanced by 55%, 120%, and 170% for all flow rates compared with that at T_{inlet} = 10 °C. The average $\dot{q}_a$ values in the heat exchanger at T_{inlet} = 40 and 50 °C are increased by 100% and 197% at all flow rates compared with that at T_{inlet} = 30 °C. Considering both cooling and heating operations, the pressure drop in the heat exchanger reaches a minimum of 0.3 kPa and a maximum of approximately 5.0 kPa for $\dot{V}$ = 0.3 to 3.0 L/min. Based on the results, T_{inlet} markedly affects the heat flux in the heat exchanger, subsequently influencing the local air temperature. Particularly, the local air temperature control and $\dot{q}_a$ in the heat exchanger are more strongly affected by T_{inlet} than by $\dot{V}$.

In the case of changing periodic air temperature field, the air temperature difference between the area below and the area above of the heat exchanger is important for crops. The periodic air temperature change was evaluated at T_{inlet}= −5 and 50 ºC for all flow rates. It was found that the air temperature difference between the areas below and above the heat exchanger of cooling and heating processes is approximately 15 ºC. This temperature difference would be sufficient for the strawberry crops because strawberry crops require the air temperature difference of around 15 ºC. As explained earlier, inlet fluid temperature has more impact on the local air temperature than the flow rate. Variation flow rate has small impact on the local air temperature. After $\dot{V}$= 0.9 L/min, the local air temperatures and air temperatures in the experimental system were not substantially changed.

When $\dot{V}$ = 0.3 to 1.3 L/min, the quick change state and moderate change state from cooling to heating (heating transition) took approximately twenty minutes and two hours, respectively. On one hand, for heating to cooling process (cooling transition), the quick change state took around forty-nine minutes and moderate change state took about one hour and forty minutes. When $\dot{V}$ = 1.5 to 3.0 L/min, the quick change state and moderate change state of heating transition took about eighteen minutes and one hour, respectively. On the other hand, quick change state and moderate change state of the cooling transition took approximately forty minutes and one hour, correspondingly. Regarding the transition time, the cooling transition seems to be more gradual compared to the heating transition, indicating that while the system heats up quickly, it cools down more slowly. The transition time reduces with $\dot{V}$ increases. When the flow rate increases, the tube surface

temperature becomes close to the value of T_{inlet} enhancing the heat exchange between the tube wall and surroundings.

The maximum system capacity requirement of the whole area control is around 62 W/m whereas that of the local area control is approximately 10 W/m which is more than 80% reduction compared to the whole area control. The total energy requirement of the whole area control was about 152 kJ/m. On the other hand, the total energy requirement of the local area control was approximately 37 kJ/m. The total energy requirement of the local area control was more than 70% reduced compared to that of the whole area control of the practical greenhouse crop cultivation.

The maximum air temperature difference can be obtained at approximately 15 °C during periodic air temperature changes even though the heat exchange is simple. This could satisfy the targeted strawberry crop requirement. Thus, the experimental inlet fluid temperatures are also applicable when this proposed heat exchanger is used in practical greenhouse cultivation. Moreover, $\dot{V}$ = 0.9 L/min could be sufficient since the local air temperatures do not markedly change more than flow rate 0.9 L/min for both cooling and heating. As a result, application of this low flow rate can reduce the pumping power leading to reduction in energy consumption of the proposed heat exchanger. In practical greenhouse cultivation, several heat exchangers will be connected in series (series connections), and these series are connected in parallel (parallel connections). Moreover, this simple and low-cost serpentine copper tube heat exchanger is sufficiently effective to provide alternate heating and cooling for strawberry crop cultivation.

Appendix

1. Thermal properties of ethylene glycol 40% by volume (Freezing point = -23.5°C)

1.1 Dynamic viscosity (μ) of ethylene glycol-based water solutions at any temperature

Temperature (°C)	μ (Pa·s)
-17.8	0.015
4.4	0.0048
26.7	0.0022
48.9	0.0013
71.1	0.0008

1.2 Density (ρ_{fluid}) of ethylene glycol-based water solutions at any temperature

Temperature (°C)	ρ_{fluid} (kg/m^3)
-8	1,075
-4	1,073
0	1,073
20	1,063
40	1,052
60	1,041

1.3 Specific heat (c_{pf}) of ethylene glycol-based water solutions at any temperature

Temperature (°C)	c_{pf} (kJ/kg·K)
-10	3.569
0	3.595
10	3.621
40	3.700
50	3.726

2. Thermal properties of air at 1 atm pressure

T Temp.(K)	ρ density(kg/m^3)	c_p specific heat (kJ/kg·K)	μ viscosity (10^{-7} Pa·s)	v kinematic viscosity (10^{-6}m^2/s)	k thermal conductivity (10^{-3}W/m·K)	Prandtl number
100	3.5562	1.032	71.1	2.00	9.34	0.786
150	2.3364	1.012	103.4	4.426	13.8	0.758
200	1.7458	1.007	132.5	7.59	18.1	0.737
250	1.3947	1.006	159.6	11.44	22.3	0.72
300	1.1614	1.007	184.6	15.89	26.3	0.707
350	0.995	1.009	208.2	20.92	30.0	0.700
400	0.8711	1.014	230.1	26.41	33.8	0.690
450	0.7740	1.021	250.7	32.39	37.3	0.686
500	0.6964	1.030	270.1	38.79	40.7	0.684
550	0.6329	1.040	288.4	45.57	43.9	0.683
600	0.5804	1.051	305.8	52.69	46.9	0.685
650	0.5356	1.063	322.5	60.21	49.7	0.690
700	0.4975	1.075	338.8	68.10	52.4	0.695
750	0.4643	1.087	354.6	76.37	54.9	0.702
800	0.4354	1.099	369.8	84.93	57.3	0.709
850	0.4097	1.110	384.3	93.80	59.6	0.716
900	0.3868	1.121	398.1	102.9	62.0	0.720
950	0.3666	1.131	411.3	112.2	64.3	0.723
1000	0.3482	1.141	424.4	121.9	66.7	0.726
1100	0.3166	1.159	449	141.8	71.5	0.728
1200	0.2902	1.175	473	162.9	76.3	0.728
1300	0.2679	1.189	496	185.1	82	0.719
1400	0.2488	1.207	530	213	91	0.703
1500	0.2322	1.23	557	240	100	0.685
1600	0.2177	1.248	584	268	106	0.688
1700	0.2049	1.267	611	298	113	0.685
1800	0.1935	1.286	637	329	120	0.683
1900	0.1833	1.307	663	362	128	0.677
2000	0.1741	1.337	689	396	137	0.672
2100	0.1658	1.372	715	431	147	0.667
2200	0.1582	1.417	740	468	160	0.655
2300	0.1513	1.478	766	506	175	0.647

List of publications

1. Peer-reviewed journals

1) Thiri Shoon Wai, Chatchawan Chaichana, Naoki Maruyama, Energy Cost Analysis of Growing Strawberries in a Controlled Environment Chamber, *Energy Reports*, Vol. 9, 2023-3, pp. 677-687, 2023, DOI: 10.1016/j.egyr.2022.11.045.
2) Thiri Shoon Wai, Naoki Maruyama, Napassawan Wongmongkol, Chatchawan Chaichana, Masafumi Hirota, Experimental Evaluation of Localized Air Temperature Profile and Performance of Serpentine Copper Tube Heat Exchanger for Energy-saving Crop Cultivation, *Case Study in Thermal Engineering*, Vol. 60, 2024-8, 15 pages, 2024, DOI: 10.1016/j.csite.2024.104816.

2. International conference proceedings, etc. with peer-reviewed

1) Thiri Shoon Wai, Naoki Maruyama, Yuttana Mona, Chatchawan Chaichana, Prediction of the Energy Consumption for Indoor Strawberry Cultivation in a Tropical Climate, *Journal of Hunan University (Natural Science)*, Vol. 49, No. 3, 2022-3, pp. 158-167, 2022, DOI:10.55463/issn.1674-2974.49.3.17.
2) Thiri Shoon Wai, Chatchawan Chaichana, Naoki Maruyama, Modelling of Cooling Load in Close-system Solar Greenhouse under Thailand Climates Using TRNSYS, *The 1st International Conference on Smart Community Development in the Asia Pacific (iSCAP2020)*, pp. 71-77, 2020-2, Chiang Mai, Thailand.
3) Thiri Shoon Wai, Chatchawan Chaichana, Naoki Maruyama, Investigation of Solar Light Intensity beneath a Solar Photovoltaic System in a Tropical Climate Region, *The 12th TSME International Conference on Mechanical Engineering (TSME-ICoME 2022)*, 2022-12, pp. 364-370, Phuket, Thailand.
4) Thiri Shoon Wai, Napassawan Khammayom, Chatchawan Chaichana, Naoki Maruyama, Masafumi Hirota, Local Air Temperature Profile Around Serpentine Pattern Copper Pipe Heat Exchanger for Crop Cultivation, *American Institute of Physics (AIP) Conference Proceeding*, Vol. 3236, 2024-10, 080011-1–080011-10, 2024, DOI: 10.1063/5.0236822.
5) Thiri Shoon Wai, Naoki Maruyama, Napassawan Wongmongkol, Chatchawan Chaichana, Masafumi Hirota, Comparisons of the Local Air Temperature Profiles of Serpentine Copper-pipe Heat Exchangers for Growing Crops, *International Conference on Mechanical System Engineering and Technology Applications (ICoMSETA 2024)*, 2024-9, 10 pages, Pulau Pinang, Malaysia. (under processing for Institute of Physics (IOP) Publishing-Journal of Physics: Conference Series).
6) Thiri Shoon Wai, Naoki Maruyama, Napassawan Wongmongkol, Chatchawan Chaichana, Masafumi Hirota, Analysis of Local Cooling Performance of Heat Exchangers suitable for Crop Cultivation in Greenhouse, *The 14th TSME International Conference on Mechanical Engineering (TSME-ICoME 2024)*, 2024-12, pp. 640-649, Pattaya, Thailand.

7) Thiri Shoon Wai, Takumi Hirose, Naoki Maruyama, Napassawan Wongmongkol, Chatchawan Chaichana, Masafumi Hirota, Comparative Study on the Local Area Cooling of Serpentine Heat Exchanger Configurations for Crop Cultivation, *The International Conference on Sustainable Energy and Green Technology (SEGT 2024)*, 2024-12, 8 pages, Bangkok, Thailand. (accepted for presentation and full paper has been submitted for peer-reviewed).

3. International workshop without peer-reviewed

1) Thiri Shoon Wai, Napassawan Khammayom, Chatchawan Chaichana, Naoki Maruyama, Masafumi Hirota, Investigation of Local Air Temperature Profile around a Serpentine Copper Pipe Heat Exchanger, *The 15th International Workshop on Regional Innovation Studies (IWRIS 2023)*, 2023-10, pp. 51-54, Tsu, Japan.
2) Thiri Shoon Wai, Takumi Hirose, Naoki Maruyama, Napassawan Wongmongkol, Chatchawan Chaichana, Masafumi Hirota, Effectiveness of a Serpentine Heat Exchanger for Local Area Heating of Crop Cultivation, *The 16th International Workshop on Regional Innovation Studies (IWRIS 2024)*, 2024-10, pp. 13-16, Tsu, Japan.

4. National conferences

1) Thiri Shoon Wai, Chatchawan Chaichana, Naoki Maruyama, Heat Transfer Characteristics of a Completely Closed Horticulture Room, *Proceedings of Japan Society of Refrigerating and Air Conditioning Engineers (JSRAE 2020)*, Paper No. E-141, 6 pages, 2020-9, Tsu, Mie, Japan.
2) Thiri Shoon Wai, Chatchawan Chaichana, Naoki Maruyama, Prediction of Heat Load of Air Conditioning for Strawberry Cultivation in Horticultural Closed Room, *The 20th National Conference on Heat and Mass Transfer*, 5 pages, 2021-3, Songkla, Thailand.
3) Thiri Shoon Wai, Chatchawan Chaichana, Naoki Maruyama, Experimented Plant Factory's Air Conditioning System Performance Evaluation, *The 32nd Environmental Engineering Comprehensive Symposium 2022*, 4 pages, 2022-6, Takamatsu, Japan.
4) Thiri Shoon Wai, Naoki Maruyama, Napassawan Wongmongkol, Chatchawan Chaichana, Masafumi Hirota, Local Heating by the Serpentine Copper Pipe Heat Exchanger for Greenhouse Crop Cultivation, *The 34th Environmental Engineering Comprehensive Symposium 2024*, pp. 340-343, 2024-7, Koyasan, Japan.

5. Oral presentations

1) Thiri Shoon Wai, Chatchawan Chaichana, Naoki Maruyama, Energy Cost Analysis of Growing Strawberries in a Controlled Environment Chamber, *The 9th International Conference on Power and Energy Systems Engineering (CPESE 2022)*, 2022-9, Kyoto, Japan.

2) Thiri Shoon Wai, Chatchawan Chaichana, Naoki Maruyama, Masafumi Hirota, Analysis of Energy Demand for Vertical Strawberry Plantation in the Closed Room, *Lecture meeting, The Heat Transfer Society of Japan*, Tokai Chapter, 2022-10, Nagoya, Japan.

6. Others

1) Jyoji Keeni, Atsuki Hatano, Thiri Shoon Wai, Naoki Maruyama, Masafumi Hirota, Flow Visualization of Compressor Oil Behavior contained in Refrigerant to Enhance Heat Transfer in the Evaporator of CO_2 Refrigerator, *The 16th International Workshop on Regional Innovation Studies (IWRIS 2024)*, 2024-10, pp. 5-8, Tsu, Japan.
2) Jyoji Keeni, Atsuki Hatano, Thiri Shoon Wai, Naoki Maruyama, Masafumi Hirota, Influence of Compressor Oil contained in the CO_2 Refrigerant on Heat Transfer of Evaporator and its Visualization, *The 14th TSME International Conference on Mechanical Engineering (TSME-ICoME 2024)*, 2024-12, pp. 754-762, Pattaya, Thailand.

7. Awards

1) Thiri Shoon Wai, Best Oral Presentation Award at the *1st International Conference on Smart Community Development in the Asia Pacific (iSCAP2020)*, 2020-2, Chiang Mai, Thailand.
2) Thiri Shoon Wai, Best Student Paper Award at the *9th International Conference on Power and Energy Systems Engineering (CPESE 2022)*, 2022-9, Kyoto, Japan.
3) Thiri Shoon Wai, Best Paper Award at the *12th TSME International Conference on Mechanical Engineering (TSME-ICoME 2022)*, 2022-12, Phuket, Thailand.
4) Thiri Shoon Wai, Outstanding Paper Award at the *15th International Workshop on Regional Innovation Studies (IWRIS 2023)*, 2023-10, Tsu, Japan.
5) Thiri Shoon Wai, Best Outstanding Paper Award at the *16th International Workshop on Regional Innovation Studies (IWRIS 2024)*, 2024-10, Tsu, Japan.
6) Thiri Shoon Wai, Best Presenter Award at the *International Conference on Sustainable Energy and Green Technology (SEGT 2024)*, 2024-12, Bangkok, Thailand.
7) Thiri Shoon Wai (Co-author), Best Paper Award at the *14th International Conference on Mechanical Engineering (TSME-ICoME 2024)*, 2024-12, Pattaya, Thailand.